

Characterization of potential source rocks of the Prince Albert,
Whitehill and Collingham Formations in the Laingsburg sub-basin,
South Africa

BY

Janine Connie Ferreira



**UNIVERSITY of the
WESTERN CAPE**

SUPERVISOR: Dr. M. Opuwari

**Department of Earth Sciences,
University of the Western Cape**

*A thesis submitted in fulfilment of the requirements for the degree of Magister Scientiae in the
Department of Earth Sciences, University of the Western Cape*

2014

Characterization of potential source rocks of the Prince Albert,
Whitehill and Collingham Formations in the Laingsburg sub-basin,
South Africa

Janine Connie Ferreira

Key Words

Karoo Basin

Sedimentology

Mineralogy

Organic geochemistry

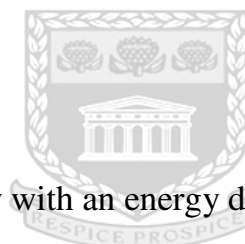
X-ray diffraction

Scanning electron microscopy with an energy dispersive spectrometer

Total organic carbon

Rock-Eval pyrolysis

Shale



UNIVERSITY *of the*
WESTERN CAPE

Abstract

The present research deals with the characterization of the Lower Ecca Group in terms of sedimentology, mineralogy and organic geochemistry. A field study was conducted in order to characterize the sedimentology and thereby determine the environments of deposition of the Prince Albert, Whitehill and Collingham Formations. In addition, shale samples were subjected to geochemical and mineralogical analyses so as to ascertain its source rock properties. The study utilized X-ray diffraction (XRD), scanning electron microscopy with an energy dispersive spectrometer (SEM-EDS), total organic carbon (TOC) and Rock-Eval pyrolysis to determine the mineralogy and organic geochemistry of shale from the formations under investigation.

The sedimentological investigation revealed that the upper Prince Albert Formation is dominated by shale with thin beds of carbonate. These shales are interpreted to have been deposited by suspension settling in a marine environment which was occasionally interrupted by deposition of carbonates that form in a shallow marine environment. The overlying Whitehill Formation consists predominantly of carbonaceous shale with relatively more resistant shale beds also present. The fine sediments are interpreted to have been deposited from suspension settling under anoxic bottom conditions which would favor the preservation of organic rich material. Deposition of the Whitehill Formation was followed by the Collingham Formation which is dominated by rhythmic deposits of shale and sandstone that are occasionally interrupted by tuff layers. The clay size sediments are interpreted to have been deposited from suspension settling which are interbedded with low density turbidite current deposits in a marine environment. Based on the findings of the field study, it is apparent that the Prince Albert and Collingham Formations were deposited in marine environments, with the Whitehill Formation being deposited in an anoxic environment. These environments are known to be dominated by phytoplanktonic organisms and algal debris, and as such shales deposited in these environments contain predominantly Type I (derived from algae) and II kerogen (derived from plankton). It can therefore be postulated that Type I and II kerogens are the dominant constituents of organic matter in the Lower Ecca Group shales.

Mineralogically, the shales consist chiefly of kaolinite, smectite and illite clay minerals, which are derived from a combination of weathering of feldspars, and the alteration of other

clay minerals. The latter being inferred from the existence of albite in all the studied shale samples, pyroclastic material observed in the field, as well as the occurrence of alteration along clay mineral edges.

The TOC values of the shale varied between 0.11 to 2.32 wt%, with an average of 0.52 wt%. The calculated production index (PI) values as determined by Rock-Eval pyrolysis ranges from 0.33 to 0.5 with an average of 0.43, this corresponds to thermally overmature organic matter. In addition, contrary to the sedimentological source characterization of organic matter, the Rock-Eval pyrolysis values and values calculated there from imply that organic matter type is predominantly Type III kerogen (derived from terrestrial plant matter), with low hydrogen index (HI) and medium to high oxygen index (OI) values. The contradiction between the geochemical and sedimentological source characterization can be considered to be evidence of the oxidization of organic matter, because well-preserved Type I/II organic matter have high HI values.



UNIVERSITY *of the*
WESTERN CAPE

Declaration

I declare that, “*Characterization of potential source rocks of the Prince Albert, Whitehill and Collingham Formations in the Laingsburg sub-basin, South Africa*” is my own work, that it has not been submitted for any degree or examination in any other university and that all the sources I have used or quoted have been indicated and acknowledge by complete references.

Full Name: Janine Connie Ferreira

Date:.....

Signed:.....



UNIVERSITY *of the*
WESTERN CAPE

Acknowledgements

This study was funded by Inkaba yeAfrica, and would not have been completed without their continued support.

Thanks go out to my supervisor, for putting his name on just about anything I write. Bless. In addition, I would like to thank my friends and family, because that's what decent human beings do...or so I've heard.

Finally, my bitches and dogs, named: Tinkles, Elizabeth, Lupo, and Al Capony. But they also respond to Duchess, Diva, Vicious-furry-little-bastard, and Handsome, respectively.



UNIVERSITY *of the*
WESTERN CAPE

Table of Contents

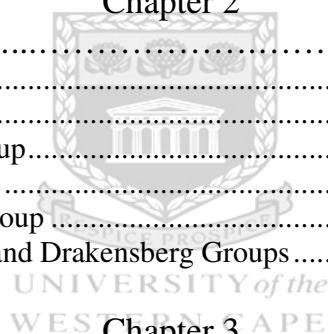
Title Page.....	i
Key words	ii
Abstract	iii
Declaration	v
Acknowledgements.....	vi
Table of Contents.....	vii
List of Figures.....	x
List of Tables.....	xii

Chapter 1

Introduction.....	1
1.1 Background.....	1
1.2 Project Scope.....	2
1.3 Study Area.....	3

Chapter 2

Geological Background.....	7
2.1 Tectonic Setting.....	10
2.2 Stratigraphy	14
2.2.1 Dwyka Group.....	14
2.2.2 Ecca Group	15
2.2.3 Beaufort Group	17
2.2.4 Stormberg and Drakensberg Groups.....	18



Chapter 3

Methods of Investigation.....	21
3.1 Field study.....	21
3.2 Mineralogical analysis	21
3.2.1 Scanning Electron Microscopy (SEM).....	21
3.2.2 X-ray diffraction (XRD).....	22
3.3 Geochemical analysis	26
3.3.1 Determination of total organic carbon content (TOC).....	26
3.3.2 Rock-Eval pyrolysis	27

Chapter 4

Sedimentology.....	31
4.1 Facies Description	31
4.1.1 Prince Albert Formation	31
4.1.1.1 Shale facies.....	31
4.1.1.2 Silty-shale facies.....	35
4.1.1.3 Dolomite facies.....	35
4.1.2 Whitehill Formation	38
4.1.2.1 Shale facies.....	38
4.1.3 Collingham Formation	41

4.1.3.1 Shale facies.....	41
4.1.3.2 Silty-shale facies.....	43
4.1.3.3 Siltstone facies.....	43
4.1.3.4 Sandstone facies	44
4.1.3.5 Tuff facies	45
4.1.3.6 Chert facies.....	45
4.2 Facies Associations.....	49
4.2.1 Prince Albert Formation	49
4.2.2 Whitehill Formation	49
4.2.3 Collingham Formation	50
4.3 Depositional Environments.....	50
4.3.1 Marine facies associations	50
4.3.2 Anoxic bottom facies associations	51
4.3.3 Distal turbidite facies associations	52

Chapter 5

Mineralogy.....	55
5.1 Clay mineralogy	55
5.2 Clay minerals in the studied shale samples.....	56
5.2.1 Kaolinite.....	56
5.2.2 Illite.....	57
5.2.3 Smectite.....	58

Chapter 6

Organic Geochemistry.....	64
6.1 Total organic carbon content.....	64
6.2 Rock-Eval pyrolysis.....	65
6.2.1 Organic matter type assessment.....	65
6.2.1.1 Hydrogen index (HI) versus oxygen index (OI).....	65
6.2.2 Organic matter abundance assessment.....	67
6.2.2.1 Total organic carbon (TOC).....	67
6.2.2.2 S ₁ and S ₂	67
6.2.3 Thermal maturity assessment.....	68
6.2.3.1 T _{max}	68
6.2.3.2 Production index (PI).....	68

Chapter 7

Discussion and Conclusions.....	71
7.1 Discussion	71
7.2 Conclusions	73

Chapter 8

Recommendations.....	75
Bibliography.....	78
Appendix A.....	96
Appendix B.....	109

Appendix C.....	112
Appendix D.....	135
Appendix E.....	137
Appendix F.....	152

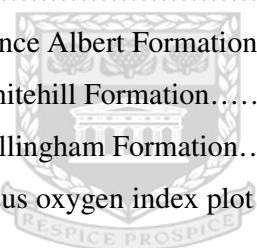


UNIVERSITY *of the*
WESTERN CAPE

List of Figures

Figure 1.1.	Location map showing the location of the Tanqua and Laingsburg sub-basins.....	4
Figure 1.2.	Geological map of the Laingsburg sub-basin, Karoo Basin, South Africa.....	5
Figure 2.1.	Lithostratigraphic column for the Cape Fold Belt and SW Karoo Basin.....	8
Figure 2.2.	Stages of foreland system evolution.....	9
Figure 2.3.	(A) Schematic map view of a ‘typical’ foreland basin, bounded longitudinally by a pair of marginal ocean basins.....	11
Figure 2.4.	(A) Schematic diagram showing the principal loads in peripheral foreland basin systems.....	12
Figure 2.5.	Outcrop distribution of the main lithostratigraphic units of the Karoo Supergroup.....	13
Figure 2.6.	Schematic plan of the main Karoo Basin showing the geographic and stratigraphic relationship of the formations of the Karoo Supergroup.....	14
Figure 3.1.	Diagram of SEM column and specimen chamber.....	22
Figure 3.2.	The diagram shows a common configuration of an X-ray diffractometer.....	23
Figure 3.3.	Diffraction of X-rays by layers of atoms.....	24
Figure 3.4.	Generation of X-rays in a modern X-ray tube.....	25
Figure 3.5.	Response of organic matter to controlled heating during pyrolysis.....	28
Figure 4.1.	Dark grey shale displaying splinter weathering found in the Witteburg area.....	33
Figure 4.2.	Greenish oxidized shale of the Prince Albert Formation in the Floriskraal area.....	33
Figure 4.3.	Elongated concretions in the dark grey to black shale found in the Witteburg area.....	34
Figure 4.4.	Creamish calcite nodules found in the brown weathered shale.....	34
Figure 4.5.	Brown weathered dolomite of the Prince Albert Formation in the Witteburg area.....	37
Figure 4.6.	Brown elephant-skin weathering of dolomite in the Witteburg area.....	37
Figure 4.7.	White weathering carbonaceous shale displaying pencil cleavage of the Whithill Formation.....	38

Figure 4.8.	Brown weathered resistant cherty and/or micaceous shale of the upper Whitehill Formation.....	39
Figure 4.9.	Brown weathered bedding displaying ripple or plumos found in the Geelbek area.....	39
Figure 4.10.	Dark grey to black shale displaying splinter cleavage in the Witteburg area.....	42
Figure 4.11.	Silt laminations on the dark grey sandstone in the Floriskraal area.....	42
Figure 4.12.	Fine to very fine grained tabular sandstone bounded by shale displaying pencil cleavage of the Collingham Formation in the Witteburg area.....	44
Figure 4.13.	Parallel- and cross-lamination on the Maatjiesfontein chert band in the Floriskraal area.....	47
Figure 4.14.	Bitumen staining on the secondary chert band in the Witteburg area.....	48
Figure 4.15.	Bitumen staining and ripple forms on the secondary chert band in the Witteburg area.....	48
Figure 5.1.	XRD plots of the Prince Albert Formation.....	60
Figure 5.2.	XRD plots of the Whitehill Formation.....	61
Figure 5.3.	XRD plots of the Collingham Formation.....	62
Figure 6.1.	Hydrogen index versus oxygen index plot of Rock-Eval pyrolysis data.....	66



UNIVERSITY *of the*
WESTERN CAPE

List of Tables

Table 3.1.	Measured and calculated parameters derived from Rock-Eval pyrolysis.....	28
Table 3.2.	Geochemical parameters describing source rock generation potential.....	29
Table 3.3.	Geochemical parameters describing the type of hydrocarbon generated.....	29
Table 3.4.	Geochemical parameters describing the maturity of organic matter.....	29
Table 6.1.	Total organic carbon (TOC) results for the Prince Albert (PA), Whitehill (WH) and Collingham (CH) Formations.....	64
Table 6.2.	TOC and Rock-Eval results of the Prince Albert (PA), Whitehill (WH) and Collingham (CH) Formations.....	65



UNIVERSITY *of the*
WESTERN CAPE



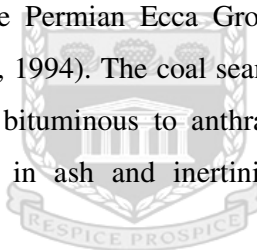
Chapter 1

UNIVERSITY *of the*
WESTERN CAPE

Introduction

1.1 Background

The main Karoo Basin, having a surface area of approximately 700 000 km², is the largest basin in South Africa (Petroleum Agency SA, 2008/9). This basin developed during the Late Palaeozoic and is a product of accretion tectonics along the southern margin of Gondwana (De Wit & Ransome, 1992; Veevers *et al.*, 1994; López-Gamundí & Rossello, 1998; Wild, 2005). Hosting numerous deposits, the Karoo Basin is responsible for approximately 98 percent of all coal production in Africa, with coal resources estimated at 115 billion metric tons (DME, 2008; Methane to Markets, 2008). The bulk of the coal mined in South Africa is consumed internally, while the remainder is exported to the European Union and East Asia (EIA, 2005; Methane to Markets, 2008). Most of the Karoo Basin's coal is contained in Artinskian-Kungurian strata of the Permian Ecca Group, with the exception of the Late Triassic Molteno coalfield (Dreyer, 1994). The coal seams are interbedded in sandstone, and range in rank from high-volatile bituminous to anthracite (Catuneanu *et al.*, 2005). The deposits are also relatively high in ash and inertinite (Falcon, 1986a; Falcon, 1986b; Catuneanu *et al.*, 2005).



UNIVERSITY of the
WESTERN CAPE

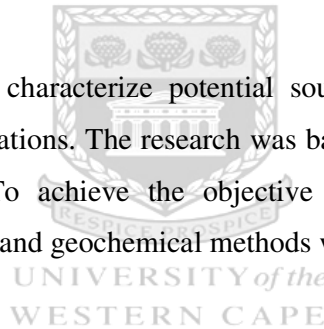
In addition to coal, uranium deposits are also found in the main Karoo Basin. These deposits are limited to fluviially-deposited sandstones (found in the Adelaide Subgroup, the Molteno Formation as well as the Elliot Formation) and to coals within the Springbok Flats Basin (specifically the uppermost part of the Hammanskraal Formation) (Cole, 2009). The absence of uranium from lithologies of similar deposition is believed to be due to the lack of a suitable uranium source during metallogenesis (Cole, 2009). Despite the fact that the main Karoo Basin is known to contain uranium, the sandstone- and coal hosted deposits are yet to be mined (Cole, 2009). However, the noteworthy increase in the price of uranium over the past few years could in future, make these deposits become economically-viable (Cole, 2009).

Furthermore, the increase in demand for hydrocarbon is motivating a new period in exploration for hydrocarbon resources in previously overlooked areas. This is supported by renewed exploration, including feasibility studies, which are currently being conducted

within the Karoo Basins of South Africa (Petroleum Agency SA, 2008/9). During previous exploration of the basin undertaken by Soekor (spanning the period of 1965 to 1975), gas was discovered within the shales of the Ecca Group (Vermeulen, 2012). The deposit was originally estimated to be as large as 485Tcf, making it the fifth largest in the world (Kuuskraa *et al.*, 2011; Vermeulen, 2012). That estimate was recently reduced to a more conservative value of 40Tcf (Business Day live, 2014). Although there was a substantial drop in the estimated recoverable reserves of shale gas, the reserve is still considered to be feasible, especially when taking into account that the Moss gas project (which is currently the only gas exploration project in South Africa) was planned on a reserve of merely 3Tcf (Vermeulen, 2012). The key focus of the present research is the characterization of potential source rocks of the Lower Ecca Group in the Laingsburg sub-basin, in terms of sedimentology, mineralogy and organic geochemistry.

1.2 Project Scope

The aim of the study was to characterize potential source rocks of the Prince Albert, Whitehill and Collingham Formations. The research was based on outcrop samples collected within the Laingsburg area. To achieve the objective of the study a combination of sedimentological, mineralogical and geochemical methods were utilized.



Objectives of study included:

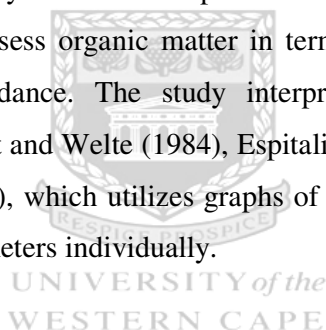
1. Interpreting lithological variations in the Prince Albert, Whitehill and Collingham Formations in Laingsburg
2. Determine the depositional environment(s) of the Prince Albert, Whitehill and Collingham Formations
3. Determine the mineralogical composition of the Prince Albert, Whitehill and Collingham Formations shale
4. Assessing the type, abundance and thermal maturity of organic matter of the Prince Albert, Whitehill and Collingham Formations shale

A field study was conducted in order to characterize the sedimentology of the formations in question. Field work included the construction and interpretation of sedimentary logs within

the study area. Interpretation included the identification of the following: lithology; sedimentary features; and bedding thickness.

In addition, shale samples were collected for geochemical and mineralogical analyses. A qualitative XRD analysis was performed on samples to determine which clay minerals were present. Clay mineral identification was then confirmed by way of SEM micrographs, through comparison of the mineral morphology with that of micrographs and data from Keller (1970), Bohor and Hughes (1971), Engelhardt (1977), Guven *et al.* (1980), Keller *et al.* (1986), Ehrenberg *et al.* (1993) and Hong and Mi (2006).

The total organic carbon content was determined using the Walkley-Black method and results were used to select samples for further analysis. Rock-Eval pyrolysis was undertaken on a total of 28 outcrop samples to ascertain the source rock potential. The total organic carbon content and Rock-Eval analyses yielded several parameters (i.e. T_{max} , S_3 , S_2 , S_1 , HI, OI, PI, and TOC) that were used to assess organic matter in terms of its geochemical properties; thermal maturation; and abundance. The study interpreted Rock-Eval data based on guidelines documented by Tissot and Welte (1984), Espitalie *et al.* (1985), Peters (1986), and Nuñez-Betelu and Baceta (1994), which utilizes graphs of various parameters in addition to evaluating the appropriate parameters individually.



1.3 Study Area

The main Karoo Basin is bordered to the south and west by the Cape Fold Belt mountain range (Bouma and Wickens, 2002). The south-western Karoo Basin is subdivided into the Tanqua, Laingsburg and southern sub-basins (Catuneanu *et al.*, 2002). The Tanqua and Laingsburg sub-basins (Figure 1.1) are separated by the Baviaanshoek and Hex River-Bontberg anticlines (Wickens, 1994; Cole *et al.*, 1998; Scott and Bouma, 1998; Catuneanu *et al.*, 2002). The Laingsburg and southern sub-basins are separated by a structural high postulated to be along the meridian 24°E (Rubidge, 1995; Catuneanu *et al.*, 2002).

The Karoo Supergroup ranges in age from Late Carboniferous to Early Jurassic (Hegenberger *et al.*, 1996). The strata that make up the Supergroup were deposited in a wide range of environments, which include glacial, deep marine, shallow marine, deltaic, fluvial, lacustrine and aeolian environments (Hegenberger *et al.*, 1996). Most of the Permian time slot for the

Karoo Supergroup is occupied by the Ecca Group which occurs between the Dwyka Group (Late Carboniferous) and the Beaufort Group (Late Permian-Middle Triassic) (Catuneanu *et al.*, 2005).

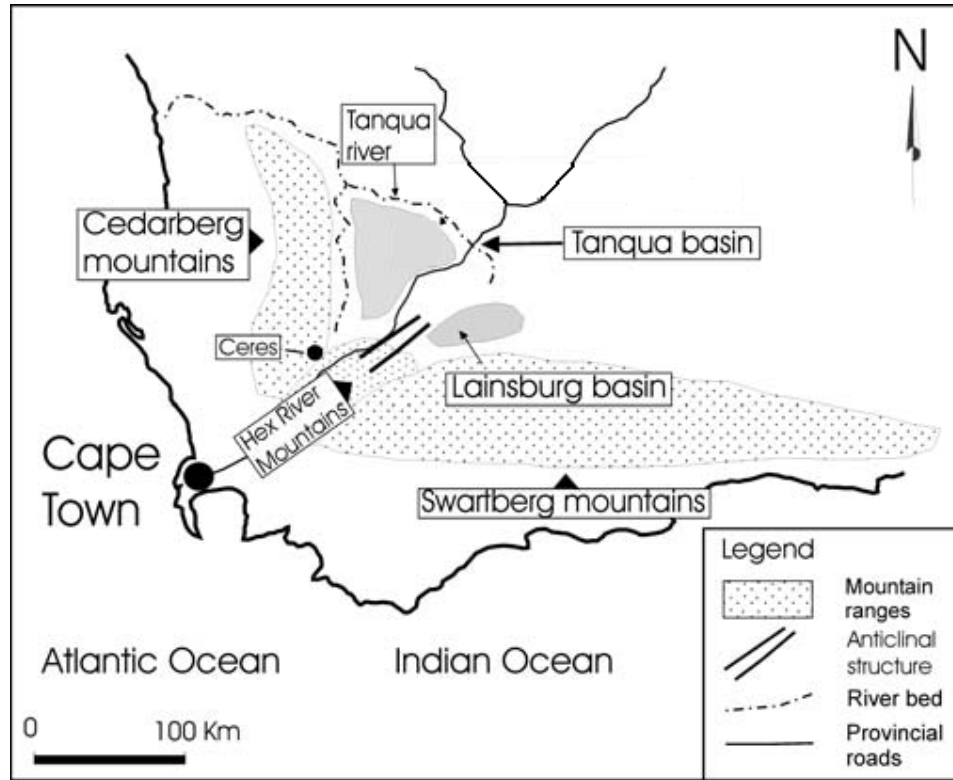
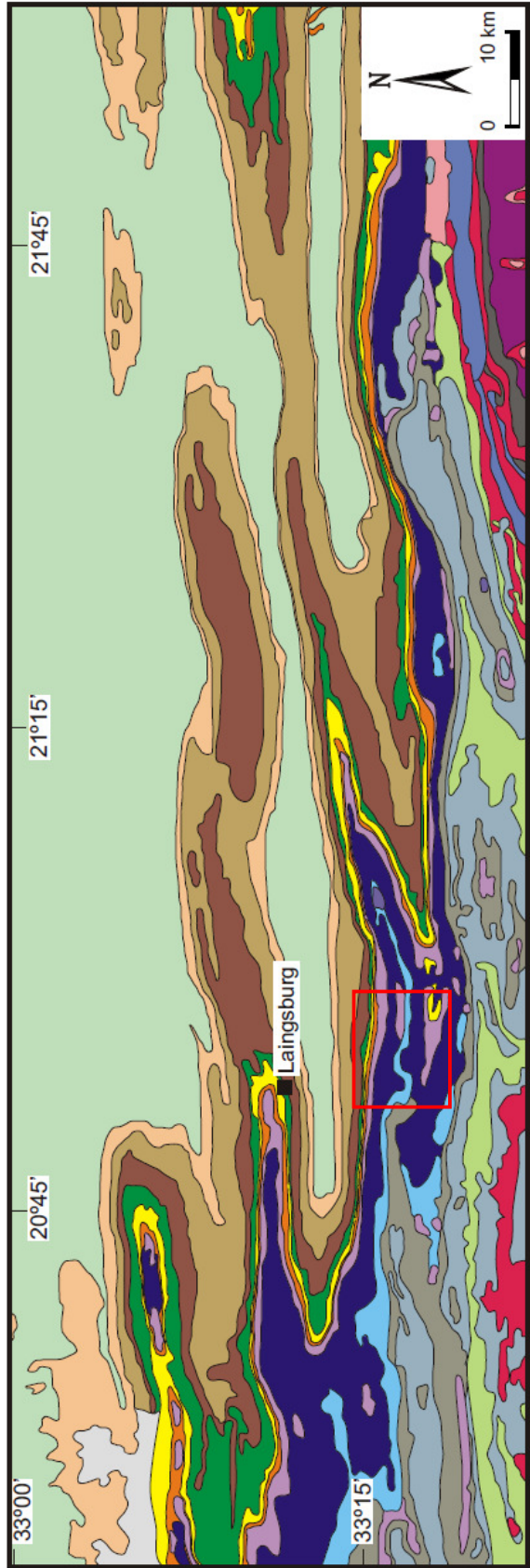


Figure 1.1. Location map showing the location of the Tanqua and Laingsburg sub-basins. The Cape Fold Belt comprises the N–S trending Cedarberg Mountains and the E–W trending Witteberg-Swartberg Mountains (van der Werff and Johnson, 2003).

The study area is located in the Laingsburg sub-basin (Figure 1.2), west of the Floriskraal dam. The entire Ecca Group is present in the study area, with the Prince Albert, Whitehill and Collingham Formations representing the sequences under study. The lowermost formation of the Ecca Group is the Prince Albert Formation, which is overlain by the Whitehill Formation followed by the Collingham Formation.

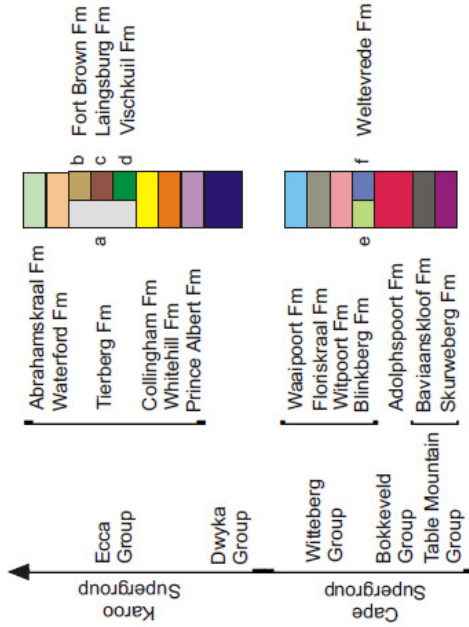
Coordinates of Study Area: 33° 13' 46.79" S; 20° 50' 36.38" E
 33° 13' 46.79" S; 20° 58' 33.87" E
 33° 17' 28.07" S; 20° 50' 36.38" E
 33° 17' 28.07" S; 20° 58' 33.87" E



Geological legend

Palaeozoic	
Permian	
Carboniferous	
Devonian	
Silurian	

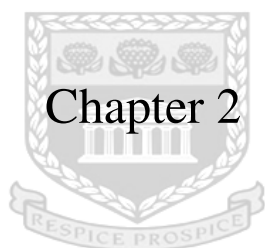
Lithostratigraphy



Lithology

- Mudstone, siltstone, sandstone, thin cherty beds
- a - Shale
- b - Shale with thin siltstone and sandstone beds
- c - Sandstone, greywacke and siltstone
- d - Arenaceous shale, siltstone and thin sandstone beds
- Siltstone, chert and sandstone with thin interbedded shale and yellow-weathering mudstone/tuff
- Dark grey shale, light grey weathering with cherty siltstone beds in upper part
- Dark grey shale with reddish brown weathering siltstone
- Tillite, diamictite, subsidiary shale
- Shale, siltstone and thin sandstone, micaceous, weathering reddish brown
- Sandstone, micaceous, light brown; alternating with shale and siltstone; subordinate grit beds with pebbles
- Quartzitic sandstone, weathering prominently white at the top, reddish brown lower down; thin siltstone beds
- e - Sandstone, quartzitic, micaceous, weathering white, subordinate shale and siltstone in places
- f - Siltstone and mudstone, micaceous impure sandstone; subordinate shale
- Siltstone, shale and argillaceous sandstone
- Brown weathering micaceous impure sandstone; subordinate shale
- Light grey, massively bedded, quartzitic sandstone, thin lenticular conglomerate and grit beds

Figure 1.2. Geological map of the Laingsburg sub-basin, Karoo Basin, South Africa (after van Lente, 2004). Study area marked in red.



Chapter 2

UNIVERSITY *of the*
WESTERN CAPE

Geological Background

The tectonostratigraphic development (from the Palaeozoic to Early Mesozoic) of southern Africa can be related to the evolution of western Gondwana, though the record for southern Africa is not as complete as for South America and Antarctica (Flint *et al.*, 2010). This is due to the removal of a great deal of the late Palaeozoic record by the major Mesozoic regional strike-slip and extensional tectonics. In southern Africa, two sedimentary mega-successions were deposited in two laterally offset major sedimentary basins (from the Early Ordovician to Early Jurassic) (Visser, 1997; Tankard *et al.*, 2009; Flint *et al.*, 2010).

The Karoo Supergroup (Figure 2.1) consists of approximately 5500 m of deep marine to fluvial deposits (Flint *et al.*, 2010). Large scale subsidence produced a series of interconnected marine basins (during the Late Carboniferous to Early Permian period). All the Karoo Basins across southern Africa were extensional intracratonic rifts, related to the N-S trending basement shear zones (Stollhofen *et al.*, 2000; Flint *et al.*, 2010). The Karoo Basin forms one of the most complete stratigraphic successions in the world, spanning from the Late Carboniferous to Middle Jurassic (Veevers *et al.*, 1994; Catuneanu *et al.*, 2002).

The Karoo sedimentary fill displays a wedge-shaped geometry with a maximum preserved thickness of 6 km adjacent to the Cape Fold Belt (Rubidge, 1995; Catuneanu *et al.*, 2002). The stratigraphy of the Karoo Supergroup is noticeably different between the proximal (southern) and distal (northern) regions of the basin (Catuneanu *et al.*, 2002). These differences between the southern and northern regions of the basin reflect contrasting tectonic histories across the flexural hinge line of the foreland system (Catuneanu *et al.*, 1998; Catuneanu *et al.*, 2002). A deep marine environment controlled the sedimentation processes in the southern region of the Karoo Basin (Catuneanu *et al.*, 2002). Simultaneous with the deposition in the south, sediment aggradation took place in non-marine to shallow marine environments in the northern region (Catuneanu *et al.*, 2002). During the underfilled phase of the foreland system (Figure 2.2), the deeper marine facies of the Dwyka and Early Ecca Groups accumulated (Catuneanu and Bowker, 2001). During the filled phase of the foreland system, the shallow marine facies of the Late Ecca Group accumulated (Catuneanu and Bowker, 2001). This was followed by the overfilled phase that was dominated by fluvial sedimentation which started with the Beaufort Group (Catuneanu and Bowker, 2001).

Time-scale	Age	Key	Formations	Key	Group	Supergroup	
~135 Ma ~225 Ma	Cretaceous - Recent			PS	Post-Stromberg		
	Trias-Jurassic			S	Stromberg		
~280 Ma	Permian	Pte	Teekloof	B	Beaufort	Karoo	
		Pa	Abrahamskraal				
		Pwa	Waterford	E	Ecca		
		Pk	Kookfontein				Fortbrown
		Pf	Skoorsteenberg				Laingsburg
		Ps	Tierberg				Vischkuil
		Pt	Collingham				
		Pv	Whitehill				
		Pw	Prince Albert				
		Pp					
C-Pd		Dwyka					
~345 Ma	Carboniferous	Cw	Waaipoort	W	Witteberg	Cape	
		Cf	Floriskraal				
~395 Ma	Devonian	Ck	Kweekvlei	B	Bokkeveld		
		Dwi	Witpoort				
		Ds	Swartruggens				
		Dbl	Blinkberg				
		Dwa	Wagen Drift				
		Dka	Karopoort				
		Do	Osberg				
		Dkl	Klipbökkop				
		Dwu	Wuppertal				
		Dw	Waboomberg				
		Db	Boplaas				
		Dt	Tra-Tra				
		Dh	Hexriver				
		Dv	Voorstehoek				
		Dga	Gamka				
Dg	Gydo						
~435 Ma	Silurian	Dr	Reitvlei	TM	Table Mountain		
		Ss	Skurweberg				
~500 Ma ~600 Ma	Cambrian Namibian	Sg	Goudini	PT	Pre-Table Mountain		
		O-Sc	Cederberge				
		Opa	Pakhuis				
		Ope	Peninsula				
		Og	Graafwater				
		Op	Piekenierskloof				

Unconformity

Unconformity

Figure 2.1. Lithostratigraphic column for the Cape Fold Belt and SW Karoo Basin (Besaans, 1973; Dingle & Siesser, 1977; Steyn, 1983; Theron, 1986; Cole, 1992; Wickens, 1994; Thomas, 1997; De Beer, 1999; Flint et al., 2004; King, 2005).

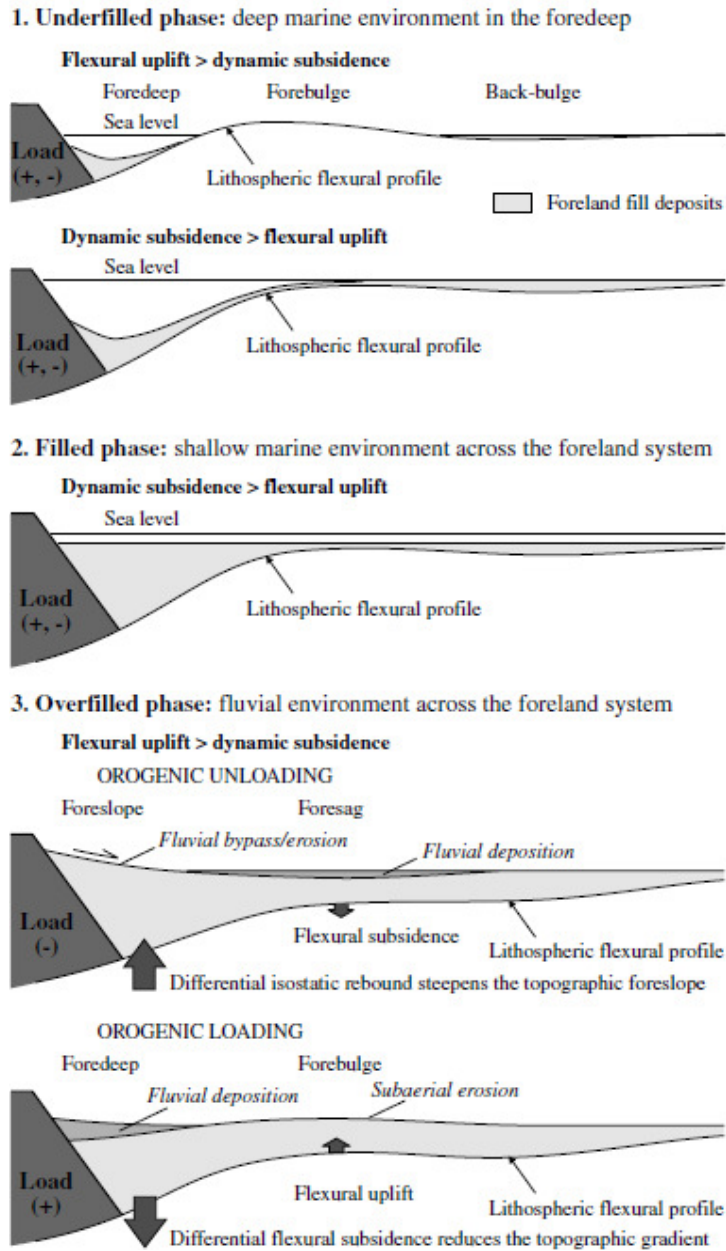


Figure 2.2. Stages of foreland system evolution. Note the difference between bathymetric/topographic profiles and the lithospheric flexural profile. (+, -) refer to increases and decreases in orogenic load, respectively (Catuneanu, 2004).

2.1 Tectonic Setting

The Karoo Basin is classified as a retroarc foreland system (Figures 2.3 and 2.4) (de Wit *et al.*, 1988; Johnson, 1991; Catuneanu *et al.*, 1998; Catuneanu *et al.*, 2002). Basin development was linked to the orogenesis of the Cape Fold Belt which was described as a single-phase, multiple event orogen (Hälbich, 1983; Catuneanu and Elango, 2001). The basin formed in front of the Cape Fold Belt in response to crustal shortening brought about by the subduction of the paleo-Pacific plate beneath the Gondwana plate (Lock, 1978, 1980; Pysklywec and Mitrovica, 1989; de Wit and Ransome, 1992; Catuneanu *et al.*, 2002). The Cape Fold Belt was part of the extensive Pan Gondwanian Belt generated through collision and terrain accretion along the southern margin of Gondwana (Catuneanu and Bowker, 2001). The associated foreland basin (Figure 2.5) is preserved today in the Karoo Basin (southern Africa), the Parana Basin (South America), the Beacon Basin (Antarctica) and the Bowen Basin (Australia) (Catuneanu and Bowker, 2001).

The Karoo foreland system is separated into three flexural provinces, which include the foredeep, the forebulge, and the back-bulge (Catuneanu *et al.*, 1998, 1999; Catuneanu and Bowker, 2001). This foreland system extended approximately 6000 km along strike, and over 1000 km along dip, prior to the break-up of Gondwana (Catuneanu and Bowker, 2001). Sedimentation was controlled by episodic supra-lithospheric loading in the Cape Fold Belt and was coupled with renewed subsidence of the foredeep, which resulted in pulsatory deposition of the sedimentary pile (Hälbich, 1983, 1992; Cole, 1992; Catuneanu *et al.*, 1998). During crustal unloading the depocentre of the foreland system migrated towards the distal part of the system. This resulted in contrasting stratigraphies between the proximal and distal regions of the basin. Eight tectonic paroxysms were recognized and dated in the Cape Fold Belt by means of K-Ar and Ar-Ar techniques (Hälbich, 1983; 1992; Catuneanu *et al.*, 1998).

Recent studies indicate that the Cape Fold Belt is Triassic in age (Flint *et al.*, 2010). It is proposed that only strata from the upper Beaufort Group and younger correspond with the Cape Fold Belt as a sedimentary source (van Lente, 2004; Flint *et al.*, 2010). Thus, the foreland basin is younger in age than the Dwyka, Ecca and lower Beaufort Groups (Flint *et al.*, 2010). There is also no evidence of extensional faults of Ecca age or later contractional reactivation of these extensional faults, though there is a lack of seismic reflection data.

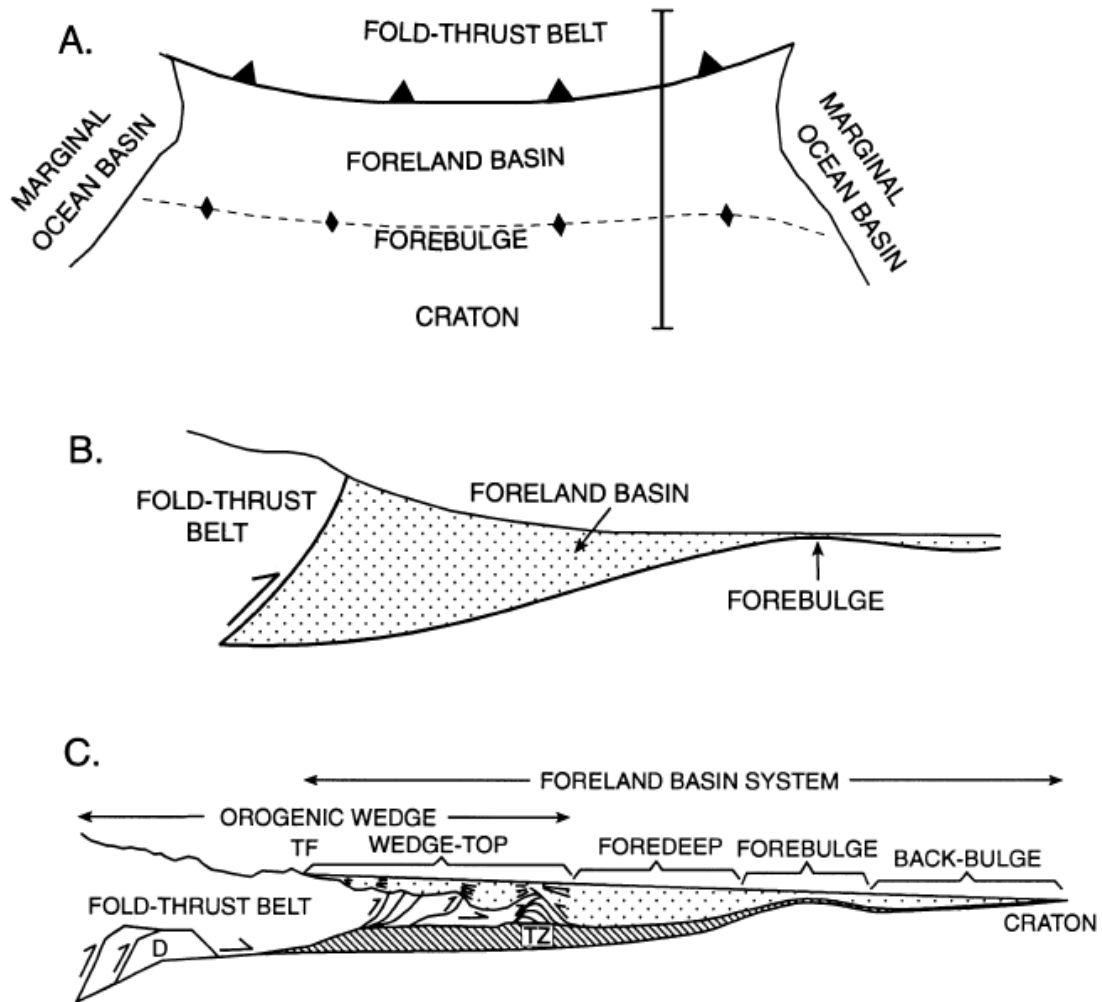


Figure 2.3. (A) Schematic map view of a ‘typical’ foreland basin, bounded longitudinally by a pair of marginal ocean basins. The scale is not specified, but would be of the order of 102–103 km. Vertical line at right indicates the orientation of a cross-section that would resemble what is shown in part B. (B) The generally accepted notion of foreland-basin geometry in transverse cross-sections. Note the unrealistic geometry of the boundary between the basin and the thrust belt. Vertical exaggeration is of the order of 10 times. (C) Schematic cross-section depicting a revised concept of a foreland basin system, with the wedge-top, foredeep, forebulge and back-bulge depozones shown at approximately true scale. Topographic front of the thrust belt is labelled TF. The foreland basin system is shown in coarse stipple; the diagonally ruled area indicates pre-existing miogeoclinal strata, which are incorporated into (but not shown within) the fold-thrust belt toward the left of diagram. A schematic duplex (D) is depicted in the interland part of the orogenic wedge, and a frontal triangle zone (TZ) and progressive deformation (short fanning lines associated with thrust tips) in the wedge-top depozone also are shown. Note the substantial overlap between the front of the orogenic wedge and the foreland basin system (DeCelles and Giles, 1996).

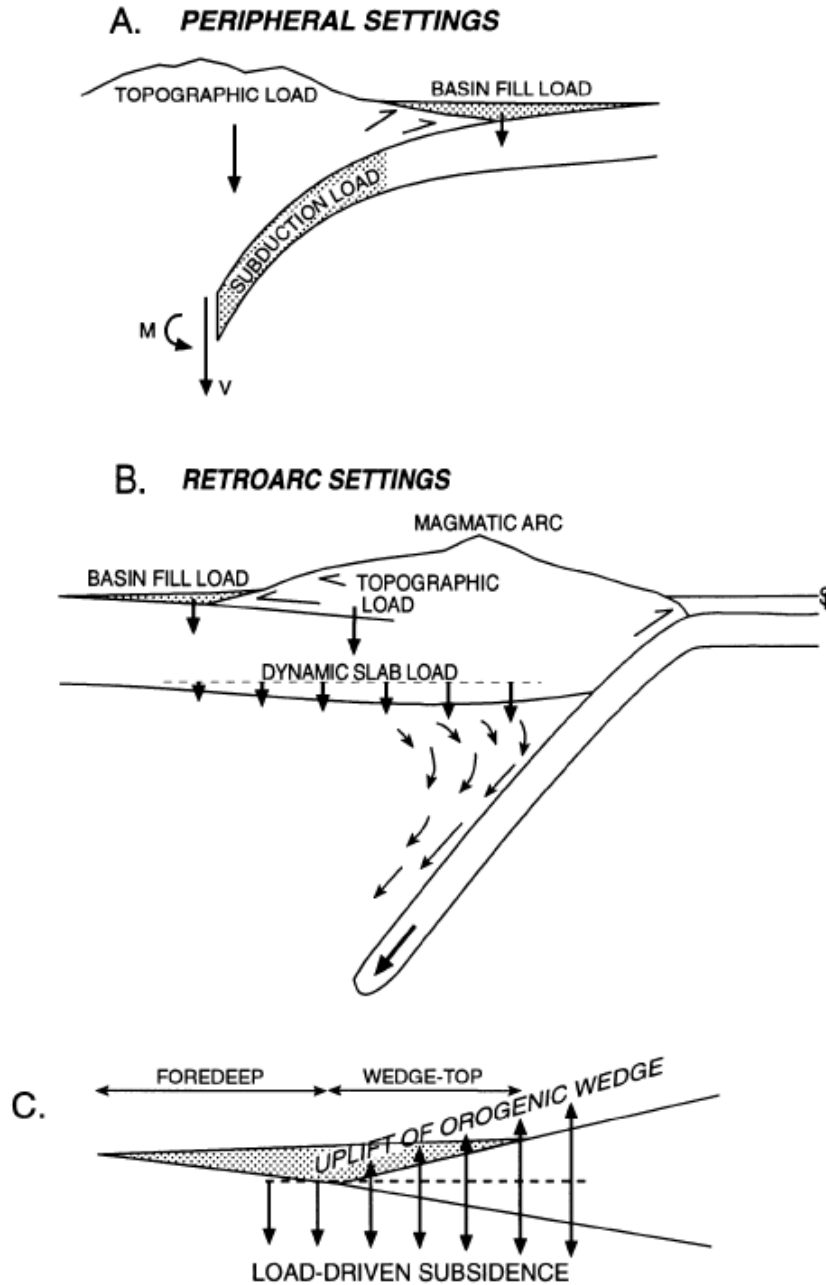


Figure 2.4. (A) Schematic diagram showing the principal loads in peripheral foreland basin systems. In addition to the topographic and sediment loads, a subduction load, due to a vertical shear force (V) and bending moment (M) on the end of the subducted slab, may exist at depths of 50–200 km (Royden, 1993). (B) Retroarc foreland basin systems involve topographic and sediment loads as well as a dynamic slab load caused by viscous coupling between the subducting slab, overlying mantle-wedge material and the base of the overriding continental plate (Mitrovica et al., 1989; Gurnis, 1992). (C) Accumulation in the wedge-top depozone takes place under competing influences of regional, load-driven subsidence (downward pointing arrows), and local uplift of the orogenic wedge in response to shortening and thickening (upward pointing arrows) (DeCelles and Giles, 1996).

It has been suggested that subsidence was partially controlled by dynamic topography (mantle flow) associated with the subducting slab (Pysklywec and Mitrovica, 1999; Flint *et al.*, 2010). This process of mantle flow was complicated by inconsistent degrees of foundering of basement blocks (Tankard *et al.*, 2009; Flint *et al.*, 2010). The basement blocks are concurrent with the Hex River area oroclinal bend (of the Cape Fold Belt) and might have acted as a buried basin boundary (at Eccca Group time) and possibly influenced the location of the shelf edge (similar to that of a passive margin) (Tankard *et al.*, 2009; Flint *et al.*, 2010). Furthermore, there was no source area in close proximity at Eccca Group time, meaning that subsidence was not a result of asymmetric crustal loading (Flint *et al.*, 2010). An approximate water depth of 1800 m for the turbidite succession was estimated by the uncompacted thickness of the succession from basin floor fans to first deltaic deposits, since there are no direct microfaunal indicators for palaeobathymetry (Flint *et al.*, 2010).

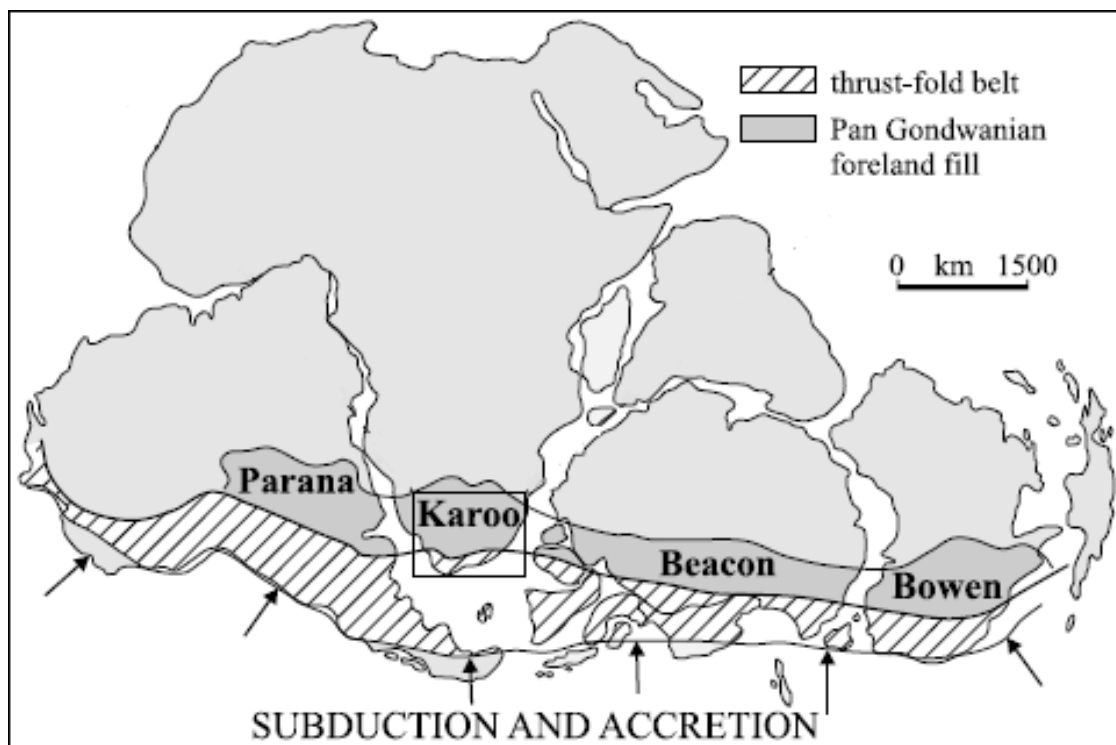


Figure 2.5. Outcrop distribution of the main lithostratigraphic units of the Karoo Supergroup. The Karoo Basin is shown in the context of the Pan Gondwanian foreland system that developed in relation to the Cape Orogeny along the southern margin of Gondwana. The Adelaide and Tarkastad subgroups together form the Beaufort Group. The stratigraphic hinge line separates the foredeep (to the south) from the forebulge (to the north) flexural provinces of the Karoo foreland system (Catuneanu and Bowker, 2001).

2.2 Stratigraphy

The Karoo Supergroup (Figure 2.6.) is subdivided into the Dwyka Group (glacial), the Ecca Group (marine), and the Beaufort and Stormberg Groups (nonmarine), which are capped by the volcanic Drakensberg Group (Smith *et al.*, 1998; Catuneanu *et al.*, 2002). Most of the Permian time slot for the Karoo Supergroup lithologies is occupied by the Ecca Group which occurs between the Dwyka Group (Late Carboniferous) and the Beaufort Group (Late Permian-Middle Triassic) (Catuneanu *et al.*, 2005).

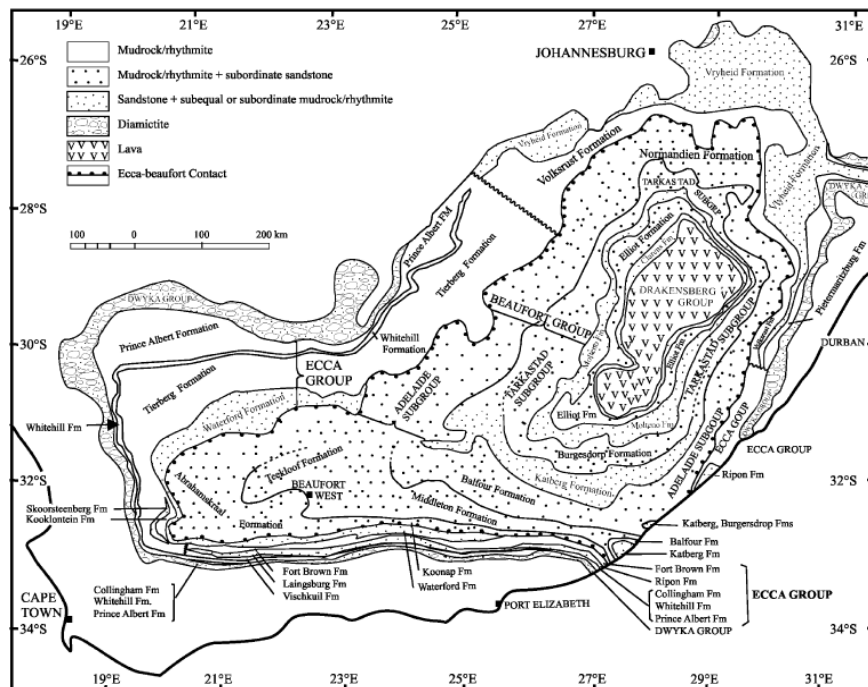


Figure 2.6. Schematic plan of the main Karoo Basin showing the geographic and stratigraphic relationship of the formations of the Karoo Supergroup (Catuneanu *et al.*, 2005).

2.2.1 Dwyka Group

The Late Carboniferous Dwyka Group time of deposition corresponds to the migration of Gondwana over the South Pole, which marked the start of Karoo sedimentation at approximately 300-310 Ma (Flint, 2010). The Dwyka Group is made up of the oldest rocks of the Karoo Supergroup (Herbert and Compton, 2007) and ranges from 600 to 750m in thickness (SACS, 1980; Visser, 1989; Johnson, 1991). Glacial sedimentation of the Dwyka Group took place from the Late Carboniferous to Early Permian (Bangert *et al.*, 1999;

Veevers and Powell, 1987; Visser, 1989, 1990, 1993; Herbert and Compton, 2007). It is believed that these sediments were deposited as a result of advancing and retreating ice sheets which bordered the basin (Crowell and Frakes, 1972; 1975; Cadle *et al.*, 1993). During the Late Carboniferous the lithosphere underlying the present day Karoo Supergroup migrated over the South Polar Region, which resulted in the southern Gondwana basins and highlands being covered by a major ice sheet (SACS, 1980; Visser, 1989; Johnson, 1991). The Dwyka Group consists of a widespread fill of subglacial till, glaciolacustrine shale, terrestrial moraine and fluvioglacial outwash (Van Brunn, 1977; Visser, 1986; Visser and Lock, 1987; Cadle *et al.*, 1993).

Four deglaciation sequences have been identified (DS1–DS4) in the southern Karoo Basin (Theron and Blignault, 1975; Herbert and Compton, 2007). Each of these consists of a basal zone of massive diamictite that is capped by a stratified terminal zone (Theron and Blignault, 1975; Herbert and Compton, 2007). The youngest units consist of clast-poor diamictite with subordinate mudstone (Visser and Loock, 1987; Visser, 1989, 1994a; Herbert and Compton, 2007). They are interpreted to be dense proximal rain-out deposits formed from melting icebergs that have been locally modified by sediment gravity flows (Visser and Loock, 1987; Visser, 1989, 1994a; Herbert and Compton, 2007). These diamictites also show higher carbonate contents than the older Dwyka diamictites, and contain numerous carbonate concretions (Herbert and Compton, 2007). The Dwyka Group progressively thins and pinches out northward (Cadle *et al.*, 1993).

2.2.2 Ecca Group

While southern Gondwana drifted towards lower latitudes, an extensive shallow sea developed (Viljoen, 1994). The Prince Albert and Whitehill Formations were deposited in this marine environment (Viljoen, 1994), which accumulated on the submerged glaciated platform (Smith, 1990; King, 2005).

With the continuous sediment infilling and the compressive regime (caused by thrusting in the Cape Fold Belt), the Karoo Basin gradually closed and became brackish and lacustrine (ceasing to be marine) (Viljoen, 1994). During this time, deposition of the sub-aqueous Collingham, Tierberg, Vischkuil, Laingsburg, Ripon, Fort Brown, Skoorsteenbergh,

Kookfontein and Waterford Formations on submarine fans, shelf and deltas took place. In the north thick accumulations of peat formed on the fluvial and delta plains, which matured into coal beds (Cadle *et al.*, 1993).

Overlying the Whitehill Formation is the Collingham Formation that consists of fine-grained silt-prone turbidites and intercalated ashes (Flint, 2010) dated as Early Permian (approximately 270 Ma; Turner, 1999; King, 2005).

In the Laingsburg depocentre the upper Ecca Group include the Vischkuil, Laingsburg, Fort Brown and Water Ford Formations (Flint, 2010). The main deepwater depositional system comprises approximately 1200 m thick Vischkuil-Laingsburg-Fort Brown Formation package (Flint, 2010). The stratigraphy displays an upward progression from distal basin floor fan through slope to mixed wave/tide-influenced and finally river-dominated shelf edge deltas (Flint, 2010). The Vischkuil Formation was interpreted to signify the initiation of turbidite deposition of the Laingsburg Formation, and consists of a series of mass transport complexes (Flint *et al.*, 2004; King, 2005). The lower Vischkuil Formation comprises of undeformed graded siltstone beds and mudstone lithofacies, while the upper Vischkuil Formation is dominated by similar facies but include three widespread 10–85 m thick syn-sedimentary deformation units (Van Der Merwe *et al.*, 2009; Flint, 2010). The overlying Laingsburg Formation is a shallowing-upward succession from basin floor fan and lower slope systems through mid-slope channel-levee systems to heterolithic upper slope channel-levee systems (Grecula *et al.*, 2003a,b; Sixsmith *et al.*, 2004; Flint *et al.*, 2007; Figueiredo *et al.*, (*in press*); Flint, 2010). The Laingsburg Formation is a sequence of five turbidite deposits intercalated with mudstones (King, 2005). Overlying the Laingsburg Formation is the shelf-edge delta deposit (Ford Brown Formation), which is interpreted to be a low order highstand systems tract (Flint, 2010). The Fort Brown Formation represents slope deposits, and consists of fine grained sandstone and mudstone (Smith, 1990; King, 2005).

In the Tanqua depocentre the Tierberg Formation (up to 1000 m thick) represents a period of regional sediment starvation, and is a thick black shale unit (King, 2005). The basin-floor to shelf-edge succession of the Tanqua depocentre is represented by the Skoorsteenberg and Kookfontein Formations. The Skoorsteenberg Formation consists of five basin floor fans intercalated with shale and mudstone (Wild, 2005; Hodgson *et al.*, (*in press*); King, 2005).

The Kookfontein Formation represents the slope succession, and is a sequence of fine sandstone interbedded with mudstone (King, 2005).

The Ripon and Fort Brown Formations represent a turbidite fan complex with a southeastern transportation direction, deposited in a deep to medium aqueous environment (Johnson, 1976). The Ripon Formation consists of dark grey, fine to very fine-grained feldspathic sandstones, interbedded with rhythmites along with mudrocks (Johnson, 1976). The Ripon Formation is overlain by the Waterford Formation which consists of upward coarsening cycles, distal sandbar, distributary mouth bar deposits, crevasse splay and interdistributary bay deposits (Johnson, 1976). The Waterford Formation represents deltaic deposits and overlies the Fortbrown, Kookfontein and Ripon Formations in the Laingsburg, Tanqua and southern depocentres, respectively.

2.2.3 Beaufort Group

During the deposition of the Beaufort Group, the environment became transitional brackish lacustrine to fluvial. The greenish-grey sandstones of the Waterford Formation graded upwards into fine-grained siltstones and mudstones of the Koonap Formation (Johnson, 1976). The Koonap Formation is overlain by the Middleton Formation which consists of cyclic deposits of lenticular sandstone bodies that grade into greenish-grey mudstone. The Middleton Formation constitutes 37% of the Beaufort Group, and 47% of the Adelaide Subgroup (Johnson, 1976). Lenses of red mudstone have been found in the formation, and were interpreted to have been deposited in a sub-aerial fluvial environment. The upper part of the Adelaide Subgroup is occupied by the Balfour Formation, and it is part of what was called the lower to middle Beaufort (Smith *et al.*, 1993). The Beaufort Group is capped by the Tarkastad Subgroup (which is made up of the Katberg and Burgersdorp Formations) (Neveling, 2003). The arenaceous Katberg Formation is believed to have been deposited in a braided fluvial system (with various amounts of red and olive-yellow mudstones) and the overlying Burgersdorp Formation was interpreted to have been deposited in a low-sinuosity fluvial system (Neveling, 2003).

The Beaufort Group contains a wealth of fossil tetrapods, which allowed biostratigraphic subdivision of the group since the age is not perfectly constrained (Keyser and Smith, 1978; Kitching, 1977; Rubidge *et al.*, 1995; Catuneanu *et al.*, 2005). The Beaufort Group is

subdivided into eight biozones which are listed in stratigraphic order: Eodicynodon, Tapinocephalus, Pristerognathus, Tropidostoma, Cistecephalus, Dicynodon, Lystrosaurus, and Cynognathus Assemblage Zones (Catuneanu *et al.*, 2005). An overlap in the ranges of Dicynodon and Lystrosaurus was first proposed by Hotton (1967); with recent works on the Permo-Triassic boundary in the south of the basin (Smith, 1995; MacLeod *et al.*, 2000) confirming the overlap (Catuneanu *et al.*, 2005). The Lystrosaurus Assemblage Zone is now considered to be in the Permian, and the Permo-Triassic boundary is within a non-fossiliferous “event bed” (Smith and Ward, 2001; Catuneanu *et al.*, 2005). This non-fossiliferous “event bed” is located above the last appearance datum of Dicynodon (Smith and Ward, 2001; Catuneanu *et al.*, 2005). Derived from the stratigraphic distribution of the Capitosaurids (Mastodontosaurids) Kestrosaurus Dreyeri, Xenotosuchus (Parotosuchus) Africanus and Paracyclotosaurus Morganorum, the Cynognathus Assemblage Zone is considered to contain three subzones (known as subzones A, B, and C) (Hancox *et al.*, 1995; Shishkin *et al.*, 1995; Hancox, 2000; Catuneanu *et al.*, 2005).

2.2.4 Stormberg and Drakensberg Groups

The Stormberg Group is made up of the Molteno, Elliot and Clarens Formations. The uppermost volcanic rocks are grouped into the succeeding Drakensberg Group (Catuneanu *et al.*, 2005). The greatest thicknesses of these units are contained in the main Karoo Basin, the Mid-Zambezi Basin, and the Cabora Bassa Basin, reaching thicknesses of 1200 m, 3000 m and 8000 m respectively (Johnson *et al.*, 1996; Catuneanu *et al.*, 2005).

The Molteno Formation consists of two major sequences (Catuneanu *et al.*, 1998). The basal sequence comprises of the Bamboesberg and Indwe Sandstones. The upper sequence consists of the Transitional Member (Catuneanu *et al.*, 1998). Tabular sheets of horizontally and cross-stratified medium to coarse grained sandstone dominate the formation, and are believed to have been deposited by braided streams on a vast braidplain (Catuneanu *et al.*, 1998).

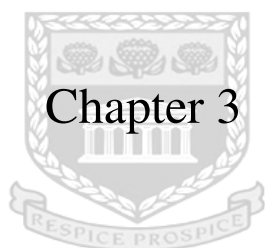
The Elliot Formation comprises of red floodplain mudstones with subordinate channel and crevasse splay deposits. The deposits were interpreted as a mixed load dominated meandering system in an increasingly arid setting (Visser and Botha, 1980, Bordy *et al.*, 2004). Furthermore, in the fluvial deposits of the Elliot Formation, aeolian sediments occur as meter-scale intercalations.

The Clarens Formation consists of yellow fine-grained sandstones, sandy siltstones and mudstones, showing a strong aridification of the climate (Beukes, 1970). The deposits are interpreted to have been deposited in a desert environment, with shallow playa lake and river deposits in the wetter parts of the basin (Smith *et al.*, 1993; Catuneanu *et al.*, 1998).

The Drakensberg Group consists of a thick succession of basalts that caps the Karoo succession. The extrusion of these basalts, and the subsequent intrusion of their associated dolerite dykes and sills, have been linked to the breakup of Gondwana. The 1370 m thick succession is mainly made up of tholeiitic andesites (Smith *et al.*, 1993; Duncan *et al.*, 1997).



UNIVERSITY *of the*
WESTERN CAPE



Chapter 3

UNIVERSITY *of the*
WESTERN CAPE

Methods of Investigation

3.1 Field study

The field investigation was carried out in the area during August, 2010. During the field investigation geological maps and toposheets on 1:50 000 and 1:250 000 scales were used. The study area is illustrated in figure 1.2.

The outcrops were examined on a meter scale by constructing several stratigraphic logs, recording grain size, bed thicknesses, type of contacts and sedimentary structures. Measurements were taken using a 5 meter measuring tape. Digital photographs were also taken of the measured outcrops. GPS readings (latitude, longitude and altitude) were collected to mark top locations of each log.

Several stratigraphic logs were measured at suitable locations. The locations of the logs were selected primarily based on outcrop quality. Good quality outcrops were generally found at the back of gullies and rock exposures on river incisions.

The resulting outcrop data (stratigraphic logs and photographs) were used for facies analysis and to establish depositional models for the Lower Ecca. Additionally, a total of 28 shale samples were collected at suitable locations for laboratory studies. The samples were properly documented and numbered.

3.2 Mineralogical analysis

3.2.1 Scanning Electron Microscopy (SEM)

Scanning Electron Microscopy (SEM) for selected shale samples of the Lower Ecca was performed in order to gain knowledge of the structures of the clays in the samples. The SEM analysis was carried out using a Scanning Electron Microscope Type X-650 HITACHI equipped with an energy dispersive spectrometer (EDS) system for determination of chemical composition of small particles. Samples were prepared from broken shale fragments which were fixed to aluminum studs using silver paint, and carbon coated prior to analysis.

In principle, SEM consists of an electron optical column (Figure 3.1), containing electromagnetic lenses, which demagnifies an electron source that focuses a small beam of electrons onto the surface of a specimen that is scanned in a rectangular raster. The resulting signal, caused by the interaction of the beam with the specimen, is collected by an electron detector and used to adjust the brightness of the cathode ray tube (CRT). A picture of the specimen on the CRT screen is thus formed by the low-energy secondary electrons (Advanced Metals Research Corporation, 1969; Bohor and Hughes, 1971).

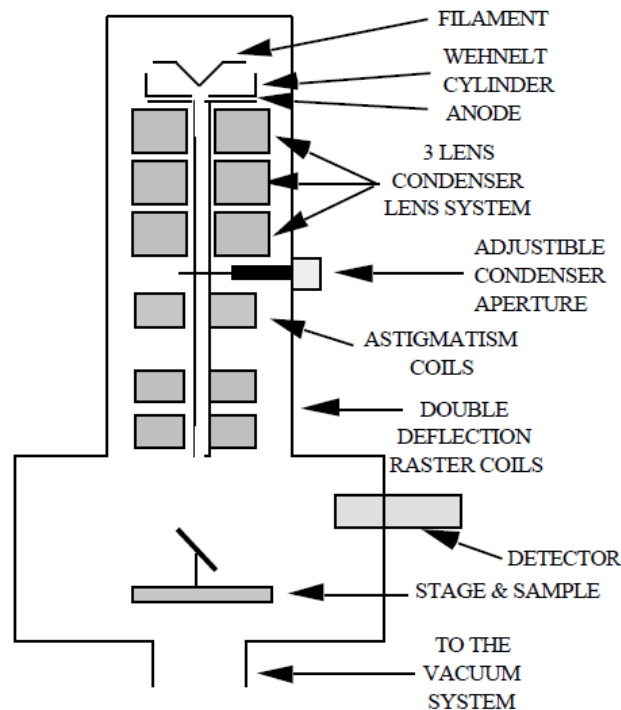


Figure 3.1. Diagram of SEM column and specimen chamber (Dunlap and Adaskaveg, 1997).

3.2.2 X-ray diffraction (XRD)

X-ray diffraction (XRD) analysis was performed on fresh outcrop samples to ascertain the mineralogy of the shale samples. A powder diffraction analysis was conducted using a multipurpose powder diffractometer known as the D8 Advance (by iThemba Labs) that has a Vantec1 detector which is a sensitive detector with a multi-channel position.

X-ray diffraction is an important tool in determining the mineralogical composition of sedimentary rocks. This method is particularly essential for shale where petrography is of limited utility (Lindholm, 1987). X-ray diffraction is a technique that uses the crystalline

properties of a material to reveal structure (UTA, 2010). Because different samples will have distinctive diffraction patterns, diffraction data can be used to characterize a sample (UTA, 2010).

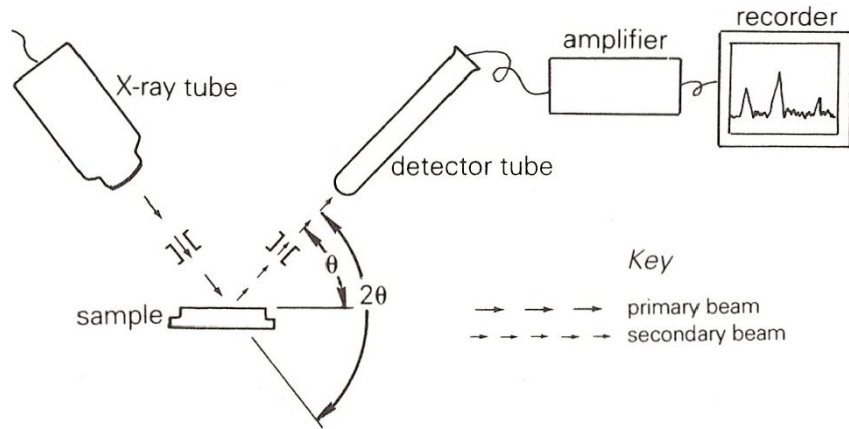


Figure 3.2. The diagram shows a common configuration of an X-ray diffractometer (Lindholm, 1987).

Monochromatic X-rays passing through a mineral are scattered by the atoms that it is composed of (Lindholm, 1987). Monochromatic X-rays are X-rays with a single wavelength (Wenk and Bulakh, 2006). Diffraction occurs when X-rays are shot at a specific angle of incidence and the scattered X-rays are in phase creating a secondary beam. W. L. Bragg and L. H. Bragg suggested that diffraction can be interpreted as a reflection of the X-ray beam by planes of atoms (Lindholm, 1987).

A first-order reflection occurs when the distance traveled by X-rays scattered from two adjacent layers of atoms is equal to the wavelength (Figure 3.3a). A second-order reflection occurs when the distance traveled by X-rays scattered from two adjacent layers of atoms equals two wavelengths (Figure 3.3b). Higher-order reflections occur when the distance traveled by X-rays scattered from two adjacent layers of atoms is a whole-number multiple of the wavelength (Lindholm, 1987). The Bragg equation expresses the general relationship as:

$$n\lambda = 2d \sin \theta$$

where:

n = a whole number,

λ = the X-ray wavelength,

d = the distance between planes of atoms (\AA),

θ = the angle of incidence.

Furthermore, Bragg's law has two conditions:

1. The lattice planes must be in a reflection orientation between the incident and diffracted X-ray waves.
2. Diffraction occurs at a specific angle that is determined by the d-spacing of the lattice planes (Wenk and Bulakh, 2006).

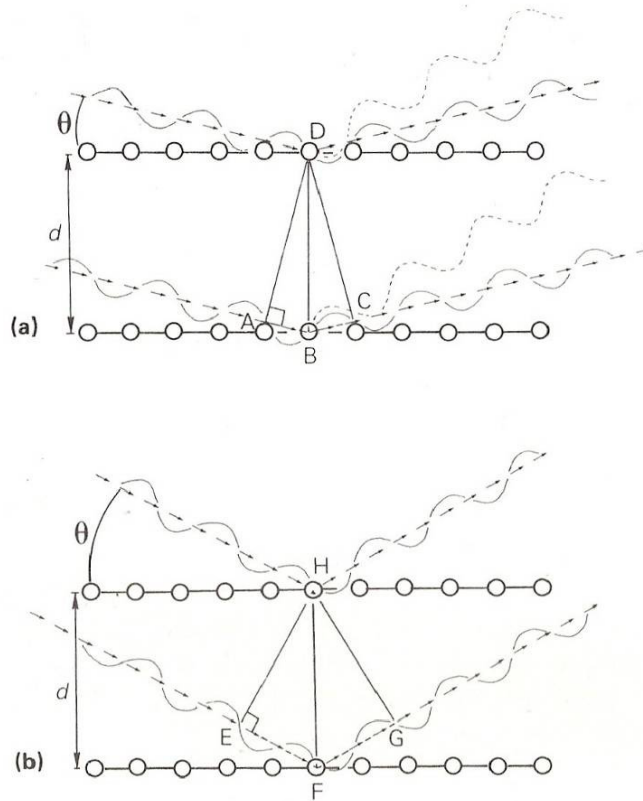


Figure 3.3. Diffraction of X-rays by layers of atoms; (a) first-order reflections occur when the path difference ($AB + BC$) between X-ray beams scattered by adjacent planes of atoms equal one X-ray wavelength. These beams are in phase and combine to form a secondary beam. Other scattered beams (e.g. those shown as dashed lines), which do not meet this condition, are out of phase and are destroyed. Note that θ = angles ADB and BDC and the side $BD = d$; (b) second-order reflections occur when the path difference ($EF + FG$) equals two wavelengths. Note that θ = angles EHF and FHG and that side $FH = d$ (Lindholm, 1987).

The powder diffractometry method is commonly used to study sedimentary materials (Lindholm, 1987). Following the sample being ground to a powder (1-50 μm) it is placed in the diffractometer. The powder consists of numerous randomly orientated crystals (Wenk and Bulakh, 2006). The path of the primary X-ray beam stays unchanged as the sample rotates around an axis normal to the beam (Lindholm, 1987). X-rays are created by an X-ray tube that is powered by an X-ray generator (Figure 3.4; Wenk and Bulakh, 2006). X-rays from a source (copper, molybdenum or cobalt) are directed at a powder sample (UTA, 2010). A diffracted beam that arrives at the detector tube (which is attached to a goniometer arm) rotates at twice the rate of the sample (Lindholm, 1987). Therefore, the sample rotates at an angle of θ and the detector tube rotates at an angle of 2θ (Figure 3.3). The powder is placed on a flat disk, and the reflections are scanned with a detector that records the intensity (as a function of diffraction angle) (Wenk and Bulakh, 2006).

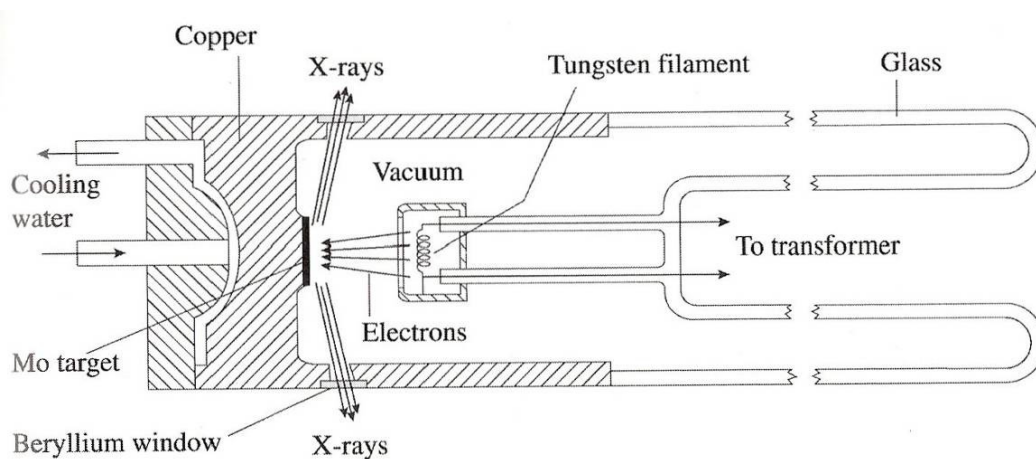


Figure 3.4. Generation of X-rays in a modern X-ray tube. A heated filament emits electrons that are accelerated and produce X-rays when they hit an anode. The anode is cooled with water (Wenk and Bulakh, 2006).

Because of the geometrical arrangement of the diffractometer only mineral grains whose lattice planes are parallel to the surface of the specimen holder will give off diffracted secondary beams (that go into the detector tube) (Lindholm, 1987). Consequently, the size of the particle must be small to guarantee that a large number of appropriately positioned grains are present (Lindholm, 1987). Rotation is not necessary since there will always be crystals with lattice planes in the right orientation to diffract (Wenk and Bulakh, 2006).

3.3 Geochemical analysis

3.3.1 Determination of total organic carbon content (TOC)

The Walkley-Black method was performed on fresh outcrop samples to ascertain the total organic carbon content of the shale samples (by Bemlabs). The Walkley-Black procedure is commonly used to determine the amount of readily oxidizable carbon by wet combustion (Walkley and Black, 1934; Walkley, 1935; Frink, 1992). The Walkley-Black procedure uses potassium dichromate ($K_2Cr_2O_2$) and concentrated H_2SO_4 , which is added to 0.5 g to 1.0 g of soil or sediment (Schumacher, 2002). The solution is then swirled and allowed to cool preceding the addition of water to stop the reaction. The sample has to be cooled as a result of the exothermic reaction when the potassium dichromate and sulfuric acids are mixed. To help eliminate interferences from the ferric (Fe^{3+}) iron that may be present in the sample, H_3PO_4 is added to the digestive mix after the sample has cooled (although in most cases, this step is not necessary) (Tiessen and Moir, 1993; Schumacher, 2002).

The Walkley-Black procedure is commonly utilized as it is simple, rapid, and has minimum equipment requirements (Nelson and Sommers, 1996; Schumacher, 2002). The procedure was initially designed to quantify the biologically active forms of carbon (e.g. raw organic material and soil humus) whilst excluding the inorganic and elemental forms (Frink, 1992). However, the procedure has been known to lead to the incomplete oxidation of organic carbon (Schumacher, 2002). The recovery of organic carbon ranges from 60 to 86% with an average recovery of 76% (Walkley and Black, 1934; Schumacher, 2002). Consequently, a correction factor of 1.33 is generally applied to the results to correct the organic carbon recovery.

The Walkley-Black procedure was modified, to overcome the concern of incomplete digestion of the organic matter, to include extensive heating of the sample during sample digestion (Mebius, 1960; Schumacher, 2002). In the modified Walkley-Black procedure the sample and extraction solutions are gently boiled at $150^\circ C$ for 30 minutes, cooled, and after that water is added to stop the reaction (Schumacher, 2002). The addition of heat to the system causes a complete digestion of the organic carbon in the sample. The temperature must be stringently controlled because the acid dichromate solution decomposes at temperatures greater than $150^\circ C$ (Charles and Simmons, 1986; Schumacher, 2002).

3.3.2 Rock-Eval pyrolysis

Outcrop samples were analyzed by Rock-Eval pyrolysis using a Rock-Eval 6 pyrolysis instrument. Guidelines to interpreting Rock-Eval data have been documented by Tissot and Welte (1984), Espitalie *et al.* (1985), Peters (1986), and Nuñez-Betelu and Baceta (1994), which utilizes graphs of various parameters in addition to evaluating the appropriate parameters individually.

During pyrolysis free or absorbed state hydrocarbons are first volatilized at moderate temperature (<300°C), which generates the S₁ peak (mg HC/g of rock) and is measured by a flame ionization detector (FID). Further pyrolysis of kerogen at temperatures between 300 and 600 °C results in the generation of the S₂ (mg HC/g of rock) and S₃ peaks (mg CO₂/g of rock), which represents the generated hydrocarbons and CO₂ respectively. The compounds generated are separated into two streams passing through a flame ionization detector (measures S₂) and a conductivity detector (measures S₃), operative between 300 and 390 °C. Furthermore, the temperature of maximum hydrocarbon generation (S₂) is also measured, and is referred to as T_{max} (Figure 3.5). Subsequently, residual organic matter is oxidized at 600 °C and the carbon released by this process is summed with S₁, S₂ and S₃ values to give the TOC (Espitalie *et al.*, 1977).

Table 3.1 is a summary of the various parameters Rock-Eval pyrolysis and other parameters calculated from them that can be used to characterize potential source rocks. Hydrocarbon source rocks are characterized based on three crucial factors: the quantity of organic matter; the type of organic matter; and its level of thermal maturity (Tissot and Welte, 1984).

The quantity of organic matter can be determined by interpreting the TOC, S₁ and S₂ values (table 3.2). The type of organic matter can be determined by interpreting the hydrogen index (HI) and oxygen index (OI) (table 3.3). In addition to providing information on the Type of organic matter, HI vs. OI plots can be used to roughly estimate the level of thermal maturity. The thermal maturity of organic matter can be determined by interpreting PI and T_{max} values (table 3.4).

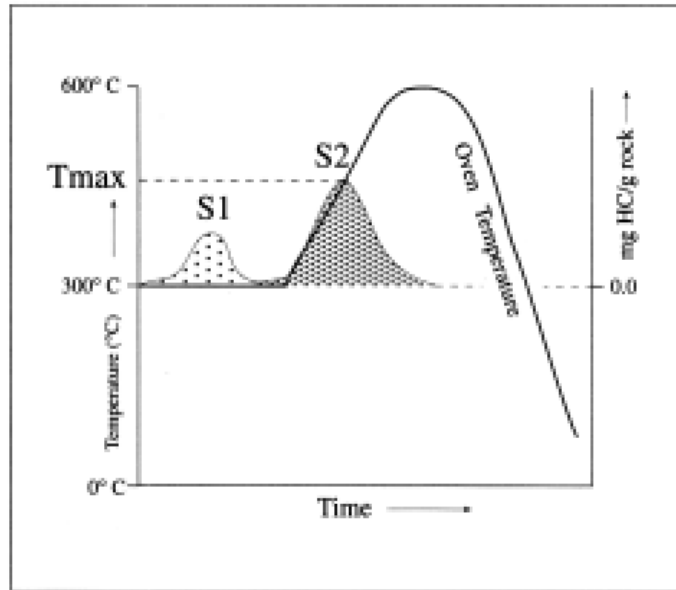


Figure 3.5. Response of organic matter to controlled heating during pyrolysis. S_1 corresponds to hydrocarbons formed in the subsurface and already present in the rock, whereas S_2 represents hydrocarbons generated during the pyrolysis process. T_{max} corresponds to the maximum generation of hydrocarbons during pyrolysis and is much higher than the temperatures governing the formation of hydrocarbons in nature (Barker, 1974).

Table 3.1. Measured and calculated parameters derived from Rock-Eval pyrolysis.

Measured Parameters
S_1 = hydrocarbons thermally distilled from the whole rock at temperature < 300 °C. Units: mg of hydrocarbon/gram of rock
S_2 = hydrocarbons generated by pyrolytic degradation of kerogen between 300 and 600°C. Units: mg of hydrocarbon/gram of rock
S_3 = a measure of organic CO_2 generated between temperature of 300 and 390°C. Units: mg of CO_2 /gram of rock
T_{max} = the temperature of maximum rate of evolution of pyrolysis hydrocarbons (S_2) in °C
TOC = carbon in ($S_1 + S_2 + S_3$) + carbon from oxidized residual organic matter
Calculated Parameters
HCP (hydrocarbon potential) = $S_1 + S_2$
PI (Production index) = $S_1/(S_1 + S_2)$
HI (hydrogen index) = $(S_2/TOC) \times 100$
OI (oxygen index) = $(S_3/TOC) \times 100$
QOM (quality of organic matter) = $(S_1 + S_2)/TOC$

Table 3.2. Geochemical parameters describing source rock generation potential (Peters, 1986).

Quantity	TOC (wt. %)	S₁ (mg HC/g rock)	S₂ (mg HC/g rock)
Poor	0 - 0.5	0 - 2.5	0 - 2.5
Fair	0.5 - 1	0.5 - 1	2.5 - 5
Good	1 - 2	1 - 2	5 - 10
Very Good	2+	2+	10+

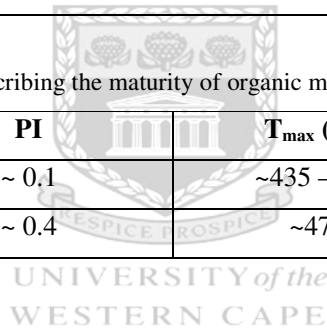
Table 3.3. Geochemical parameters describing the type of hydrocarbon generated (Peters, 1986).

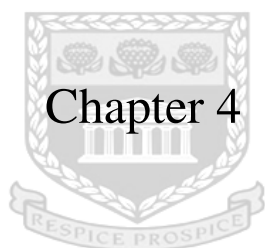
Type	HI	S₂/S₃
Type III OM	0 - 150	0 - 3
Type II OM	150 - 300	3 - 5
Type I OM	300+	5+

Assuming a level of thermal maturation equivalent to R_o=0.6%
OM = organic matter

Table 3.4 Geochemical parameters describing the maturity of organic matter (Peters, 1986).

Maturation	PI	T_{max} (°C)	R_o (%)
Top of oil window	~ 0.1	~435 - 445	~0.6
Bottom of oil window	~ 0.4	~470	~1.4





Chapter 4

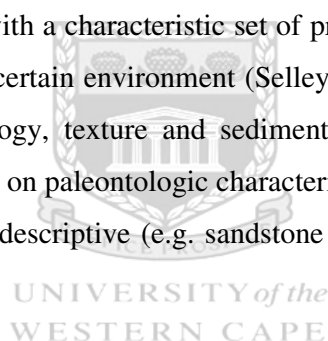
UNIVERSITY *of the*
WESTERN CAPE

Sedimentology

Sedimentology can be defined as the study of sedimentary strata and the processes by which they were formed (Hall, 2007). Sedimentology is based on the principle of “uniformitarianism” whereby processes affecting the Earth today are the same as the processes that affected the Earth in the past (Selley, 1982). By applying this principle, the depositional environment of ancient sedimentary rocks can be determined by studying modern sedimentary processes and products. Depositional environments are routinely reconstructed by the identification and interpretation of certain aspects such as sedimentary structures, facies, facies association and depositional models (Neveling, 2003).

4.1 Facies Description

A facies is a stratigraphic unit with a characteristic set of properties formed under conditions of sedimentation that reflects a certain environment (Selley, 1982). Facies based on physical properties such as color, lithology, texture and sedimentary structures are referred to as lithofacies, whereas facies based on paleontologic characteristics are biofacies (Boggs, 2001). The facies concept can also be descriptive (e.g. sandstone facies) and/or interpretative (e.g. deltaic facies).



4.1.1 Prince Albert Formation

A total of three facies were identified for the Prince Albert Formation and they are shale, silty-shale and dolomite (sedimentary log illustrated in Appendix A, taken at Lat: E 20°57.050' and Long: S 33°16,762').

4.1.1.1 Shale facies

Description:

Mudstone with planar horizontal laminae is commonly referred to as shale. The shale (Figure 4.1) is usually dark grey to black in color and displays flaky, pencil weathering. It reaches a maximum thickness of 15 m in the Witteburg area, with an average thickness of 1.1 m. The facies is usually bordered by dolomite, with both sharp and gradational contacts. In the

uppermost part of the formation, greenish-oxidized iron rich shale (Figure 4.2) displays flaky weathering and is usually bounded above and below by black shale with sharp contacts. Layers containing elongated concretions (Figure 4.3) as well as calcite nodules (Figure 4.4) are commonly found within the shales. In addition, dolerite intrusions are also observed in some locations.

Interpretation:

Shale has a composition of more than two thirds clay particles (< 0.06 mm) (Boggs, 2006) and represents deposition of fine-grained silts and clays which settle out from suspension (Selley, 1982). Variation in color is owed to the varying composition of shale (Twenhofel, 1950). The Prince Albert shales are generally clay-rich and can consequently be interpreted to be argillaceous. Argillaceous sediments have the finest grain size of sediments and are composed primarily of clay sized particles (Hall, 2007). These argillaceous shales break along the bedding and are platy.

Concretions are secondary sedimentary structures that can consist of calcite, siderite, haematite or dolomite. The shape of a concretion is dependent on the permeability of the host sediment and is diagenetic in origin. They grow concentrically around a nucleus by precipitation of carbonate that is drained from the adjacent sediment (Seilacher, 2001; Boggs, 2006).

Nodules are typically derived from the shells of silica secreting organisms (e.g. diatoms, radiolarians and sponges) which were dissolved by fluids flowing through the rock during diagenesis, with individual grains of chert forming as a result of recrystallization or precipitation of the shells of these organisms (Nelson, 2011).

Dolerite intrusions are present throughout the Karoo sedimentary sequence (Du Toit, 1920; Chevallier and Woodford, 1999; Aarnes *et al.*, 2011) and are believed to be contemporaneous with the Drakensberg flood basalts (Cole and McLachlan, 1994; Branch *et al.*, 2007). However, the thickest and most extensive sills are found within the Ecca Group (Du Toit, 1920; Chevallier and Woodford, 1999; Aarnes *et al.*, 2011).



Figure 4.1. Dark grey shale displaying splinter weathering found in the Witteburg area.



Figure 4.2. Greenish oxidized shale of the Prince Albert Formation in the Floriskraal area.



Figure 4.3. Elongated concretions in the dark grey to black shale found in the Witteburg area.



Figure 4.4. Creamish calcite nodules found in the brown weathered shale.

4.1.1.2 Silty-shale facies

Description:

The silty-shale is grey to dark grey in color and exhibits flaky weathering in some places. It has an average thickness of 0.11 m in the Floriskraal area. The facies is typically bounded above and below by shale with sharp contacts.

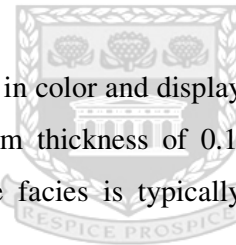
Interpretation:

Silty-shale represents deposition of fine-grained silts and clays which settle out from suspension (Selley, 1982). Silty-shale has slightly more silt sized particle than that of typical shales, giving it a gritty texture (Boggs, 2006).

4.1.1.3 Dolomite facies

Description:

The dolomite (Figure 4.5) is brown in color and displays distinctive elephant-skin weathering (Figure 4.6). It reaches a maximum thickness of 0.16 m in the Floriskraal area, with an average thickness of 0.12 m. The facies is typically bordered by shale, with sharp and gradational contacts.



UNIVERSITY of the
WESTERN CAPE

Ooids are also observed in some places.

Interpretation:

Dolomite is interpreted to have been formed in the shallow marine environment by precipitation of carbonates. Carbonates are shallow water deposits that form at depths <10 to 20 m, because the organisms that produce carbonate are photosynthetic or require the presence of photosynthetic organisms (Nelson, 2011). Seeing as photosynthesis requires sunlight, the organisms can only flourish at shallow depths because light cannot penetrate to great depths in the oceans. Carbonates are mainly composed of allochems, mud, cement and terrigenous grains (Folk, 1959, 1962; Reading, 1996). Sedimentation of carbonates are controlled by temperature, salinity, carbon dioxide balance, water depth, nature of local current regimes, light penetration, effective day length, nature of substrate and turbidity (Reading, 1996), with temperature and salinity being the primary controls on a global scale (Lees, 1975). Carbonates are typically formed on carbonate platforms and shelves (Nelson,

2011) which are shallow-water areas (Reading, 1996). Carbonate platforms are buildups (with reef building organisms usually forming the framework) of carbonates in deeper parts of the sea on top of continental blocks that are left behind during continental breakup (Nelson, 2011). Furthermore, carbonates are also known to form in tidal flats (Nelson, 2011) which are comprised of intertidal and supratidal zones, which lie below and above the reach of the highest normal spring tides respectively (Reading, 1996). Within the tidal flats, carbonate sands (transported by tides) are cemented together by carbonate secreting organisms, resulting in the formation of algal mats and stromatolites (Nelson, 2011).

Despite the fact that no dolomite is being directly formed in modern environments, it is believed that most dolomites appear to form as a result of diagenetic conversion of calcite (or Mg-rich calcite) to dolomite. Furthermore, dolomitization of carbonates (i.e. limestones) can take place via two mechanisms, which are: evaporative reflux; and mixing of seawater and meteoric water. Evaporative reflux involves the evaporation of seawater to form brine. The brine then precipitates gypsum, which causes the enrichment of the brine in Mg (relative to Ca) and a higher density. The brine then enters the groundwater system and moves downward into buried limestones, where the Mg-rich brine then reacts with the calcite in the limestone to create dolomite. Mixing of seawater and meteoric water involves the combination of groundwater (derived from the surface) with saline groundwater (beneath the oceans). Dolomitization is considered to occur in the porous and permeable limestone, where the two groundwater components mix (Nelson, 2011). Weathered dolomite is prone to have brownish color resulting from oxidation of ferrous iron in the dolomite (Selley, 1982).

Ooids are spherical particles that have a concentric or radial laminae coating a nucleus (Flügel, 2009). The nucleus of each particle consists of quartz or carbonate particles enclosed by concentric or radial layer of chemically precipitated calcite (Nelson, 2011). These chemically precipitated coatings are formed as grains roll around in agitated water.



Figure 4.5. Brown weathered dolomite of the Prince Albert Formation in the Witteburg area.



Figure 4.6. Brown elephant-skin weathering of dolomite in the Witteburg area.

4.1.2 Whitehill Formation

A total of three sub-facies were identified for the Whitehill Formation and they are shale, carbonaceous shale and tuffaceous shale. For the purpose of this study it was decided to discuss the sub-facies collectively as the shale facies. Due to the extreme weathering of outcrops, construction of a detailed sedimentary log was unachievable (sedimentary log illustrated in Appendix B, taken at Lat: E 20°57.107' and Long: S 33°16.832').

4.1.2.1 Shale facies

Description:

The shale facies consist of carbonaceous shale (Figure 4.7), tuffaceous shale as well as resistant shale beds found in the uppermost parts (Figure 4.8). The formation reaches a maximum thickness of 30 m in the study area. The Whitehill Formation shales are bounded above by shale of the Collingham Formation and below by shale of the Prince Albert Formation, with sharp and gradational contacts respectively. Pencil weathering and plumose weathering (Figure 4.9) can be observed in some locations with dispersed coal found throughout the formation.



Figure 4.7. White weathering carbonaceous shale displaying pencil cleavage of the Whitehill Formation.



Figure 4.8. Brown weathered resistant cherty and/or micaceous shale of the upper Whitehill Formation.



Figure 4.9. Brown weathered bedding displaying ripple or plumose weathering structures found.

Interpretation:

Shale has a composition of more than two thirds clay particles (< 0.06 mm) (Boggs, 2006) and represents deposition of fine-grained silts and clays which settle out from suspension (Selley, 1982).

Carbonaceous shale is dark, thinly laminated shale with unusually high organic carbon content ($\geq 5\%$), sulfide (particularly iron sulfide), and trace element concentrations (Jackson, 1997). Carbonaceous shale is known to form under anoxic conditions found in stratified lakes, restricted marine basins, and on the open shelves in areas of high productivity (Demaison and Moore, 1980). The environment of deposition of the Whitehill Formation has previously been established to range from brackish to deep marine (Smith, 1990; Visser, 1992b; Catuneanu *et al.*, 2005; Aarens *et al.*, 2011).

Tuffaceous shales are considered to be mixed pyroclastic-epiclastic deposits. These mixed pyroclastic-epiclastic deposits comprise 25% to 75% tuffites, with an average clast size of $< 1/256$ mm (Schmid, 1981). Thin tuffaceous beds have been observed in the southern and western outcrops of the Whitehill Formation (Johnson *et al.*, 1997). Tuffaceous rock, in addition to dark colored chert, carbonate rock and mudrock, make up a special sedimentary facies (known as the Black shale series) which represents an anoxic environment (Delian *et al.*, 1998).

Dispersed coal found in the Whitehill Formation is a result of maturation of carbonaceous shale (Cole and McLachlan, 1994; Branch *et al.*, 2007). This maturation is a consequence of contact metamorphism from pervasive dolerite intrusions that are contemporaneous with the Drakensberg flood basalts. Maturation of organic material as a result of contact metamorphism causes an elevation in vitrinite reflectance, loss of TOC, increased aromatization and changes in carbon isotope compositions of the residual organic material (Clayton and Bostick, 1986; Barker and Bone, 1995; Meyers and Simoneit, 1999; Aarnes *et al.*, 2010). These intrusions are potentially important in numerous sedimentary basins for the maturation of source rocks and subsequent methane (CH_4) generation in the areas surrounding sill-complexes (Aarnes *et al.*, 2010).

4.1.3 Collingham Formation

A total of six facies were identified for the Collingham Formation and they are shale, silty-shale, siltstone, sandstone, tuff and chert (sedimentary log illustrated in Appendix C, taken at Lat: E 20°51.951' and Long: S 33°14.436').

4.1.3.1 Shale facies

Description:

The shale (Figure 4.10) is dark grey to black in color and exhibits flaky weathering. Shales are also occasionally cherty and carbonaceous. The shale reaches a maximum thickness of 0.8 m in the Witteburg area, with an average thickness of 0.34 m. It is usually bordered by fine to very fine sandstone, with sharp contacts. Parallel lamination and plumose weathering can be observed in some places. Shale with silt lamination (Figure 4.11) is present in the Floriskraal area.

Interpretation:

Shale has a composition of more than two thirds clay particles (< 0.06 mm) (Boggs, 2006) and represents deposition of fine-grained silts and clays which settle out from suspension (Selley, 1982). These suspension-deposited shales occur interbedded with turbidite sands.

Laminations are small differences in the type of sediment that occur throughout the rock which are caused by cyclic changes in the supply of sediment. These changes include: grain size, clay percentage, microfossil content, organic material content or mineral content (Boggs, 1987). In fine grained sediments, lamination develops when fine grained particles settle in quiet water.



Figure 4.10. Dark grey to black shale displaying splinter cleavage in the Witteburg area.



Figure 4.11. Silt laminations on the dark grey sandstone in the Floriskraal area.

4.1.3.2 Silty-shale facies

Description:

The silty-shale is grey to dark grey in color and displays splinter weathering in some places. It has an average thickness of 0.12 m in the Floriskraal area. The facies is usually bounded above and below by shale with sharp contacts.

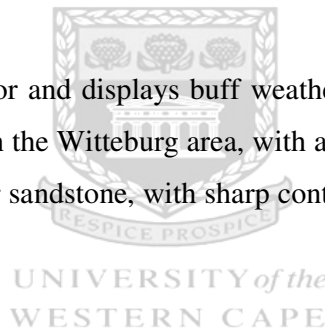
Interpretation:

Silty-shale, as previously discussed, represents deposition of fines which settle out from suspension (Selley, 1982). Silty-shale has slightly more silt sized particles than that of typical shales, giving it a gritty texture (Boggs, 2006).

4.1.3.3 Siltstone facies

Description:

The siltstone is creamish in color and displays buff weathering in some places. It reaches a maximum thickness of 0.16 m in the Witteburg area, with an average of 0.07 m. The facies is usually bordered by shale and/or sandstone, with sharp contacts. Ripple cross-laminations are also observed in some places.



Interpretation:

Siltstone has a composition of more than two thirds silt particles (Boggs, 2006). Siltstone facies represent deposition of fine-grained silt size particles which settle out from suspension (Selley, 1982).

Ripple cross-laminae are a result of deposition of sediment during migration of current or wave ripples and are always orientated ninety degrees to the direction of flow, meaning perpendicular to the paleoflow (Boggs, 2006). It has been proposed that current drag or the slowing of current velocity, during deposition is responsible for ripple cross-laminae (Potter and Pettijohn, 1977).

4.1.3.4 Sandstone facies

Description:

The sandstone is grey to dark grey in color and fine to very fine grained. The sandstone (Figure 4.12) reaches a maximum thickness of 0.85 m in the Witteburg area, with an average thickness of 0.29 m. It is usually bounded above and below by shale, with sharp contacts. Small concretions as well as ripple marks can be observed at the top of some beds.

Interpretation:

Sandstone represents deposition by low density distal turbidity currents which are interbedded with the shale and siltstone beds.



Figure 4.12. Fine to very fine grained tabular sandstone bounded by shale displaying pencil cleavage of the Collingham Formation in the Witteburg area.

Ripples marks occur in fine grained sediments that are subjected to gentle traction currents (Selley, 1982). The ripple index (RI) is a statistical parameter calculated by dividing the wavelength by the ripple height. Ripple marks in the formation are symmetrical in shape and has a wavelength of 9.96 cm and height of 0.5 cm, giving it a ripple index of 19.92. This RI

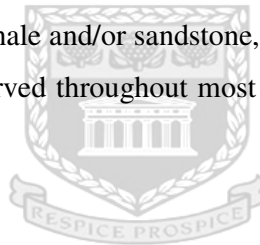
value corresponds to that of current ripples (Lindholm, 1987). These symmetrical current ripples were formed by the oscillating motion of water current (Selley, 1982).

Concretions, as previously discussed, are secondary sedimentary structures that can consist of calcite, siderite, haematite or dolomite. The shape of a concretion is dependent on the permeability of the host sediment and is diagenetic in origin. They grow concentrically around a nucleus by precipitation of carbonate that is drained from the adjacent sediment (Seilacher, 2001; Boggs, 2006). Concretions present in the sandstones are significantly smaller than those of the Prince Albert Formation.

4.1.3.5 Tuff facies

Description:

The tuff is yellowish cream in color and reaches a maximum thickness of 6 cm in the Witteburg area. It is bordered by shale and/or sandstone, with sharp contacts. In addition, thin tuff layers (+/-2 mm) can be observed throughout most of the Collingham Formation, but is absent in the uppermost 8 m.



Interpretation:

The volcanogenic sediments can be divided into ash-fall material and sediment gravity flows (Reading, 1996). Ash-fall material is generally distributed through the biogenic hemipelagic sediment but occasionally forms widespread layers (after a very large eruption). Sediment gravity flows consist of pyroclastic debris flows but also include turbidites (Reading, 1996). Pyroclastics that become part of other sedimentary deposits (e.g. hemipelagic sediment and turbidites) may lose their identity (Twenhofel, 1950). Thus, the widespread tuff layers can be interpreted to be air-fall tuffs.

4.1.3.6 Chert facies

Description:

A prominent chert bed found throughout the study area, known as the Matjiesfontein chert band (Figure 4.13), has a thickness of 0.41 m and is cream in color. A secondary chert bed is present in the Witteburg area, that is absent in the Geelbek and Floriskraal area, has a

thickness of 0.16 m. These chert beds are commonly bounded by shale (with contacts being sharp in nature).

Distinct parallel laminations can be observed at the base of the Maatjiesfontein chert band with ripple cross lamination at the top. Bitumen staining, in addition to ripple forms, (Figure 4.14 and Figure 4.15) are observed on the secondary chert bed.

Interpretation:

Chert can be defined as a mineralogically simple rock composed of microcrystalline quartz. Chert can form as beds that formed along tectonically active continental margins. These bedded cherts occur in association with turbidites, ophiolites, and mélanges. Although chert is believed to represent deep water accumulations of silica secreting organisms, it can also form in warm nutrient rich shallow water environments. Most cherts exhibit a microcrystalline texture that results from recrystallization during diagenesis, but sometimes the remains of silica secreting organisms (such as radiolaria, sponge spicules, or diatoms) are preserved (Nelson, 2011).

Laminations, as discussed previously, are small differences in the type of sediment that occur throughout the rock which are caused by cyclic changes in the supply of sediment. These changes include: grain size, clay percentage, microfossil content, organic material content or mineral content (Boggs, 1987). Ripple cross-laminae on the other hand form as a result of deposition of sediment during migration of current or wave ripples and are always orientated ninety degrees to the direction of flow, meaning perpendicular to the paleoflow (Boggs, 2006). It has been proposed that current drag or the slowing of current velocity, during deposition is responsible for ripple cross-laminae (Potter and Pettijohn, 1977). A change from parallel-lamination to ripple cross-lamination can be interpreted as a result of a change in the flow regime (Johnson *et al.*, 2001; Boggs, 2006).

Bitumen is the portion of organic matter that is soluble in normal petroleum solvents (Peters and Cassa, 1994) and occurs within both infilling sediment pores as well as within fractures (Selley, 1982). Bitumen can form by a number of mechanisms, which include: cracking of a hydrocarbon charge (caused by increasing temperatures during burial); an influx of a secondary gas charge (which causes the exsolution of bitumen); and/or by biodegradation (Lomando, 1992; Wilkinson *et al.*, 2006). Bitumen staining (also known as matrix bitumen

stain) refers to bitumen that impregnates the mineral matrix (Jacob, 1989; Ortoleva, 1994). The occurrence of bitumen staining in the Collingham Formation is considered to be strong evidence for the presence of oil in the past.



Figure 4.13. Parallel- and cross-lamination on the Maatjiesfontein chert band in the Floriskraal area.



Figure 4.14. Bitumen staining on the secondary chert band in the Witteburg area.



Figure 4.15. Bitumen staining and ripple forms on the secondary chert band in the Witteburg area.

4.2 Facies Associations

Facies that occur together and are environmentally related can be grouped into facies associations (Reading, 1996). The use of facies associations makes environmental interpretation easier since it provides additional evidence as compared to evaluating individual facies (Reading, 1996).

4.2.1 Prince Albert Formation

The upper Prince Albert Formation is dominated by the shale facies that averages 2.5 m in thickness with occasional thin beds of carbonate facies, averaging 12 cm, at the base or roof. It occurs in the north and south of the study area and is anomalously thickest in the southwestern portion of Floriskraal due to extensive folding. The Prince Albert Formation is overlain by carbonaceous shale of the Whitehill Formation with the contact generally being gradational in nature.

The occurrence of shale and carbonate in the upper Prince Albert sequence indicates that the sediments are deposited in an environment with little to no clastic input. The fine-grained sediments are deposited by suspension settling in a marine environment which was occasionally interrupted by deposition of carbonates that form in a shallow marine environment.

4.2.2 Whitehill Formation

The Whitehill Formation is dominated by carbonaceous shale that averages 8 m in thickness in the Witteburg area with relatively more resistant shale beds also present, averaging 6 cm in thickness. Resistant beds generally occur in the uppermost part of the Whitehill Formation, though these beds are observed throughout the Floriskraal exposures. A sharp contact separates the sequence from the overlaying shale of the Collingham Formation.

Based on the dominance of the carbonaceous shale, the Whitehill sequence was formed in an environment which would allow for the preservation of organic rich material. Thus, the fine sediments are interpreted to have been deposited from suspension settling under anoxic bottom conditions.

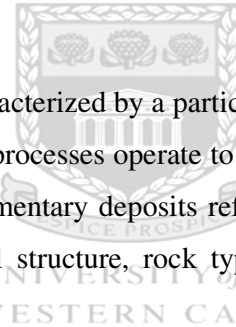
4.2.3 Collingham Formation

The Collingham Formation is dominated by the shale and sandstone facies that average 34 and 29 cm in thickness, respectively. The thin rhythmic deposits of shale and sandstone are occasionally interrupted by tuff layers. These tuff beds are approximately 2cm in thickness and are absent in the uppermost 8 m. Overlying the sequence is the Vischkuil Formation with the contact generally being sharp.

Inferred from the presence of both the thin beds of shale and sandstone; the Collingham Formation was formed in a quiet low energy environment with cyclic influx of clastic material that would allow rhythmic deposition of fine to very fine-grained sands and clays. The clay size sediments are deposited from suspension settling which are interbedded with low density turbidite current deposits in a marine environment.

4.3 Depositional Environments

Depositional environments are characterized by a particular setting in which a combination of physical, chemical, and biological processes operate to produce a certain type of sedimentary deposit (Boggs, 2001). These sedimentary deposits reflect the environment of deposition in their gross structure, their internal structure, rock type and biological activity (Neveling, 2003).



Based on the findings of the facies and facies associations it can be expected that the depositional sequences present within the Laingsburg sub-basin would be dominated by marine sequences.

4.3.1 Marine facies associations

Facies found in the deep marine comprises of siliciclastic turbidite sandstones, shale, and conglomerates; pelagic and hemipelagic shales that occasionally occur in association with bedded cherts; chalks and marls; limestone breccias; and carbonate turbidites (Boggs, 2001). These deposits are generally fine grained in nature (with the exception of turbidites and carbonate breccias). A further distinction of deep marine deposits is the sedimentary structures that comprise primarily out of thin, horizontal laminations. Deep marine deposits

are also characterized by the occurrence of larger concentrations of planktonic organisms (e.g. diatoms, radiolarians, foraminifers and coccoliths; in addition to graptolites and ammonites in older deposits) as compared to shallow marine deposits. Shale can be deposited by a number of processes that typically control fine-grained sedimentation in deep water (Stow *et al.*, 2001). Depositional processes most commonly involved are pelagic settling, hemipelagic sedimentation and turbidity currents.

Wilson (1975) identified the occurrence of carbonates and pelagic sediments and described it to be a basinal facies which is interbedded, organic-rich argillaceous and pelagic muds that accumulate in deep intracratonic and marginal cratonic depressions. The lack of light and depth hinder the formation of carbonates but lime-mud may enter from adjacent platforms or from platform as well as pelagic sources. Numerous ancient pelagic limestone deposits occur close to carbonate platforms which produce aragonite and calcite materials that are continually washed into deeper water (Wilson, 1969; Reading, 1996). Therefore, apparently pelagic carbonates might consequently have been wafted down the water-column from shallow-water areas (Reading, 1996).

The shale facies is interpreted to be deposited from suspension settling with dolomite making up the carbonate facies. The presence of nodules in shale of the Prince Albert Formation indicates slow sedimentation rate (Reading, 1996). The formation of carbonates is likely to be a result of tidal influences, as opposed to formation from nearby carbonate platform. The presence of ooids within the dolomite, resulting from particles rolling around in agitated water, indicates tidal influences (Nelson, 2011). Thus, the upper Prince Albert Formation is considered to have been deposited in a marine to shallow marine environment.

4.3.2 Anoxic bottom facies associations

Although the depositional environment of the Whitehill Formation is a question still in debate, the general consensus is that it was deposited under anoxic bottom conditions. The Whitehill Formation is dominated by carbonaceous shale which formed in conditions that favor the preservation of organic matter. Preservation of organic matter is widely believed to be a direct result of bottom water anoxia (Demaison and Moore, 1980; Demaison *et al.*, 1984; Calvert and Pedersen, 1993). Based on this, organic-rich rocks are assumed to have been formed in anoxic bottom conditions (Woolnough, 1937; Calvert and Pedersen, 1993). Anoxic

bottom conditions form in an anoxic environment where water is so depleted in oxygen that it caused practically all aerobic biological activity to stop (Demaison and Moore, 1980). These conditions are found where water columns do not mix, which include: stratified lakes; restricted basins; and on open shelves.

In anoxic environments a special sedimentary facies, known as the black shale series, is found (Delian et al., 1998). The black shale series is made up of dark colored chert, carbonate rock and mudstone (as well as tuffaceous rock). The dark color of the black shale series is caused by the organic carbon ($C_{org} > 1\%$), disseminated sulfides and ultrastructure. The black shale series is typically composed of two of the aforementioned rocks (Delian *et al.*, 1973, 1998). However, it could also be dominated by end members (Delian *et al.*, 1998), in the case of the Whitehill Formation, organic matter-rich shale. Thus, the Whitehill Formation represents formation of organic matter rich sediments under anoxic condition in an anoxic environment.



4.3.3 Distal turbidite facies associations

Facies produced by turbidity flow are characterized by interbedded sand and shale sequences (Kuenen and Migliorini, 1950; Selley, 1982). Turbidity flows are divided into high-density and low-density flows (Lowe, 1982). High-density flow deposits are coarse-grained, thick-bedded and generally display poor grading (little to no basal scour features). These turbidites are typically deposited in the main submarine transport channels (Lowe, 1976; Boggs, 2006). Low-density flow deposits are fine-grained, thin-bedded and generally display laminations and grading (with basal scour features) (Lowe, 1982). These turbidites are typically deposited on the overbank adjacent to the submarine transport channels or further away from the source as thin sheetlike deposits (Lowe, 1976; Boggs, 2006).

Sands generated by turbidity flows are termed turbidites and generally have abrupt bases, transitional tops and tend to fine-upwards (Selley, 1982). Turbidites are composed of sands, silty sands, or gravelly sands and are found in submarine canyons, deep-sea channels, and cone-shaped fans (Boggs, 2001). Clay- and silt-sized particles are carried in low concentrations and at low velocities by low-density turbidite currents (Reading, 1996), with the bulk of the subaqueous particles transported in suspension (Selley, 1982). These

suspension-deposited mudrocks occur interbedded (or interlaminated) with turbidites (or traction deposits) (Selley, 1982).

The fine- to very fine-grained sandstone of the Collingham Formation sequence resembles the typical profile described by Selley (1982); hence the sequence is interpreted to be low-density turbidite deposit. With suspension deposited sediments making up the shale facies. The presence of pyroclastics throughout most of the Collingham Formation sequence indicates volcanic activity during the time of deposition. These widespread tuff layers found within the formation represent ash-fall tuffs (Reading, 1996).



UNIVERSITY *of the*
WESTERN CAPE



Chapter 5

UNIVERSITY *of the*
WESTERN CAPE

Mineralogy

The identification of the mineralogical composition of shale is routinely determined through the utilization of X-ray diffraction (XRD). Qualitative XRD analysis was conducted on shale (sample localities shown in Appendix D) of the Prince Albert, Whitehill and Collingham Formations in order to detect changes in mineral composition. The XRD analysis results were then confirmed through scanning electron microscopy (SEM). The following is a brief discussion of the main clay group minerals identified by means of XRD and SEM analyses.

5.1 Clay mineralogy

Clay minerals are important components of shale and are fundamentally hydrous aluminous sheet silicates (Wenk and Bulakh, 2006) with the type of clay found in shale being a function of provenance and diagenetic history (Russell, 1970). They are the products of weathering and hydrothermal alteration of feldspars, mica, pyroxenes, and volcanic glasses (Wenk and Bulakh, 2006). The majority of clay minerals form from weathering and hydrothermal alteration of feldspar, as it is the most abundant mineral in the upper crust and is sensitive to chemical alteration processes (Füchtbauer, 1988). Furthermore, factors such as climate, assemblage, topography, transport and diagenetic changes can bring about the modification of the original clay assemblage (Yuretich *et al.*, 1999). The main clay group minerals include: kaolinite, illite, smectite, and chlorite.

The kaolinite group minerals consist of kaolinite, dickite, and halloysite. Kaolinite group minerals consist of serpentine-type structures with single tetrahedral nets (1:1) (Wenk and Bulakh, 2006). Kaolinite ($\text{Al}_2\text{Si}_2\text{O}_5(\text{OH})_4$) has varying degrees of crystallinity and a distinct, platy form. Halloysite ($\text{Al}_2\text{Si}_2\text{O}_5(\text{OH})_4 \cdot 2\text{H}_2\text{O}$) consists of a poorly ordered arrangement of kaolinite-like units, with variable amounts of water between the layers and often with a tabular form. They typically occur as fine-grained aggregates in flour-like or clay-like white masses and cannot be identified on the basis of their morphology (Wenk and Bulakh, 2006).

Illite can be defined as water-rich sheet-silicates, which are deficient in potassium in the interlayer space of the structure (Wenk and Bulakh, 2006). Illite group minerals have a di- or trioctahedral 2:1 layer structure. The structure is charged due to ionic substitution in both the

tetrahedral and octahedral sheets, and contains interlayer non-exchangeable cations. Illite ($K_{0.5}(Al,Fe,Mg)_3(Si,Al)_4O_{10}(OH)_2$) is closely related to muscovite ($H_2KAl_3Si_3O_{12}$) and has formerly also been called hydromuscovite. Increasing temperature is thought to cause illite to undergo a transformation into muscovite (Gharrabi *et al.*, 1998). Muscovite is almost pure aluminous mica with very little iron (Wenk and Bulakh, 2006).

The smectite group includes numerous clay minerals, with the ideal end members being saponite ($Mg_3Si_4O_{10}(OH)_2 \cdot 4H_2O$), beidellite ($Al_2Si_4O_{10}(OH)_2 \cdot 4H_2O$), and nontronite ($Fe^{3+}_2Si_4O_{10}(OH)_2 \cdot 4H_2O$) (Wenk and Bulakh, 2006). Smectite group minerals have a dioctahedral or a trioctahedral 2:1 layer structure (Wenk and Bulakh, 2006), with the main dioctahedral minerals being Al-rich montmorillonite-beidellites and Fe^{3+} -rich nontronites (Velde, 1992). The dioctahedral montmorillonite-beidellites are predominantly octahedrally charged and are generally associated (interlayered) with the mica-like minerals (Velde, 1992).

The chlorite group minerals have a large variety of chemical compositions with Mg^{2+} , Fe^{2+} , Fe^{3+} and Al^{3+} contending for octahedral positions (Wenk and Bulakh, 2006). The two major members of the chlorite group are clinochlore ($Mg_3(OH)_6Mg_2Al(HO)_2Si_3AlO_{10}$) and chamosite ($Fe^{2+}_3(HO)_6Fe^{2+}_{2.5}Al_{0.5}(HO)_2Si_{3.5}Al_{0.5}O_{10}$). These minerals are usually 14 Å in thickness with a sheet plane parallel to 001 (Wenk and Bulakh, 2006).

5.2 Clay minerals in the studied shale samples

Kaolinite, illite and smectite are the most abundant clay minerals encountered. Qualitative results obtained are shown in figure 5.1 – 5.3 (individual result of all analyzed samples illustrated in Appendix E).

5.2.1 Kaolinite

The formation of kaolinite is favored in tropical to subtropical climates (Chamley, 1989; Hallam *et al.*, 1991). The formation of kaolinite requires the complete removal of potassium (or else illite or montmorillonite will be formed) (Murray, 1988). Kaolinite formation is excluded from marine sedimentary systems since it demands acidic environments (Millot, 1970). Additionally, kaolinite can also develop through diagenetic processes as a result of

circulation of acid solutions (Ghandour *et al.*, 2003). Kaolinite deposits have been associated with several environments that include: lacustrine, paludal, deltaic, and lagoonal environments (Murray, 1988).

Kaolinite is present in both the Prince Albert and Collingham Formations. In addition to kaolinite, halloysite is also found in samples from the Prince Albert Formation. The occurrence of kaolinite in the lower Ecca Group sediments of the southern Karoo Basin has previously been described by Scheffler (2004) and Scheffler *et al.* (2006). The presence of kaolinite in the studied samples is in agreement with the obtained results from previous studies. The origin of kaolinite in the upper Prince Albert shales was believed to be a product of the replacement of chlorite by smectite/montmorillonite (as magnesium carrier) with further chemical alteration resulting in the appearance of kaolinite. The occurrence of kaolinite in the Collingham Formation on the other hand, is believed to be a consequence of the alteration of smectite to kaolinite, which is deduced from the widespread occurrence of pyroclastic material but lack of smectite in the studied samples. SEM micrographs revealed the absence of characteristic vermicular and booklet shape of authigenic kaolinite, in addition to the blocky crystals of diagenetic kaolinite as described by Bohor and Hughes (1971). In general, during diagenesis of kaolinite, the morphology changes from vermicular or aggregates of books into individual blocky crystals (Ehrenberg *et al.* 1993). Halloysite with lamellar particles; tubular or club-like particles; and needle-like or fibrous particles described by Hong and Mi (2006) are also completely absent.

5.2.2 Illite

Illite in general forms under conditions different from those under which kaolinite and smectite are formed (Ghandour *et al.*, 2003). Illite can form in soils with little chemical weathering, cold and/or dry climates and areas of high relief where physical erosion is predominant. It appears to be the most stable clay mineral in marine environments and is formed from different precursors which include muscovite, kaolinite and feldspar (Deer *et al.*, 1992). The majority of illite found in nature contains smectite layers (that are regularly or randomly interstratified) which are common in brackish sedimentary environments.

Illite was found to be present in the Prince Albert, Whitehill and Collingham Formations. It can be assumed that the illite of the Prince Albert, Whitehill and Collingham Formations are

formed from weathering of feldspar, since albite ($\text{NaAlSi}_3\text{O}_8$) is present in all the studied shale samples. This supports the findings of Scheffler (2004) which interpreted the occurrence of illite to be predominantly related to the breakup of feldspar during chemical weathering processes in the provenance. SEM micrographs showed the presence of clay flakes as described by Bohor and Hughes (1971), as well as white fibrous growths described by Güven *et al.* (1980). In addition to the formation of illite derived from the weathering of igneous rocks that are rich in feldspars (Keller, 1970), it may also have been formed from reworked sedimentary rocks and/or muscovite that sustain for many sedimentary cycles (Engelhardt, 1977).

5.2.3 Smectite

There are four main genetic hypotheses for the formation of smectite, which are: reworking of soils and enrichment by differential settling; alteration of volcanic material; transformation of detritals; and authigenesis (Chamley, 1989; Thiry and Jaquin, 1993). Montmorillonite has also been interpreted to form from simultaneous weathering of feldspars and ferromagnesian minerals, accumulated in moderate pH and low Eh conditions (Fairbridge, 1967). During burial diagenesis, di-octahedral and tri-octahedral smectites are transformed into illite and chlorite respectively (facilitated by increasing depth and temperature). Smectite can also be transformed into kaolinite (via smectite/kaolinite) (Deer *et al.*, 1992). Montmorillonite has also been used to differentiate different sedimentary environments, with its presence often associated with open marine conditions. Increasing marine conditions can be monitored by the transformation of montmorillonite to chlorite (Velde, 1995). The occurrence of smectite (as well as kaolinite) in marine sediments have been attributed to chemical weathering in warm humid environments (Weaver, 1989). Furthermore, smectite can also form from the alteration of illite, kaolinite, and/or chlorite (Moore and Reynolds, 1989).

Smectite (in the form of montmorillonite) was present in all of the Whitehill Formation samples, and has a composition of $\text{Na}_{0.3}(\text{AlMg})_2\text{Si}_4\text{O}_{10}\text{OH}_2 \cdot 4\text{H}_2\text{O}$. Therefore the montmorillonite of the studied shale samples can be classified as Al-rich montmorillonite-beidellite based on its chemical composition. The occurrence of albite in the studied shales, as well as the presence of tuff indicates that smectite may have formed from weathering of feldspar and pyroclastics respectively. SEM micrographs revealed montmorillonite particles with lamellar aggregate structure or papery structure, as well as crinkly, ridged, honeycomb-

like texture. The papery structure of montmorillonite may be a consequence of the expulsion of water and gas during compaction and oxidation of organic matter (Keller *et al.* 1986). The crinkly, ridged, honeycomb-like texture is believed to develop as a result of the shrinkage of the expandable clay minerals as they dry (Bohor and Hughes, 1971).



UNIVERSITY *of the*
WESTERN CAPE

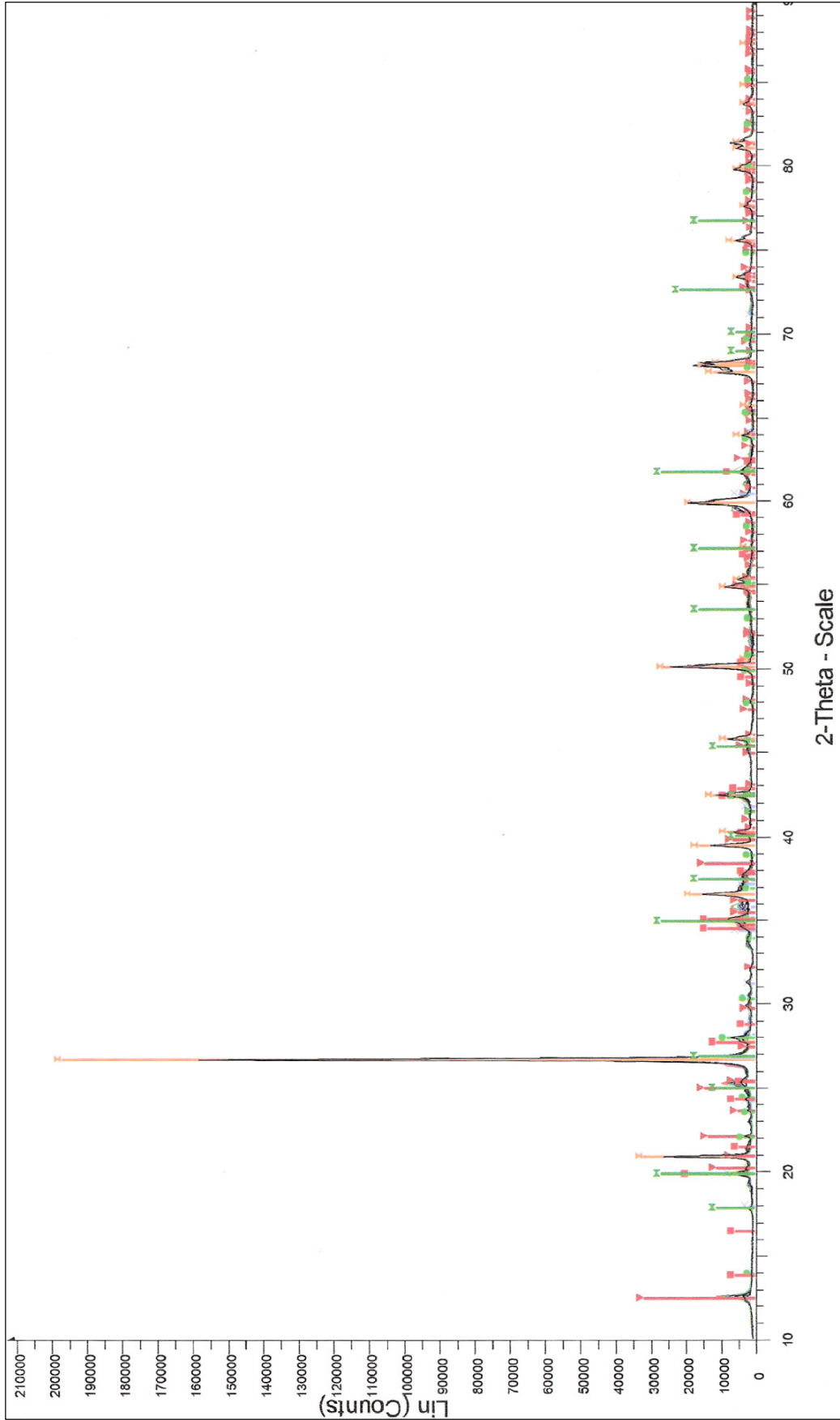


Figure 5.1. XRD plots of the Prince Albert Formation. Mineral phases include: quartz (orange); albite (green circles); palygorskite (pink squares); illite (light blue); and halloysite (green bowtie).

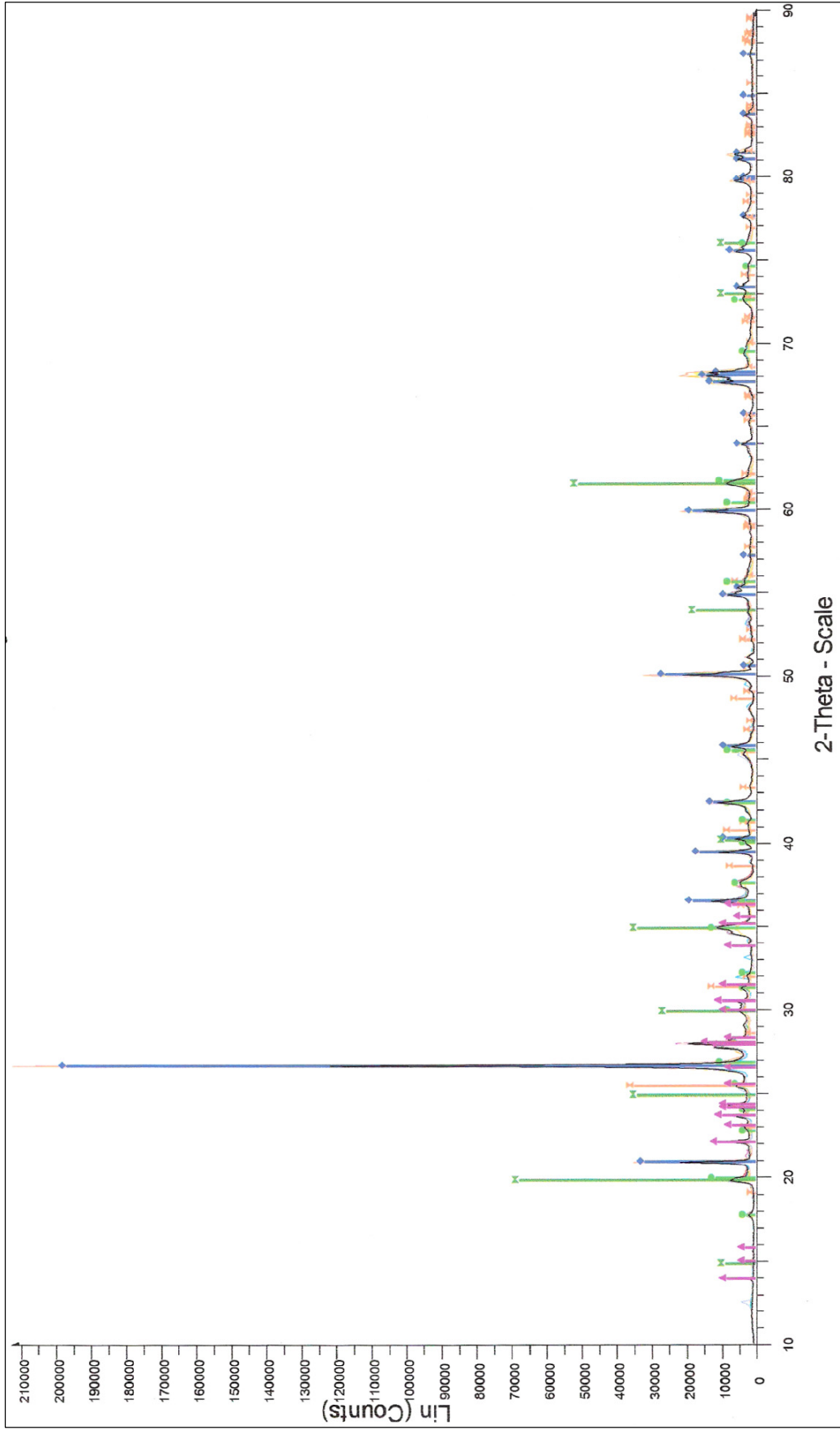


Figure 5.2. XRD plots of the Whitehill Formation. Mineral phases include: quartz (blue); albite (purple); anhydrite (orange); montmorillonite (green bowtie); muscovite (green circle).

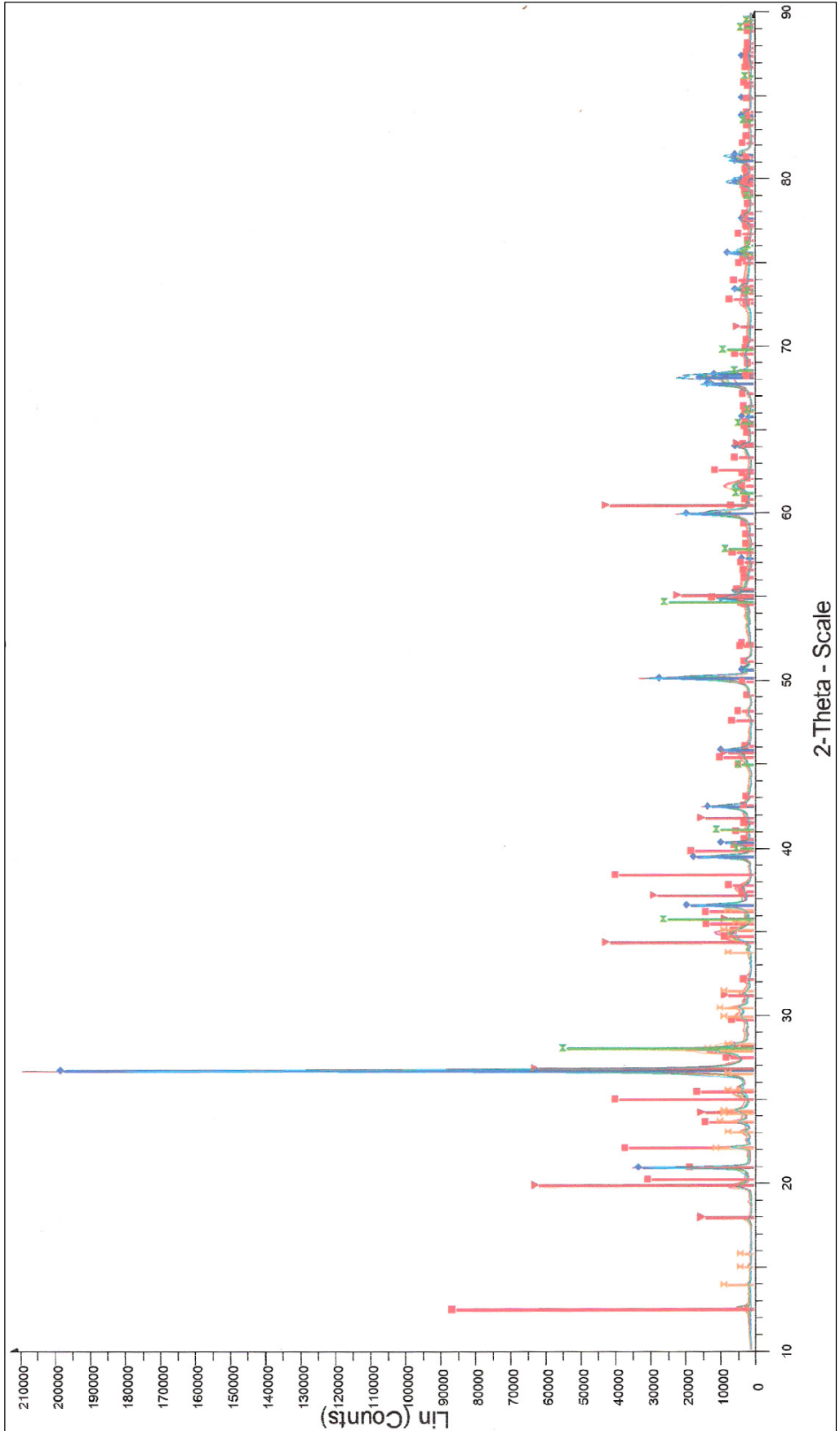
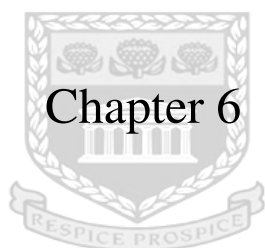


Figure 5.3. XRD plots of the Collingham Formation. Mineral phases include: quartz (blue); rutile (green); albite (orange); illite (red triangle); and kaolinite (pink square).



Chapter 6

UNIVERSITY *of the*
WESTERN CAPE

Organic Geochemistry

In this study total organic carbon (TOC) and Rock-Eval pyrolysis determination for outcrop samples have been done to ascertain the hydrocarbon potential of the Prince Albert, Whitehill and Collingham Formations in the studied area.

6.1 Total organic carbon content

High organic matter content is one of the criteria for the identification of petroleum source rocks (Tissot and Welte 1984). Organic carbon-rich sediments can form as a result of high primary production of coastal waters, a stratified water column, anoxic bottom waters, low influx of clastic material, and high supply of organic matter (Calvert and Petersen, 1992; Meyers, 1997). Preservation of the organic matter is controlled by several conditions, including: bottom water circulation rates; degree of oxygenation of bottom water; deposition rates; supply rate of organic matter from the source; and productivity in the surface water (Tissot and Welte 1984). The organic carbon analyses in the study consist of 28 samples from the Witteburg, Geelbek and Floriskraal areas (sample localities shown in Appendix D). The total organic carbon content was determined and results were used to select samples for Rock-Eval pyrolysis (Figure 6.1)

UNIVERSITY of the
WESTERN CAPE

Table 6.1. Total organic carbon (TOC) results for the Prince Albert (PA), Whitehill (WH) and Collingham (CH) Formations. * indicates samples selected for Rock-Eval pyrolysis.

Sample No.	TOC (wt.%)	Sample No.	TOC (wt.%)	Sample No.	TOC (wt.%)
PA 1	0.24	WH 1	2.05	CH 1	0.45*
PA 2	0.60*	WH 2	2.18*	CH 2	0.25
PA 3	0.23	WH 3	0.14	CH 3	0.23
PA 4	0.35	WH 4	2.32*	CH 4	0.28
PA 5	0.12	WH 5	1.75*	CH 5	0.11
PA 6	0.12	WH 6	0.11	CH 6	0.37*
PA 7	0.22	WH 7	0.11	CH 7	0.11
PA 8	0.21	WH 8	0.23	CH 8	0.27
PA 9	0.21	WH 9	0.74*		
PA 10	0.39*				
PA 11	0.19				

6.2 Rock-Eval pyrolysis

Rock-Eval pyrolysis provides information on the type, abundance and thermal maturity of organic matter in addition to its hydrocarbon potential. Rock-Eval pyrolysis and TOC results are listed in table 6.2.

Table 6.2. TOC and Rock-Eval results of the Prince Albert (PA), Whitehill (WH) and Collingham (CH) Formations.

Sample No.	RE			T _{max} (°C)	TOC	HI	OI	S ₂ /S ₃	S ₁ /TOC *100	PI
	S ₁	S ₂	S ₃							
CH 1	0.09	0.14	0.19	349	0.45	31.11	42.22	0.8	20	0.39
CH 6	0.04	0.06	0.34	341	0.37	16.22	91.89	0.2	10.81	0.4
PA 2	0.04	0.04	0.43	370	0.6	6.67	71.67	0.1	6.67	0.5
PA 10	0.05	0.06	0.25	344	0.39	15.38	64.1	0.2	12.82	0.45
WH 2	0.05	0.05	0.84	610	2.18	2.29	38.53	0.1	2.29	0.5
WH 4	0.03	0.06	0.83	321	2.32	2.58	35.78	0.1	1.29	0.33
WH 5	0.03	0.03	0.84	347	1.75	1.71	48	0	1.71	0.5
WH 9	0.07	0.11	1.25	308	0.74	14.86	168.92	0.1	9.45	0.39

6.2.1 Organic matter type assessment

The type of organic matter is a crucial factor in the determination of petroleum potential of source rock, with hydrogen index (HI) versus oxygen index (OI) diagram commonly used to estimate type (Nuñez-Betelu and Baceta, 1994).

6.2.1.1 Hydrogen index (HI) versus oxygen index (OI)

Hydrogen index (HI) and oxygen index (OI) can often be directly related to the atomic H/C and O/C ratios, and interpreted in the same way as a van Krevelen diagram (Espitalie 1977; Tissot and Welte 1984). In addition to providing information on the type of organic matter, HI vs. OI plots can be used to roughly estimate the level of thermal maturity. The thermal maturation of each kerogen type is described by a pathway on the van Krevelen diagram, where the most mature samples plot near the lower left corner.

Three main types of organic matter and their thermal alteration pathways are defined in the HI vs. OI diagram. Type I organic matter originates from algae and microbial biomass and is rich in aliphatic hydrocarbons and hydrocarbon-like components (Tissot and Welte, 1984). Type II organic matter originates from the waxy coatings of land plants and partially degraded algae and is moderately rich in aliphatic components. Type III organic matter typically represents woody land-plant matter, but it may also represent poorly preserved algal organic matter and is poor in hydrocarbon-like materials, but rich in cellulose and lignin.

Oxidation of organic matter affects both HI and OI values that can blur the source distinction between continental and marine organic matter from Rock-Eval pyrolysis (Katz, 1983; Peters, 1986). As Type I or II organic matter is oxidized, its hydrogen content decreases and its oxygen content increases, and it takes on the characteristics of Type III organic matter. An additional limitation on the use of Rock-Eval pyrolysis for determination of organic matter source is that samples should contain at least 0.5 wt% TOC to yield meaningful results.

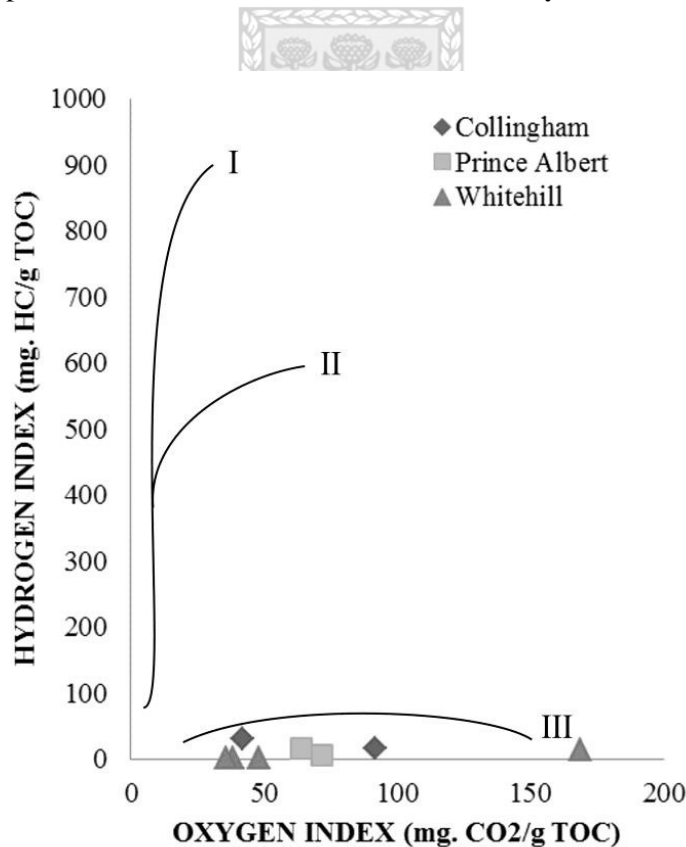


Figure 6.1. Hydrogen index versus oxygen index plot of Rock-Eval pyrolysis data.

The entire sample set plots within the Type III kerogen field (Figure 6.1), with very low HI (6.67 and 15.38 mg HC/g TOC), and medium OI (71.67 and 64.1 mg CO₂/g TOC) values observed for the Prince Albert Formation. The Whitehill Formation has very low HI (1.71 to 14.86 mg HC/g TOC) and medium to high OI (35.78 to 168.92 mg CO₂/g TOC) values. The Collingham Formation has very low HI (16.22 and 31.11 mg HC/g TOC) and medium OI (91.89 and 42.22 mg CO₂/g TOC) values.

6.2.2 Organic matter abundance assessment

High organic matter content is one of the criteria for the identification of petroleum source rocks, with a total organic carbon content of 0.5 wt.% needed for samples to be considered source rocks (Tissot and Welte 1984). In addition to TOC, S₁ and S₂ can also be used to assess the quantity of organic matter.

However, if the TOC value is less than 0.5 wt.% the values of S₂ are considered to be unreliable, because of absorption of pyrolytic compounds onto the mineral matrix (Peters, 1986). Type III kerogen is most prone to this problem, as it generates lesser amounts of S₂ per gram of organic matter than that of Type I and II kerogen (Peters, 1986).

6.2.2.1 Total organic carbon (TOC)

The formations show variable amounts of organic matter, with the samples of the Prince Albert Formation recording TOC values of up to 0.6 %, classifying it as a fair source rock (Peters, 1986). The shales of the Whitehill Formation gave the highest values: 2.05 %, 2.18 % and 2.35 %, classifying it as a very good source rock (Peters, 1986). On the other hand the samples of the Collingham Formation show a maximum value of only 0.45 %, making it a poor source rock (Peters, 1986).

6.2.2.2 S₁ and S₂

While the TOC values (discussed in section 6.2.2.1) of some of the samples show adequate quantities of organic matter, to be termed a source rock, S₁ and S₂ value are anomalously low. The studied samples of the Prince Albert, Whitehill and Collingham Formations yield S₁ and S₂ values that indicate a poor source rock potential. The Prince Albert Formation has S₁

values of 0.4 and 0.5, and S_2 values of 0.4 and 0.6. The Whitehill Formation has S_1 values ranging from 0.3 to 0.7, and S_2 values ranging from 0.3 to 0.11. The Collingham Formation has S_1 values of 0.9 and 0.4, and S_2 of values 0.14 and 0.6. The validity of the S_1 and S_2 values are questionable when taking into account the TOC values obtained.

6.2.3 Thermal maturity assessment

The degree of thermal maturity is an essential parameter in the determination of petroleum source rock, with PI and T_{max} commonly used to estimate maturity (Nuñez-Betelu and Baceta, 1994).

6.2.3.1 T_{max}

T_{max} is the temperature at which the maximum amount of hydrocarbons is generated from kerogen cracking, and represents a relative value of the level of thermal maturity (Nuñez-Betelu and Baceta, 1994). T_{max} is a good maturation indicator between 420 and 460 °C in Type II kerogen, and between 400 and 600 °C in terrestrially derived Type III kerogen (Tissot *et al.*, 1987). T_{max} values less than about 435 °C indicate immature organic matter, with values greater than 470 °C indicating the end of the oil window (Peters, 1986). The T_{max} value is regarded as being inaccurate when the S_2 value is lower than 0.2. This inaccurate T_{max} values is attributed to extremely low TOC value and oxidized character of organic matter, which can generate an invalid T_{max} value.

Although T_{max} was determined for all the samples, the samples all have S_2 values lower than 0.2. The studied samples have T_{max} values below 370 °C, with the exception of a Whitehill sample (WH2) from the Witteburg area showing 610 °C. These erroneous results are considered to be invalid, making the thermal maturity determination based on T_{max} values inconclusive.

6.2.3.2 Production index (PI)

The production index (PI) is to some extent indicative of the level of thermal maturity (Peters, 1986; Nuñez-Betelu and Baceta, 1994). The ratio $S_1/(S_1 + S_2)$ is an evaluation of the PI or transformation ratio (TR) (Espitalie *et al.*, 1985; Peters, 1986). The PI is the ratio of

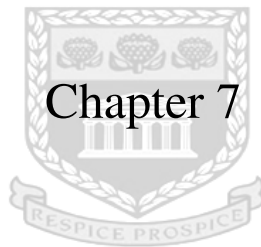
hydrocarbons formed by the kerogen (S_1) to the total amount of hydrocarbons that the kerogen can generate ($S_1 + S_2$). This ratio depends on the nature of the organic matter along with the geological (temperature vs. time) history and is often used to assess the relative thermal maturity of organic matter, as well as the presence of migrated hydrocarbons (Tissot and Welte, 1984). PI values less than about 0.1 indicates immature organic matter with values greater than 0.4 indicating the end of the oil window (Peters, 1986).

Weathering of outcrop samples usually causes depletion in S_1 and S_2 and high S_3 values, since PI is the ratio $S_1/(S_1+S_2)$, depletion of S_1 and S_2 may induce changes in PI values (Nuñez-Betelu and Baceta, 1994).

The Prince Albert Formation has PI values of 0.5 and 0.45. PI values of the Whitehill Formation range from 0.33 to 0.5. The Collingham Formation has PI values of 0.4 and 0.39. Most of the PI values of the studied samples of the Prince Albert, Whitehill and Collingham Formations indicate the end of the oil window, in other words the post-mature stage of maturity (Peters, 1986).



UNIVERSITY *of the*
WESTERN CAPE



Chapter 7

UNIVERSITY *of the*
WESTERN CAPE

Discussion and Conclusions

7.1 Discussion

Sedimentology

The sedimentological investigation revealed that the upper Prince Albert Formation is dominated by shale with thin beds of carbonate. These shales are deposited by suspension settling in a marine environment which was occasionally interrupted by deposition of carbonates that form in a shallow marine environment. The overlying Whitehill Formation is predominantly carbonaceous shale with relatively more resistant shale beds also present. The clay size sediments are interpreted to have been deposited from suspension settling under anoxic bottom conditions which would favor the preservation of organic rich material. Deposition of the Whitehill Formation was followed by the Collingham Formation which is dominated by rhythmic deposits of shale and sandstone that are occasionally interrupted by tuff layers. The fine sediments are deposited from suspension settling which are interbedded with low density turbidite current deposits in a marine environment.

Marine environments are known to be dominated by phytoplanktonic organisms as well as algal debris (Nuñez-Betelu and Baceta, 1994). Type I kerogen is derived from extensive bacterial reworking of lipid-rich algal organic matter such as Tasmanites (in marine waters) and Botryococcus (in fresh water) (Peters and Cassa, 1994). Type II kerogen is derived mainly from phytoplanktonic organisms (Nuñez-Betelu and Baceta, 1994). A marine environment would therefore be dominated by Type I and II kerogen. Based on the depositional environment of the Lower Ecce Group, Type I and II kerogen would be the dominant constituent of the organic matter of the shales.

Mineralogy

Mineralogically, the Prince Albert Formation consists predominantly of illite, kaolinite as well as halloysite. The Whitehill Formation clays consist mainly of smectite (in the form of montmorillonite) in addition to muscovite. The clay minerals of the Collingham Formation consist mainly of illite and kaolinite. The presence of plagioclase feldspar (albite) in all the studied shale samples is an indication of the formation of clay minerals as a consequence of weathering of feldspar. Furthermore, formation of clay minerals from weathering of

pyroclastic material can be inferred from the presence of tuff beds noted in the field observations. Lastly, the formation of clay minerals from alteration of other clay minerals can be deduced from the presence of alteration along clay mineral edges. Thus, it can be concluded that these clay minerals are derived from a combination of weathering of feldspars and pyroclastics as well as alteration of other clay minerals.

Organic geochemistry

The total organic carbon (TOC) of the shale varied between 0.11-2.32 wt%, with an average of 0.52 wt%. The TOC analysis shows high values in the carbonaceous shales of the Whitehill Formation. The obtained values in the Prince Albert Formation are significantly lower than that of the Whitehill Formation, with the Collingham Formation showing the lowest values, which could be an indication of the oxidation of organic matter in outcrop. In addition to oxidation, a decrease in TOC values may also be a result of thermal maturation. TOC values of thermally mature rocks containing Type I, II, and III kerogens can be reduced by up to 70, 50 and 12-20 wt% (Daly and Edman, 1987; Peters and Cassa, 1994), with Type IV kerogen showing little effect of thermal maturation. The Rock-Eval pyrolysis values and values calculated there from imply that organic matter type is predominantly Type III kerogen, with low hydrogen index (HI) and medium to high oxygen index (OI) values. Type III kerogen is derived from higher land plants and makes up common terrestrial organic matter (Nuñez-Betelu and Baceta, 1994). The calculated production index (PI) values as determined by Rock-Eval pyrolysis ranges between 0.33-0.5 with an average of 0.43, this indicates over-mature organic matter for oil generation. However, the samples are in the gas window.

The contradiction between the Rock-Eval source characterization and the sedimentological source characterization is evidence that the organic matter has been degraded, because well-preserved Type I/II organic matter has high HI values (Katz, 1983; Peters, 1986). The most common form of degradation of organic matter is oxidation which removes hydrogen and adds oxygen to the kerogen (Nuñez-Betelu and Baceta, 1994), and therefore, all pyrolysis values and values calculated there from are considered to be inaccurate.

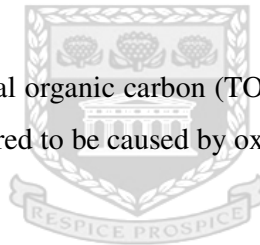
7.2 Conclusions

The present investigation comprises insights into the sedimentology, mineralogy and geochemical composition of shales from the Lower Ecca Group in Laingsburg.

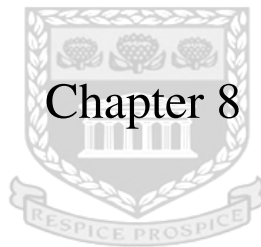
Sedimentological characteristics of the Prince Albert Formation indicate that the formation was deposited in a marine to shallow marine environment. The Whitehill Formation indicates that the formation was deposited in an anoxic environment. The Collingham Formation indicates that the formation was deposited in a marine environment.

Mineralogically, the clay minerals of the Prince Albert, Whitehill and Collingham Formations consist predominantly of illite, kaolinite in addition to smectite which were derived from a combination of weathering of feldspars and pyroclastics as well as alteration of other clay minerals.

Results obtained from both the total organic carbon (TOC) analysis and Rock-Eval pyrolysis indicates erroneous values considered to be caused by oxidation of outcrop samples.



UNIVERSITY *of the*
WESTERN CAPE



Chapter 8

UNIVERSITY *of the*
WESTERN CAPE

Recommendations

The major drawback of the study is the poor quality of samples used for the organic geochemical analyses. Similar results have been recorded in previous studies done in the Laingsburg area which also made use of outcrop samples for geochemical analyses of potential source rocks of the Ecca Group (e.g. Arnold and Akinlua, 2009). The results obtained in the Rock-Eval pyrolysis and total organic carbon analysis can be enhanced by making use of alternative sample type (e.g. core and/or side wall core samples). These core and/or side wall core samples should be taken at a depth greater than 30m to ensure that the samples have not been subjected to any surface weathering.

In addition to using alternative types of samples for organic geochemical analysis, additional analyses should be used to strengthen the organic matter assessment (e.g. gas chromatography–mass spectrometry (GC-MS), vitrinite reflectance (R_o), Leco TOC, etc.). GC-MS is routinely used for molecular organic geochemical investigations, which analyses biological markers (biomarkers). Biomarkers can be defined as organic compounds whose carbon skeleton suggests a clear link to a known natural precursor (Mackenzie *et al.*, 1982). These complex organic compounds are composed essentially of carbon, hydrogen, and other elements and are found in oil, bitumen, rocks, and sediments (Peters and Moldowan, 1993). In petroleum exploration the use of biomarkers is crucial since it provides invaluable information regarding (1) depositional environments and source-related parameters, (2) maturation parameters, (3) migration, (4) biodegradation, and (5) basin modeling (Philp and Lewis, 1987).

Leco TOC is a method by which the total organic carbon content of rock samples is measured by combustion of the organic matter in an oxygen atmosphere at a temperature of 1500°C in a Leco induction oven (Bordenave *et al.*, 1993). The advantage of Leco TOC as opposed to the Walkley-Black method is that it also provides an estimate of the mineral carbon. Leco TOC also yields better results (as compared to Rock-Eval) for mature organic matter since the carbon combustion is complete at a temperature greater than 1000°C. However, results obtained from Leco could be disturbed by interference of sulfated minerals (for instance gypsum and anhydrite), on account of the high temperature needed.

Other than geochemical analyses, organic petrography (such as vitrinite reflectance (R_o)) is also frequently implemented in petroleum exploration. Vitrinite is defined as a group of macerals with certain definite, optical as well as chemical properties (Carr, 2000). Vitrinite is frequently used for reflectance measurements, as its optical properties change more uniformly than that of the other maceral groups (Dow, 1977). Vitrinite reflectance is a means of identifying the temperature history of sediments. The vitrinite reflectance is extremely sensitive to temperature ranges that largely correspond to those of hydrocarbon generation (that is 60 to 120°C); this means that vitrinite reflectance can be used as an indicator of maturity in hydrocarbon source rocks.



UNIVERSITY *of the*
WESTERN CAPE

The crest of the University of the Western Cape, featuring a shield with three flowers at the top, a building facade in the center, and a banner at the bottom with the motto 'RESPICE PROSPICE'.

Bibliography

UNIVERSITY *of the*
WESTERN CAPE

- Aarnes, I., Svensen, H., Polteau, S., & Planke, S. (2011). Contact metamorphic devolatilization of shales in the Karoo Basin, South Africa, and the effects of multiple sill intrusions. *Chemical Geology*, (281), 181-194.
- Advanced Metals Research Corporation. (1969). AMR High Resolution Scanning Electron Microscope, Model 900. Burlington, Mass: Advanced Metals Research Corporation.
- Arnold, A.A., & Akinlua, A. (2009). Source rock potential, palaeoenvironment and thermal maturity of the lower Ecca group, South Africa: Implications for hydrocarbon exploration. *11th SAGA Biennial Technical Meeting and Exhibition Swaziland*, (p. 573).
- Barker, C. (1974). Pyrolysis techniques for source-rock evaluation. *The American Association of Petroleum Geologists Bulletin*, 58 (11), 2349-2361.
- Barker, C.E., & Bone, Y. (1995). The minimal response to contact metamorphism by the Devonian Buchan Caves Limestone, Buchan Rift, Victoria, Australia. *Organic Geochem.*, 22 (1), 151–164.
- Besaans, A.J. (1973). Geological Map of South Africa. Ladismith, southwestern sheet, 3320, 1:250 000, Pretoria: Geological Survey of the Republic of South Africa.
- Beukes, N.J. (1970). Stratigraphy and sedimentology of the Cave Sandstone Stage, Karoo System. In S.H. Haughton (Ed.), *2nd IUGS Symposium on Gondwana Stratigraphy and Palaeontology* (p. 321-341). Pretoria.
- Boggs, S. Jr. (1987). *Principles of sedimentology and stratigraphy*. Columbus, OH: Merrill Publishing Company.
- Boggs, S. Jr. (2001). *Principles of Sedimentology and Stratigraphy* (3rd ed.). New Jersey, USA: Prentice-Hall, Inc.
- Boggs, S. Jr. (2006). *Principles of Sedimentology and Stratigraphy* (4th ed.). New Jersey, USA: Prentice-Hall, Inc.

- Bohor, B.F., & Hughes, R.E. (1971). Scanning Electron Microscopy of Clays and Clay Minerals. *Clays and Clay Minerals*, (19), 49-54.
- Bordenave, M.L., Espitalié, J., LePlat, P., Oudin, J.L., & Vandenbroucke, M. (1993). Screening techniques for source rock evaluation. In M.L. Bordenave (Ed.), *Applied Petroleum Geochemistry* (pp. 217-278). Éditions Technip.
- Bordy, E.M., Hancox, J.P., & Rubidge, B.S. (2004). Provenance study of the Late Triassic – Early Jurassic Elliot Formation, main Karoo Basin, South Africa. *South African Journal of Geology*, 107, 587-602.
- Bouma, A.H., & Wickens, H.deV. (2002). The Tanqua Fan Complex, Karoo Basin, South Africa – Outcrop Analog for Fine-Grained, Deepwater Deposits. In A.H. Bouma, & C.G. Stane (Eds.), *Fine-grained turbidite systems* (pp. 153-164). AAPG Memoir 72 /SEPM Special Publication, 68.
- Branch, T., Ritter, O., Weckmann, U., Sachsenhofer, R. F., & Schilling, F. (2007). The Whitehill Formation – a high conductivity marker horizon in the Karoo Basin. *South African Journal of Geology*, 110, 465-476.
- Business Day live. (2014). *SA petroleum agency's Karoo shale-gas estimate 'far lower'*. Retrieved 2014, from <http://www.bdlive.co.za/business/energy/2014/02/21/sa-petroleum-agencys-karoo-shale-gas-estimate-far-lower.html>
- Cadle, A.B., Cairncross, B., Christie, A.D.M., & Roberts, D.L. (1993). The Karoo basin of South Africa: type basin for the coal-bearing deposits of southern Africa. *International Journal of Coal Geology*, 23, 117–157.
- Calvert, S.E., & Pedersen, T.F. (1993). Geochemistry of Recent oxic and anoxic marine sediments: Implications for the geological record. *Marine Geology*, 113, 67-88
- Carr, A.D. (2000). Suppression and retardation of vitrinite reflectance, part 1. Formation and significance for hydrocarbon generation. *Journal of Petroleum Geology*, 23, 313-343.

- Catuneanu, O. (2004). Retroarc foreland systems—evolution through time. *Journal of African Earth Science*, 38, 225-242.
- Catuneanu, O., & Bowker, D. (2001). Sequence stratigraphy of the Koonap and Middleton fluvial formations in the Karoo foredeep South Africa. *African Earth Sciences*, 33, 579-595.
- Catuneanu, O., Cairncross, B., Eriksson, P.G., Hancox, P.J., Rubidge, B.S., Smith, R.M.H., & Wopfner, H. (2005). The Karoo basin of south-central Africa. *Journal of African Earth Science*, 43, 211-253.
- Catuneanu, O., & Elango, H.N. (2001). Tectonic control on fluvial styles: the Balfour Formation of the Karoo Basin, South Africa. *Sedimentary Geology*, 140, 291-313.
- Catuneanu O., Hancox P.J., Cairncross B. & Rubidge B.S. (2002). Foredeep submarine fans and forebulge deltas: orogenic off-loading in the underfilled Karoo Basin. *Journal of African Earth Sciences*, 35, 489–502.
- Catuneanu, O., Hancox, P.J., & Rubidge, B.S. (1998). Reciprocal flexural behaviour and contrasting stratigraphies: a new basin development model for the Karoo retroarc foreland system, South Africa. *Basin Research*, 10, 417-439.
- Chamley, H. (1989). *Clay Sedimentology*. Heidelberg: Springer – Verlag.
- Clayton, J.L., & Bostick, N.H. (1986). Temperature effects on kerogen and on molecular and isotopic composition of organic matter in Pierre Shale near an igneous dike. *Organic Geochem.*, 10(1-3), 135-143.
- Cole, D. (2009). *A review of uranium deposits in the Karoo Supergroup of South Africa*. Retrieved 2010, from Search and Discovery Article (Online Journal for E&P Geoscientists): <http://www.searchanddiscovery.net/documents/2009/80047cole/index.htm>

- Cole, D.I., & McLachlan, I.R. (1994). Oil shale potential and depositional environment of the Whitehill Formation in the main Karoo basin. *SOEKOR, now PASA, South African Petroleum Agency, Cape Town. Unpublished Report No. 1994-0213.*
- Crowell, J.C., & Frakes, L.A. (1975). The late Palaeozoic glaciation. In K.S.W. Campbell (Ed.), *Gondwana Geology: Papers from the 3rd Gondwana Symposium* (pp. 313–331). Australian National Univ. Press.
- Crowell, J.C., & Frakes, L.A. (1972). Late Paleozoic glacial geography between the Parana Basin and the Andean Geosyncline. *An. Acad. Bras. Cienc.*, 44, 139-45.
- Daly, A.R., & Edman, J.D. (1987). Loss of organic carbon from source rocks during thermal maturation. *American Association Petroleum Geologists Bulletin*, 71, 546.
- De Beer, C.H. (1999). Structure of the Cape Fold belt in the Ceres Arc. *Geological Survey of South Africa Bulletin*, 123, p.93.
- De Celles, P.G., & Giles, K.A. (1996). Foreland Basin Systems. *Basin Research*, (8), 105-123.
- De Wit, M.J., & Ransome, I.G.D. (1992). Regional inversion tectonics along the southern margin of Gondwana. In M.J. de Wit, & I.G.D. Ransome (Eds.), *Inversion Tectonics of the Cape Fold Belt, Karoo and Cretaceous Basins of Southern Africa* (pp. 217-278). Balkema Publishers.
- Deer, F.R.S., Howie, R.A., & Zussman, J. (1992). *An introduction to the rock-forming minerals*. London: Longman Group Limited.
- Delian, F., Tao, Z., & Jie, Y. (1998). Anoxic environment and formation of superlarge ore deposits. *Science in China*, 41, 37-46.
- Delian, F., Xiuzhen, Y., & Lianfang, W. (1973). Petrological and geochemical characteristics of a nickel-molybdenum-multielement- bearing Lower Cambrian black shale from a certain district in South China. *Geochimica*, 3, 143.

- Demaison, G.J., & Moore, G.T. (1980). Anoxic environments and oil source bed genesis. *Organic Geochemistry*, 2, 9-31.
- Dingle, R. V. & Siesser, W.G. (1977). Geology of the continental margin between Walvis Bay and Ponta Do Ouro: Volume two of Marine Geosciences Series. Geological Survey (South Africa), Pretoria: The Government Printer.
- DME. (2008). "Coal" *South Africa Department of Minerals and Energy*. Retrieved 2010, from <http://www.dme.gov.za/energy/coal.stm>
- Dow, W.G. (1977). Kerogen studies and geological interpretations. *Journal of Geochemical Exploration*, 7, 79-99.
- Dreyer, J.C. (1994). Total utilization of the coal resource: the Grootegeluk experience. In: C.R. Anhaeusser (Ed.), *XVth CMMI Congress, Symposium Series, S14* (pp. 153-167). Johannesburg.
- Du Toit, A.L. (1920). The Karoo dolerites of South Africa: a study in hypabyssal injection. *Trans. Geol. Soc. SA*, 23, 1-42.
- Duncan R.A., Hooper P.R., Rehacek J., Marsh J.S. & Duncan A.R. (1997). The timing and duration of the Karoo igneous event, southern Gondwana. *Journal of Geophysical Research*, 102, 18127-18138.
- Dunlap, M., & Adaskaveg, J.E. (1997). Introduction to the Scanning Electron Microscope. Theory, practice, & procedures. 52. Facility for Advance Instrumentation.
- Engelhardt, W.V. (1977). *Sedimentary Petrology: The origin of sediments and sedimentary rocks*. Stuttgart: Schweizerbart.
- Ehrenberg J.N., Aagard P., Wilson M.J., Fraser A.R., & Duthie D.H.L. (1993). Depth-dependent transformation of kaolinite to dickite in sandstones of the Norwegian continental shelf. *Clay Mineral.*, 28, 325-352.

- Espitalie, J., Deroo, G., & Marquis, F. (1985). La pyrolyse Rock-Eval et ses applications. *Rev. Inst. Fr. Petr.*, 40(6), 765.
- Espitalie, J., Laporte, J.L., Madec, M., Marquis, F., Lelplat, P., Paulet, J., & Boutefeu, A. (1977). Methode rapide de caracterisation des roches meres de leur potential petrolier et de leur degre d, evolution. *Inst. Fr. Petr.*, 32, 23-42.
- Espitalie J., Makadi K. S., & Trichet J. (1984). Role of the mineral matrix during kerogen pyrolysis. *Organic Geochem.*, 6, 365-382.
- Fairbridge, R.W. (1967). Phases of diagenesis and authigenesis. In G. Larsen & G.V. Chilinger (Eds.), *Diagenesis in Sediment* (pp. 19-89). Elsevier Scientific Publishing Co.
- Falcon, R.M.S. (1986a). A brief review of the origin, formation and distribution of the coal in Southern Africa. In C.R. Anhaeusser & S. Maske (Eds.), *Mineral Deposits of Southern Africa* (Vol. I and II, pp. 1879-1898). Geological Society of South Africa.
- Falcon, R.M.S. (1986b). Classification of coals in Southern Africa. In C.R. Anhaeusser & S. Maske (Eds.), *Mineral Deposits of Southern Africa* (Vol. I and II, pp. 1899-1921). Geological Society of South Africa.
- Flint, S.S., Hodgson, D.M., King, R.C., Potts, G.J., Van Lente, B., & Wild, R.J. (2004). *The Karoo Basin Slope Project: Phase 1. Industry consortium report*. University of Liverpool.
- Flint, S.S., Hodgson, D.M., Sprague, A.R., Brunt, R.L., Van der Merwe, W.C., Figueiredo, J., Prélat, A., Box, D., Di Celma, C., & Kavanagh, J.P. (2010). Depositional architecture and sequence stratigraphy of the Karoo basin floor to shelf edge succession, Laingsburg depocentre, South Africa. *Marine and Petroleum Geology*, 28(3), 658-674.
- Flügel, E. (2009). *Microfacies of Carbonate Rocks: Analysis, Interpretation and Application*. Springer.
- Frink, D.S. (1992). The chemical variability of carbonized organic matter through time. *Archaeology of Eastern North America*, 20, 67-79.

- Füchtbauer, H. (1988). *Sedimente und Sedimentgesteine* (4th ed.). Stuttgart, Schweizerbart.
- Ghandour, I.M., Harue, M., & Wataru, M. (2003). Mineralogical and chemical characteristics of Bajocian-Bathonian shales, G. Al-Maghara, North Sinai, Egypt: Climatic and environmental significance. *Geochemical Journal*, 37, 87-108.
- Gharrabi, M., Velde, B., & Sagon, J.P. (1998). The transformation of illite to muscovite in pelitic rocks: Constraints from X-ray diffraction. *Clays and clay minerals*, 46, 79-88.
- Grecula, M., Flint, S.S., Wickens, H. de V., & Johnson, S.D. (2003a). Upward-thickening patterns and lateral continuity of Permian sand-rich turbidite channel fills, Laingsburg Karoo, South Africa. *Sedimentology*, 50, 831-853.
- Grecula, M., Flint, S.S., Potts, G., Wickens, H. de V., & Johnson, S.D. (2003b). Partial ponding of turbidite systems in a basin with subtle growth-fold topography; Laingsburg-Karoo, South Africa. *Journal of Sedimentary Research*, 73, 603-620.
- Gurnis, M. (1992). Rapid continental subsidence following the initiation and evolution of subduction. *Science*, 255, 1556-1558.
- Güven, N., Hower W., & Davies, D.K. (1980). Nature of autogenic illites in sandstone reservoirs. *Journal of Sedimentary Petrology*, 50 (3), 761-766.
- Hälbich, I.W. (1983). A tectonogenesis of the Cape Fold Belt (CBF). *Special Publication of Geological Society of South Africa*, 12, 165-175.
- Hälbich, I.W. (1992). The Cape Fold Belt Orogen: State of the art 1970's -1980's. In M.J. de Wit, & I.G.D. Ransome (Eds.) *Inversion Tectonics of the Cape Fold Belt, Karoo and Cretaceous Basins of Southern Africa* (pp. 141-158). A.A. Balkema Rotterdam.
- Hall, C.A. (2007). *Introduction to the geology of southern California and its native plants*. University of California Press, pp. 493.

- Hallam, A., Grose, J.A., & Ruffell, A.H. (1991). Paleoclimatic significance of changes in clay mineralogy across the Jurassic-Cretaceous boundary in England and France. *Palaeogeog. Palaeoclimat. Palaeoecol.*, 81, 173-187.
- Hancox, P.J. (2000). The continental Triassic of South Africa. *Zentralblatt für Geologie und Paläontologie Teil 1*, 1998, 1285-1324.
- Hegenberger, W.F., Johnson, M.R., Key, R., Shoko, U., & van Vuuren, C.J. (1996), Stratigraphy of the Karoo Supergroup in southern Africa: an overview. *Journal of African Earth Sciences*, 23 (1), 3-15.
- Herbert C.T., & Compton J.S. (2007). Depositional environments of the lower Permian Dwyka diamictite and Prince Albert shale inferred from the geochemistry of early diagenetic concretions, southwest Karoo Basin, South Africa. *Sedimentary Geology*, 194, 263-277.
- Hong, H.L., & Mi, J.X. (2006). Characteristics of halloysite associated with rectorite from Hubei, China. *Mineralogical Magazine*, 70, 257-264.
- Hotton, N. (1967). Stratigraphy and sedimentation in the Beaufort Series (Permian-Triassic), South Africa. In C. Teichert, & E.I. Yochelson (Eds.), *Essays In Palaeontology and Stratigraphy* (pp. 390–427). Special Publication of the University of Kansas.
- Hotton, N. (1986). Dicynodonts and their role as primary consumers. In N. Hotton, P.D. MacLean, J.J. Roth, & E.C. Roth (Eds.), *The ecology and biology of mammal-like reptiles* (pp. 71-82). Washington: Smithsonian Institutional Press.
- Jackson, J.A. (Ed.). (1997). *Glossary of geology*, (4th ed.). American Geological Institute, Alexandria, VA.
- Jacob, H. (1989). Classification, structure, genesis and practical importance of natural solid oil bitumen (“migrabitumen”). *International Journal of Coal Geology*, 11, 65-79.
- Johnson, M.R. (1976). *Stratigraphy and sedimentology of the Cape and Karoo Sequences in the Eastern Cape Province*. Unpublished PhD thesis, Rhodes University.

- Johnson, M.R. (1991). Sandstone petrography, provenance and plate tectonic setting in Gondwana context of the south-eastern Cape Karoo Basin. *South African Journal of Geology*, 94 (2/3), 137-154.
- Johnson, M.R., van Vuuren, C.J., Visser, J.N.J., Cole, D.J., Wickens, H.deV., Christie, A.D.M., & Roberts, D.L. (1997). The foreland Karoo Basin, South Africa. In R.C. Selley (Ed.), *African Basins—Sedimentary Basins of the World* (pp. 269-317). Elsevier, Amsterdam.
- Keller, W.D. (1970). Environmental aspects of clay minerals. *Journal of Sedimentary Petrology*, 40, 788-813.
- Keller, W.D., Reynolds, R.C., JR., & Inoue, A. (1986). Morphology of clay minerals in the smectite- to –illite conversion series by scanning electron microscopy. *Clays and Clay Minerals*, 34, 187-197.
- Keyser, A.W., & Smith, R.M.H. (1978). Vertebrate biozonation of the Beaufort group with special reference to the Western Karoo Basin. *Annals of the Geological Survey of South Africa*, 12, 1–36.
- King, R.C. (2005). *Structural evolution of the Cape Fold Belt; implications for sediment routing to the SW Karoo Basin*. Unpublished PhD thesis, University of Liverpool.
- Kuenen, P.H., & Migliorini, C.I. (1950). Turbidity currents as a cause of graded bedding. *Journal of Geology*, 58, 91-127.
- Lees, A. (1975). Possible influence of salinity and temperature on modern shelf carbonate sedimentation. *Marine Geology*, 19, 159-198.
- Lock, B.E. (1978). The Cape Fold Belt of South Africa; tectonic control of sedimentation. *Proc. Geol. Ass.*, 89, 263–281.
- Lock, B.E. (1980). Flat-plate subduction and the Cape Fold Belt of South Africa. *Geology*, 8, 35-39.

- Lomando, A.J. (1992). The influence of solid reservoir bitumen on reservoir quality. *American Association of Petroleum Geologists Bulletin*, 76, 1137-1152.
- López-Gamundí, O.R., & Rossello, E.A. (1998). Basin-fill evolution and paleotectonic patterns along the Samfrau geosyncline: the Sauce Grande basin - Ventana foldbelt (Argentina) and Karoo basin - Cape foldbelt (South Africa) revisited. *Geologische Rundschau*, 86, 819-834.
- Lindholm, R.C. (1987). *A practical approach to sedimentology*. London: Allen and Unwin Ltd.
- Lowe, D.R. (1982). Sediment gravity flow: II. Depositional models with special reference to the deposits of high-density turbidity currents. *Journal of Sedimentary Research*, 52, 279-297.
- Mackenzie, S.C., Brassell, S.C., Eglinton, G., & Maxwell, J.R. (1982). Chemical fossils: The geological fate of steroids. *Science*, 217, 491-504.
- MacLeod, K.G., Smith, R.M.H., Koch, P.L., & Ward, P.D. (2000). Timing of mammal-like reptile extinctions across the Permian-Triassic boundary in South Africa. *Geology*, 28, 227-230.
- Mebius, L.J. (1960). A rapid method for the determination of organic carbon in soil. *Analytica Chimica Acta*, 22, 120-124.
- Methane to Markets. (2008). *Coal Mine Methane Global Overview*. Retrieved 2010, from http://www.methanetomarkets.org/m2m2009/documents/toolsres_coal_overview_ch27.pdf
- Meyers, P.A. (1997). Organic geochemical proxies of paleoceanographic, paleolimnologic, and paleoclimatic processes. *Organic Geochem.*, 27, 213-250.
- Millot, G. (1970). *Geology of Clays: Weathering, Sedimentology, Geochemistry*. Heidelberg-Berlin: Springer-Verlag.

- Mitrovica, J.X., Beaumont, C., & Jarvis, G.T. (1989). Tilting of Continental Interiors by the Dynamical Effects of Subduction. *Tectonics*, 8 (5), 1079–1094.
- Moore, D.M., & Reynolds, Jr. R.C. (1989). *X-ray Diffraction and the Identification and Analysis of Clay Minerals*. New York: Oxford University Press.
- Murray, H.H. (1988). Kaolin minerals; their genesis and occurrences. *Reviews in Mineralogy*, 19, 67-89.
- Nelson, S.A. (2011). *Petrology: Carbonates and Other Rocks*. Retrieved 2011, from www.tulane.edu/~sanelson/geol212/index.html
- Nelson, D.W., & Sommers, L.E. (1996). Total carbon, organic carbon, and organic matter. In A.L. Page, D.L. Sparks, P.A. Helmke, R.H. Loeppert, P.N. Soltanpour, M.A. Tabatabai, C.T. Johnston, & M.E. Sumner (Eds.), *Methods of Soil Analysis, Part 2* (pp. 961-1010). American Society of Agronomy Inc.
- Neveling, J. (2003). Stratigraphy and sedimentological investigation of the contact between the Lystrosaurus and the Cynognathus Assemblage Zones (Beaufort Group: Karoo Supergroup). *Council for Geoscience Bulletin*, 137, 165.
- Nuñez-Betelu, L., & Baceta, J.I. (1994). Basics and application of Rock-Eval/TOC Pyrolysis: An example from the uppermost Paleocene/lowermost Eocene in the Basque Basin, Western Pyrenees. *Munibe Natural Sciences - Natur Zientziak*, 46, 43-62.
- Ortoleva, P.J. (1994). Basin compartments and seals. *American Association of Petroleum Geologists*, 477.
- Peters, K. E. (1986). Guidelines for evaluating petroleum source rock using programmed pyrolysis. *American Association of Petroleum Geologists Bulletin*, 70 (3), 318-329.
- Peters, K. E., & Cassa, M. R. (1994). Applied Source Rock Geochemistry. In L.B. Magoon, & W. G. Dow (Eds.), *The petroleum system—from source to trap* (pp. 93-120). American Association of Petroleum Geologists Memoir 60.

- Peters, K.E., & Moldowan, J.M. (1993). *The biomarker guide, interpreting molecular fossils in petroleum and ancient sediments*. Englewood Cliff, New Jersey: Prentice Hall.
- Petroleum Agency SA. (2008/9). South African Exploration Opportunities. Cape Town: South African Agency for Promotion of Petroleum Exploration and Exploitation.
- Philp, R.P., & Lewis, C.A. (1987). Organic geochemistry of biomarkers. *Annual Rev. Earth Planet. Sci.* 15. 363-395.
- Potter, P.E., & Pettijohn F.J. (1977), *Paleocurrents and Basin Analysis* (2nd ed.). New York: Springer-Verlag.
- Pysklywec, R.N., & Mitrovica, J.X. (1989). The role of subduction induced subsidence in the evolution of the Karoo Basin. *J. Geol.*, 107, 155-164.
- Reading, H.G. (Ed.). (1996). *Sedimentary Environments and Facies* (2nd ed.). London: Blackwell Sciences Ltd.
- Royden, L.H. (1993). The tectonic expression of slab pull at continental convergent boundaries. *Tectonics*, 12, 303-325.
- Rubidge, B.S. (1995). Biostratigraphy of the Beaufort Group (Karoo Supergroup). *Geological Survey of South Africa, South African Committee for Stratigraphy, Biostratigraphic Series*, 1, 1-46.
- Russell, C.A. (1970). Geochemistry and halmyrolysis of clay minerals, Rio Ameca, Mexico. *Geochim. Cosmochim. Acta*, 34, 893-907.
- SACS. (1980). Stratigraphy of South Africa, Part 1. *Geol. Surv. S. Afr. Handbook*, 8, 690pp.
- Schumacher, B.A. (2002). Methods for the determination of total organic carbon (TOC) in soils and sediments. *Ecological Risk Assessment Support Center*, 25.

- Scheffler, K. (2004). *Reconstruction of sedimentary environment and climate conditions by multi-geochemical investigations of Late Palaeozoic glacial to postglacial sedimentary sequences from SW-Gondwana*. Unpublished PhD thesis, University of Bonn.
- Scheffler, K., Buehmann, D., & Schwark, L. (2006). Analysis of late Palaeozoic glacial to postglacial sedimentary successions in South Africa by geochemical proxies – response to climate evolution and sedimentary environment. *Palaeogeography, Palaeoclimatology, Palaeoecology*, 240, 184-203.
- Schmid, R. (1981). Descriptive nomenclature and classification of pyroclastic deposits and fragments: Recommendations of the International Union of Geological Sciences Subcommittee on the Systematics of Igneous Rocks. *Geology. Geological Society of America*, 9, 41-43.
- Scott, E.D., & Bouma, A. (1998). Influence of tectonics on basin shape and deep water sedimentary fill characteristics: Tanqua and Laingsburg subbasins, southwest Karoo Basin. In J. Almond, J. Anderson, P. Booth, A. Chinsamy-Turan, D. Cole, M.J. de Wit, B.S. Rubidge, R. Smith, J. van beven Donker, & B.C. Storey (Eds.), *Gondwana 10: Event stratigraphy of Gondwana (Abstracts)* (pp. 174). *J. Afr. Earth Sci.*, 27 (1A).
- Seilacher, A. (2001). Concretion morphologies reflecting diagenetic and epigenetic pathways. *Sedimentary Geology*, 143, 41-57.
- Selley, R.C. (1982). *Introduction to sedimentology* (2nd ed.). London: Academic Press Inc.
- Smith, R.M.H. (1990). A review of stratigraphy and sedimentary environments of the Karoo Basin of South Africa. *Journal of African Earth Sciences*, 10 (1-2), 117-137.
- Smith, R.M.H., Eriksson P.G., & Botha W.J. (1993). A review of the stratigraphy and sedimentary environments of the Karoo-aged basins of Southern Africa. *Journal of African Earth Sciences*, 16, 143-169.
- Steyn, J. H. (1983). Geological Map of South Africa. Sutherland, 3320, 1:250 000, Pretoria: Geological Survey of the Republic of South Africa.

- Stollhofen, H., Stanistreet, I.G., Bangert, B., & Grill, H. (2000). Tuffs, tectonism and glacially related sea-level changes, Carboniferous-Permian, southern Namibia. *Palaeogeography, Palaeoclimatology, Palaeoecology*, 161, 127-150.
- Stow, D.A.V., Huc, A.-Y., & Bertrand, P. (2001). Depositional processes of black shales in deep water. *Marine and Petroleum Geology*, 18, 491-498.
- Tankard, A., Welsink, H., Aukes, P., Newton, R., & Stettler, E. (2009). Tectonic evolution of the Cape and Karoo basins of South Africa. *Marine and Petroleum Geology*, 26, 1379-1412.
- Theron, J.N. (1986). Geological Map of South Africa. Ladismith, 3320, 1:250 000, Pretoria: Geological Survey of the Republic of South Africa.
- Theron, J.N., & Blignault, H.J. (1975). A model for the sedimentation of the Dwyka glacials in the southwestern Cape. In K.S.W. Campbell (Ed.), *Gondwana Geology* (pp. 347-356). Australian National University Press.
- Thiry, M., & Jaquin, T. (1993). Clay mineral distribution related to rift activity, sea-level changes and paleoceanography in the Cretaceous of the Atlantic Ocean. *Clay Minerals*, 28, 61-84.
- Thomson, K. (1999). Role of continental break-up, mantle plume development and fault reactivation in the evolution of the Gamtoos Basin, South Africa. *Marine and Petroleum Geology*, 16, 409-429.
- Tiessen, H., & Moir, J.O. (1993). Total and organic carbon. In M.E. Carter (Ed.), *Soil Sampling and Methods of Analysis* (pp. 187-211). Lewis Publishers.
- Tissot, B.P., Pelet, R., & Ungerer, P. (1987). Thermal history of sedimentary basins, maturation indices, and kinetics of oil and gas generation. *American Association of Petroleum Geologists Bulletin*, 71, 1445-1466.

- Tissot, B.P., & Welte, D.H. (1984). *Petroleum formation and occurrence; a New approach to oil gas exploration*. Berlin, Heidelberg, New York: Springer-Verlag.
- Twenhofel, W.H. (1950). *Principles of sedimentology*. New York: McGraw-Hill Book Company, Inc.
- UTA. (2010). *X-ray Diffraction*. Retrieved 2010, from <http://www.uta.edu/ra/cnm/tutorials/images/xrd1.html>
- Van Lente, B. (2004). *Chemostratigraphic trends and provenance of the Permian Tanqua and Laingsburg depocentres, southwestern Karoo basin, South Africa*. Unpublished PhD thesis, University of Stellenbosch.
- Van der Werff, W., & Johnson, S.D. (2003). Deep-sea fan pinch-out geometries and their relationship to fan architecture, Tanqua Karoo basin (South Africa). *International Journal of Earth Science (Geol Rundsch)*, 92, 728-742.
- Veevers, J.J., Cole, D.I., & Cowan, E.J. (1994). Southern Africa: Karoo Basin and Cape Fold Belt. In J.J. Veevers, & C.Mc.A. Powell (Eds.), *Permian-Triassic Pangean Basins and foldbelts along the Panthalassan margin of Gondwanaland* (pp. 223-279). Geological Society of America Memoir, 184.
- Veevers, J.J., & Powell, C.M. (1987). Late Paleozoic glacial episode in Gondwanaland reflected in transgressive-regressive depositional sequences in Euramerica. *Geological Society of America Bulletin*, 98, 475-487.
- Velde, B. (1992). *Introduction to Clay Minerals*. London: Chapman & Hall.
- Velde, B. (1995). *Origin and mineralogy of clays*. Berlin: Springer Verlag.
- Vermeulen, P.D. (2012). A South African perspective on shale gas hydraulic fracturing. In C.D. McCullough, M.A. Lund & L. Wyse (Eds.), *International Mine Water Association Symposium* (pp.755-763). Bunbury.

- Viljoen, J.H.A. (1994). Sedimentology of the Collingham formation, Karoo Supergroup, South Africa. *Journal of Geology*, 97, 167-183.
- Visser, J.N.J. (1989). The Permo-Carboniferous Dwyka Formation of South Africa: deposition by a predominantly subpolar marine ice sheet. *Palaeogeography, Palaeoclimatology and Palaeoecology*, 70, 377-391.
- Visser, J.N.J., & Botha, B.J.V. (1980). Meander belt, point bar, crevasse splay and aeolian deposits from the Elliot Formation in Barkly Pass, northeastern Cape. *Transactions of the Geological Society of South Africa*, 83, 55-62.
- Visser, J.N.J. & Loock, J.C. (1987). Water depth in the main Karoo Basin in South Africa during Permian sedimentation. *Transactions of the Geological Society of South Africa*, 81, 185-191.
- Von Brunn, V. (1977). A furrowed intratillite pavement in the Dwyka Group of northern Natal. *Trans. geol. Soc. S. Afr.*, 80, 125-30.
- Walkley, A. (1935). An Examination of Methods for Determining Organic Carbon and Nitrogen in Soils. *Journal of Agricultural Science*, 25, 598-609.
- Walkley, A., & Black, I.A. (1934). An examination of the Degtjareff method for determining organic carbon in soils: Effect of variations in digestion conditions and of inorganic soil constituents. *Soil Sci.*, 63, 251-263.
- Weaver, C.E. (1989). Clays, muds, and shales. *Developments in Sedimentology*, 44, 819.
- Wenk, H.-R. & Bulakh, A. (2006). *Minerals: their constitution and origin*. New York: Cambridge University Press.
- Wickens, H. de V. (1994). *Basin floor fan building turbidites of the southwestern Karoo Basin, Ecca Group, South Africa*. Unpublished PhD thesis, University of Port Elizabeth.
- Wild, R.J. (2005). *Sedimentological and Sequence Stratigraphic evolution of a Permian Lower Slope to Shelf Succession, Tanqua Depocentre, SW Karoo Basin, South Africa*. Unpublished PhD thesis, University of Liverpool.

- Wilkinson, M., Haszeldine R.S., & Fallick, A.E. (2006). Hydrocarbon filling and leakage history of a deep geopressed sandstone, Fulmar Formation, United Kingdom North Sea. *American Association of Petroleum Geologists Bulletin*, 90(12), 1945-1961.
- Wilson, J.L. (1975). *Carbonate Facies in Geologic History*. Berlin: Springer-Verlag.
- Wilson, H.H. (1969). Late Cretaceous and eugeosynclinal sedimentation, gravity tectonics and ophiolite emplacement in Oman Mountains, southeast Arabia. *American Association of Petroleum Geologists Bulletin*, 53, 626-671.
- Woolnough, W.G. (1937). Sedimentation in barred basins and source rocks of oil. *American Association of Petroleum Geologists Bulletin*, 21, 1101-1157.
- Yuretich, R., Melles, M., Sarata, B., & Grobe, H. (1999). Clay minerals in the sediments of Lake Baikal: A useful climate proxy. *Journal of Sedimentary Research*, 69(3), 588-596.



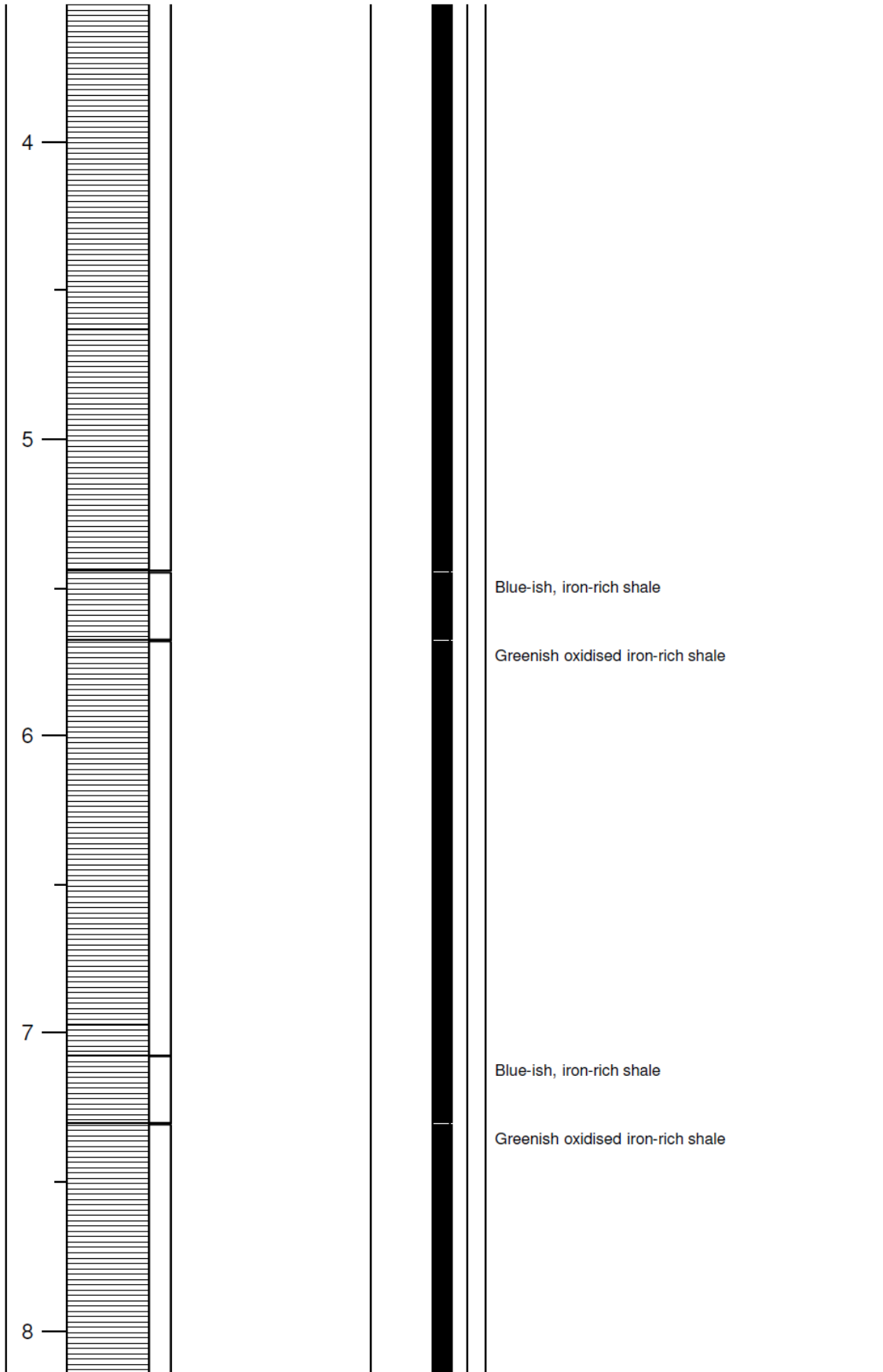
UNIVERSITY of the
WESTERN CAPE

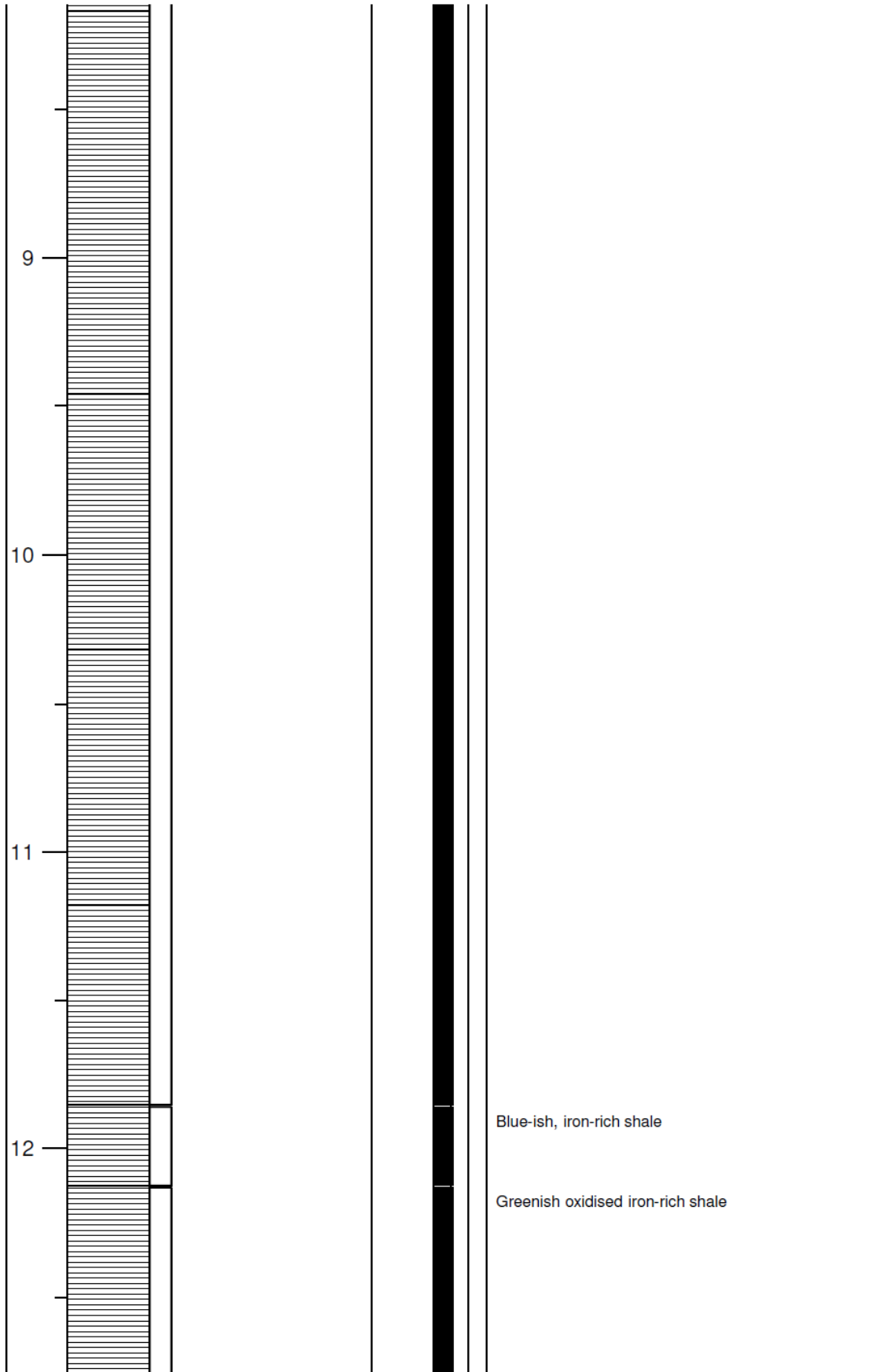


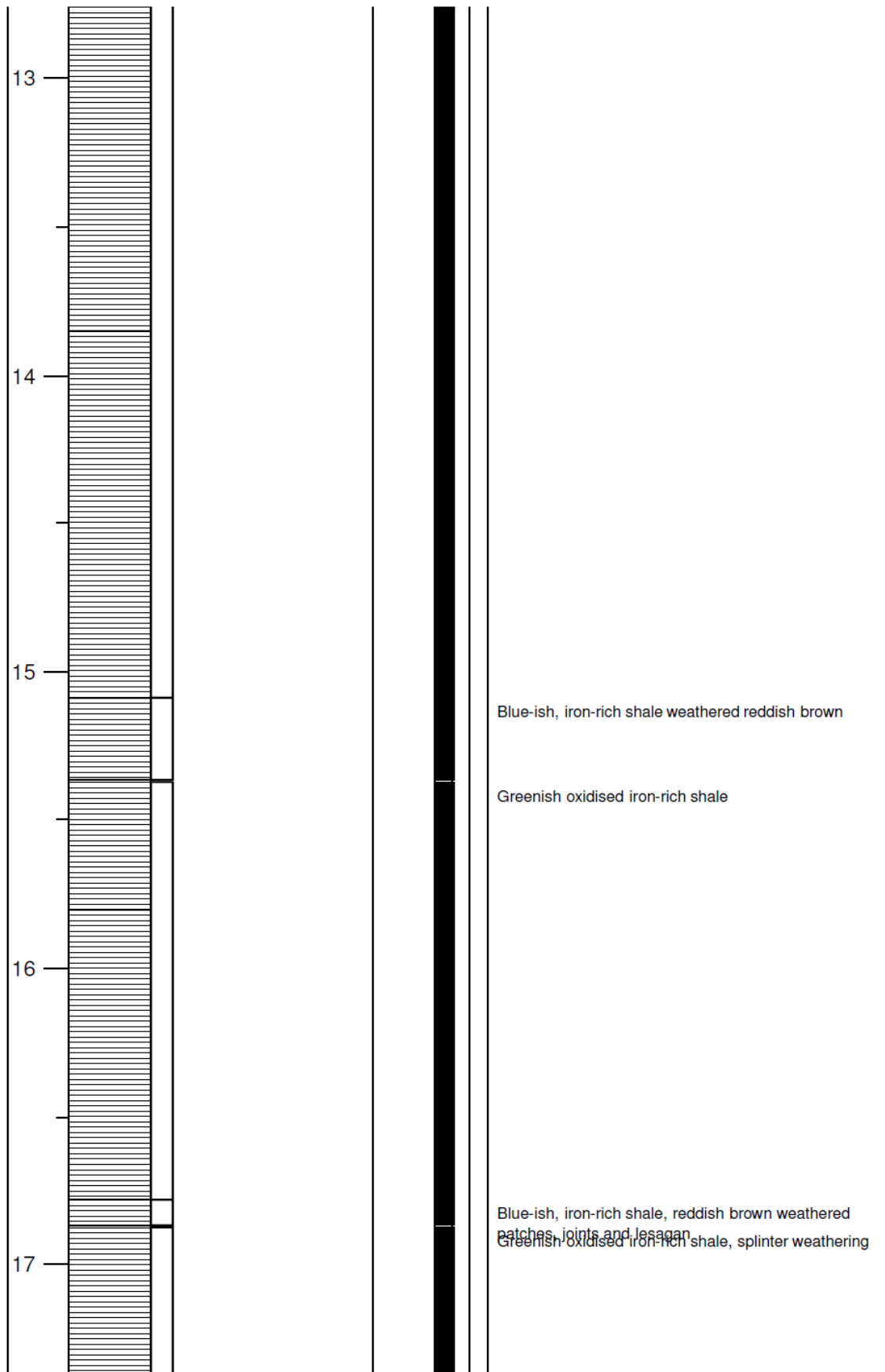
Appendix A

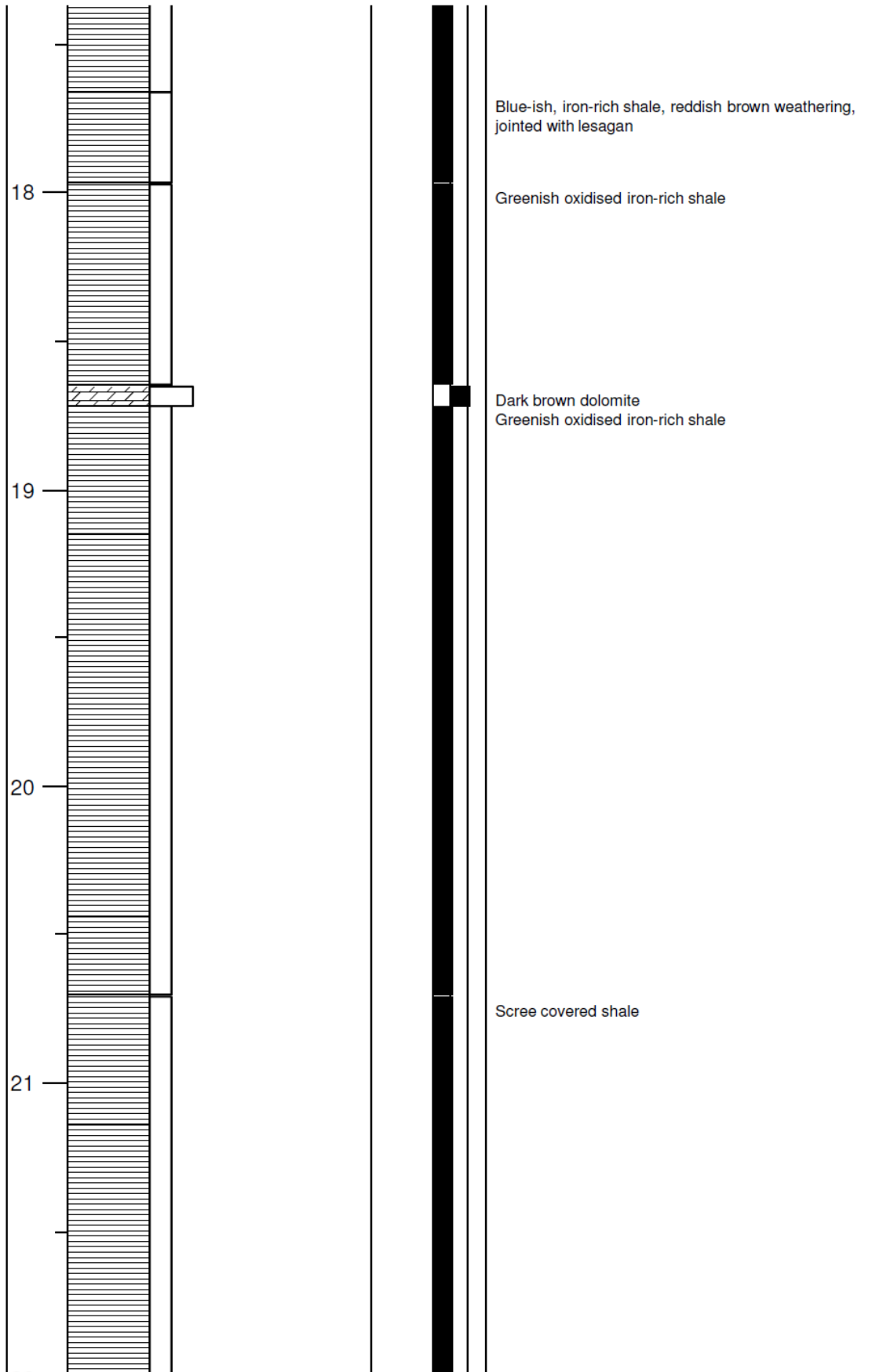
UNIVERSITY *of the*
WESTERN CAPE

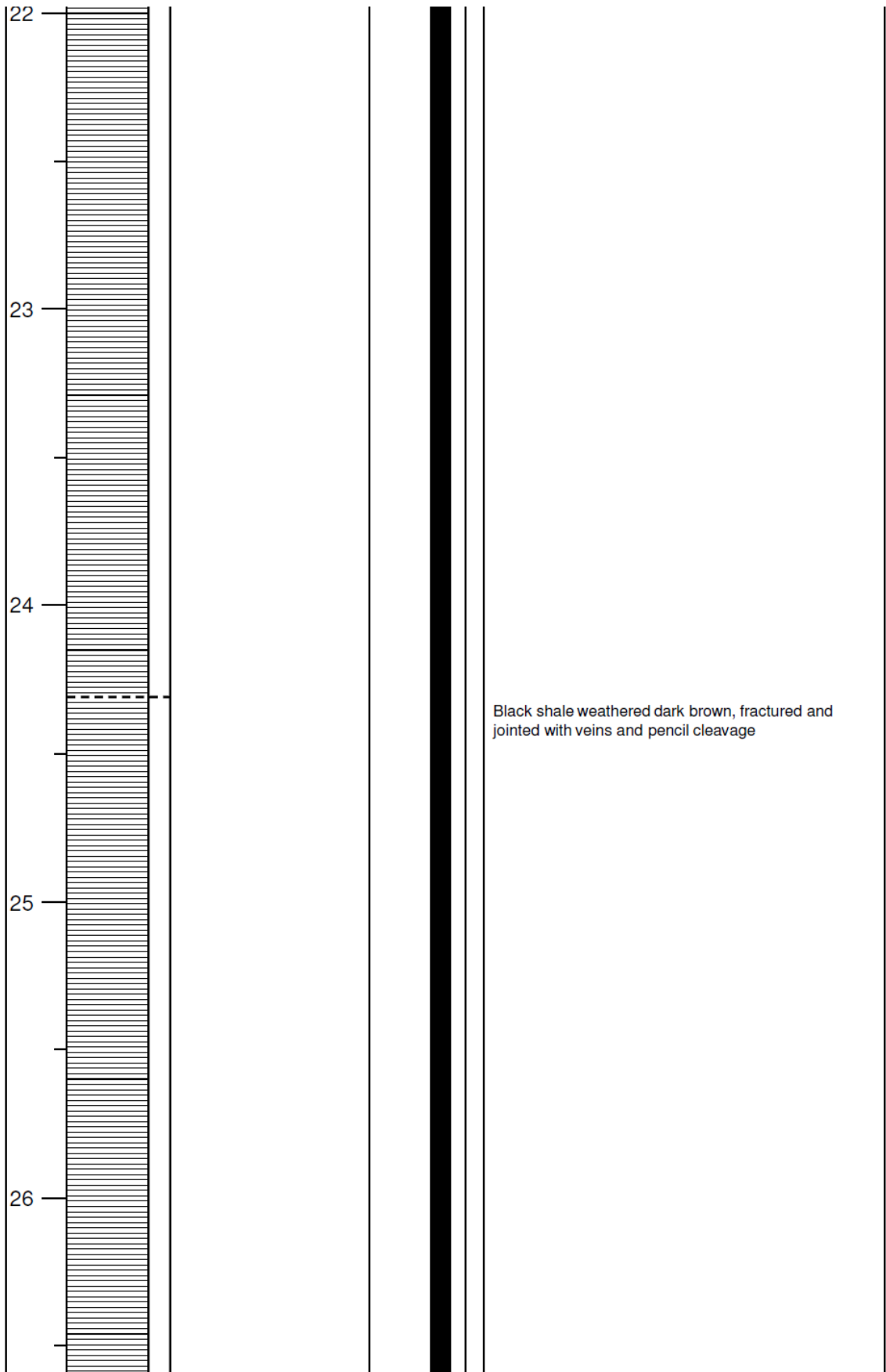
Prince Albert Formation						
SCALE (m)	LITHOLOGY	LIMESTONES		STRUCTURES / FOSSILS	FACIES	NOTES
		mud wacke pack grain	rud & bound			
		clay silt vf f c	m vc	gran pebb cobb boul		
1						Black shale, fractured and jointed with veins
2						Greenish oxidised iron-rich shale
3						Blue-ish, iron-rich shale
						Greenish oxidised iron-rich shale
						Blue-ish, iron-rich shale
						Greenish oxidised iron-rich shale

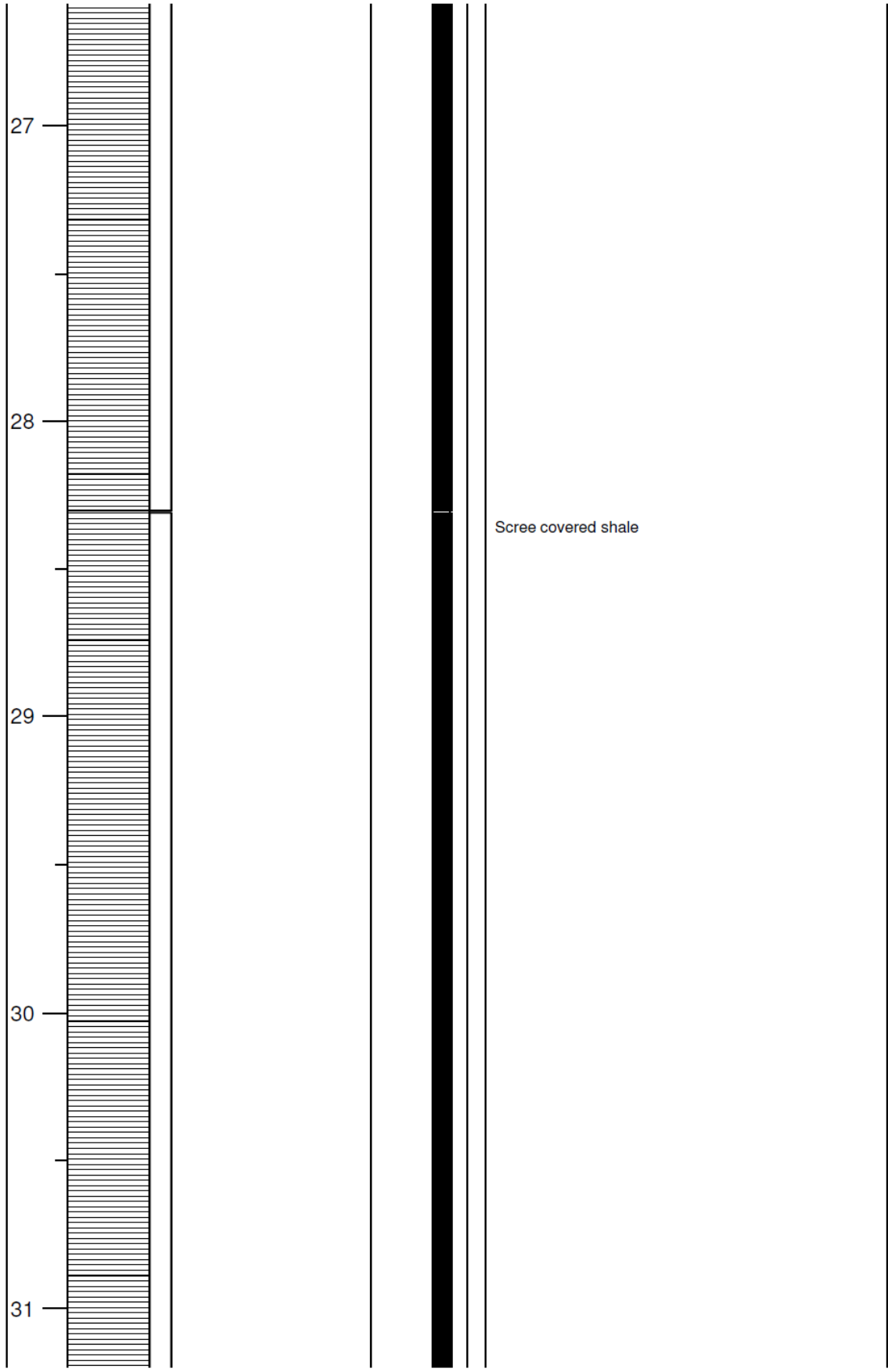


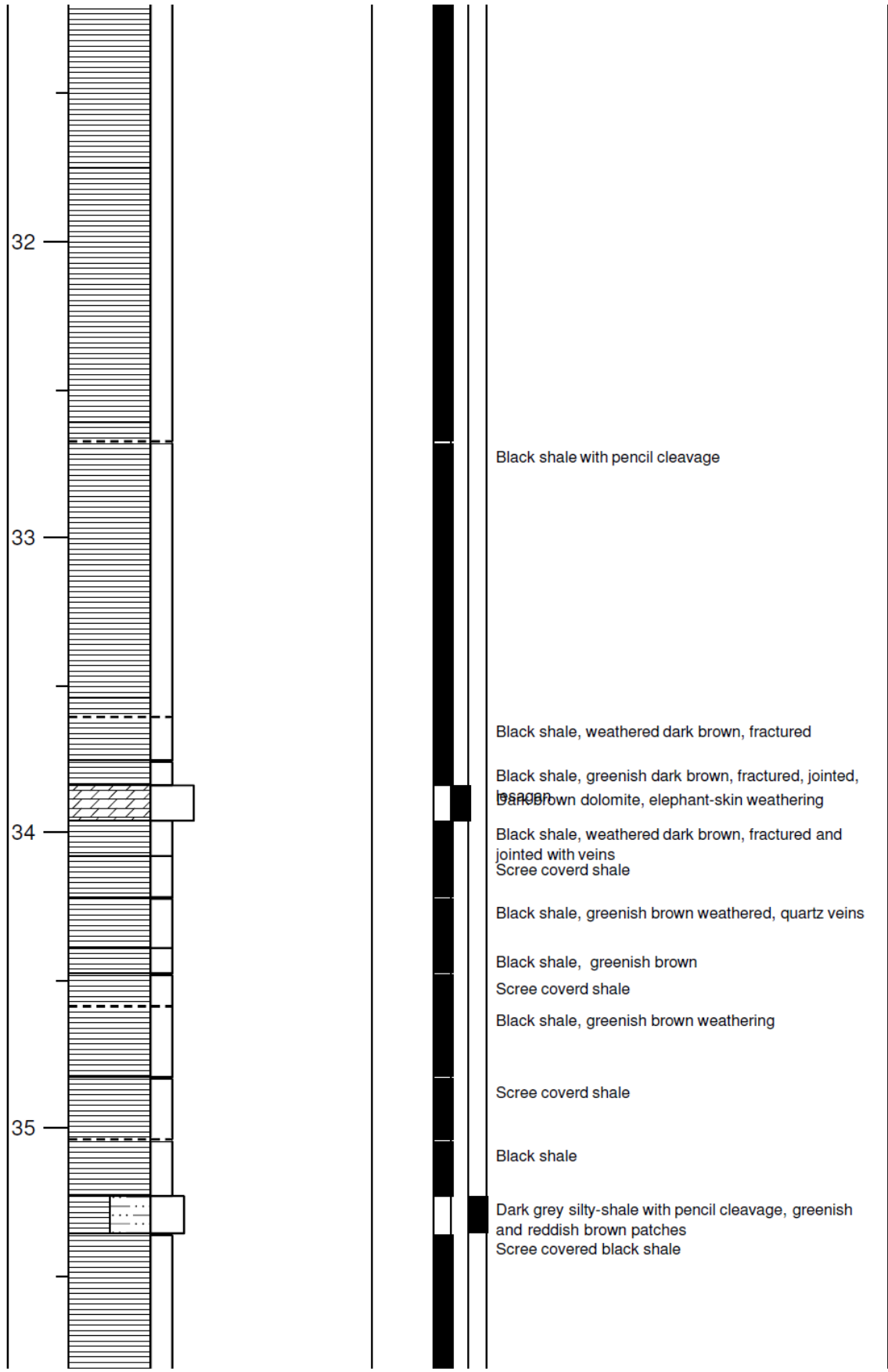


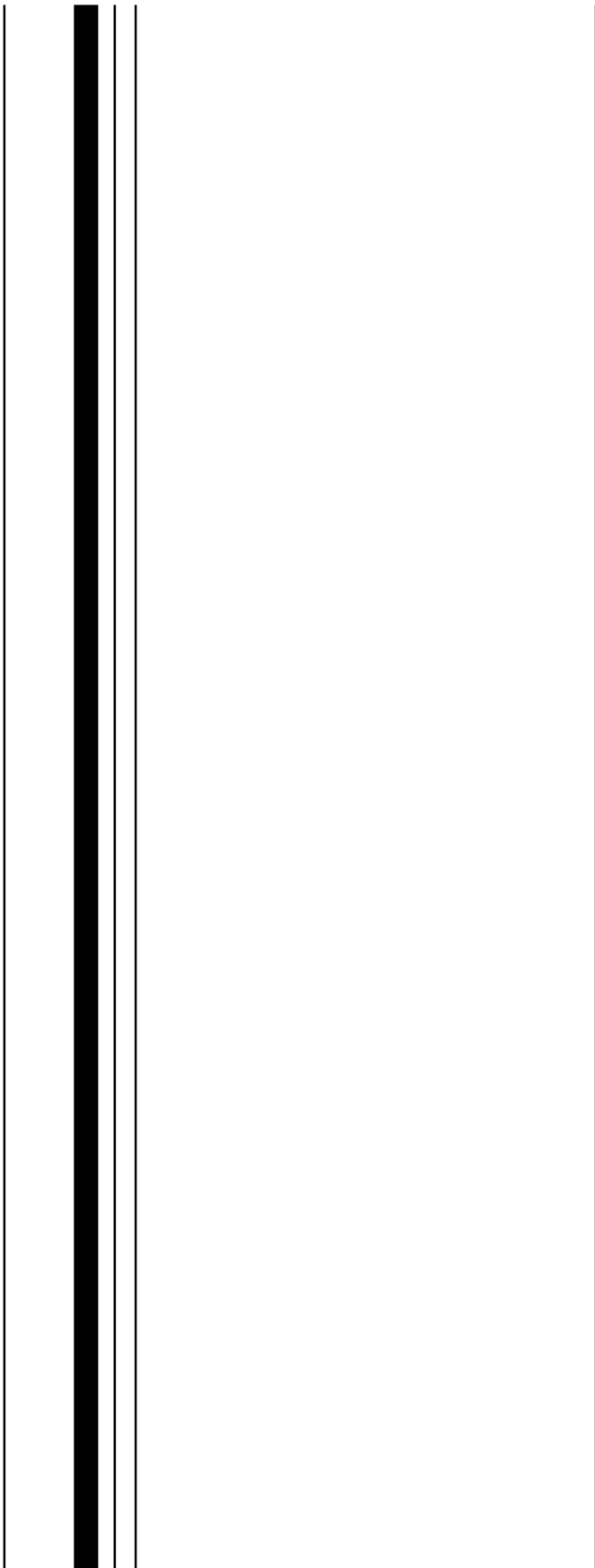
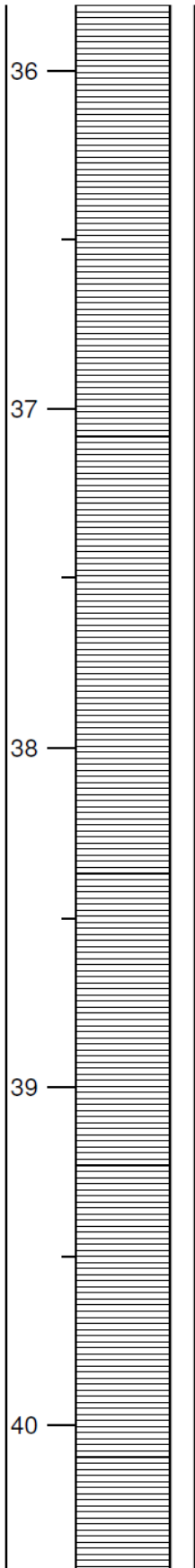


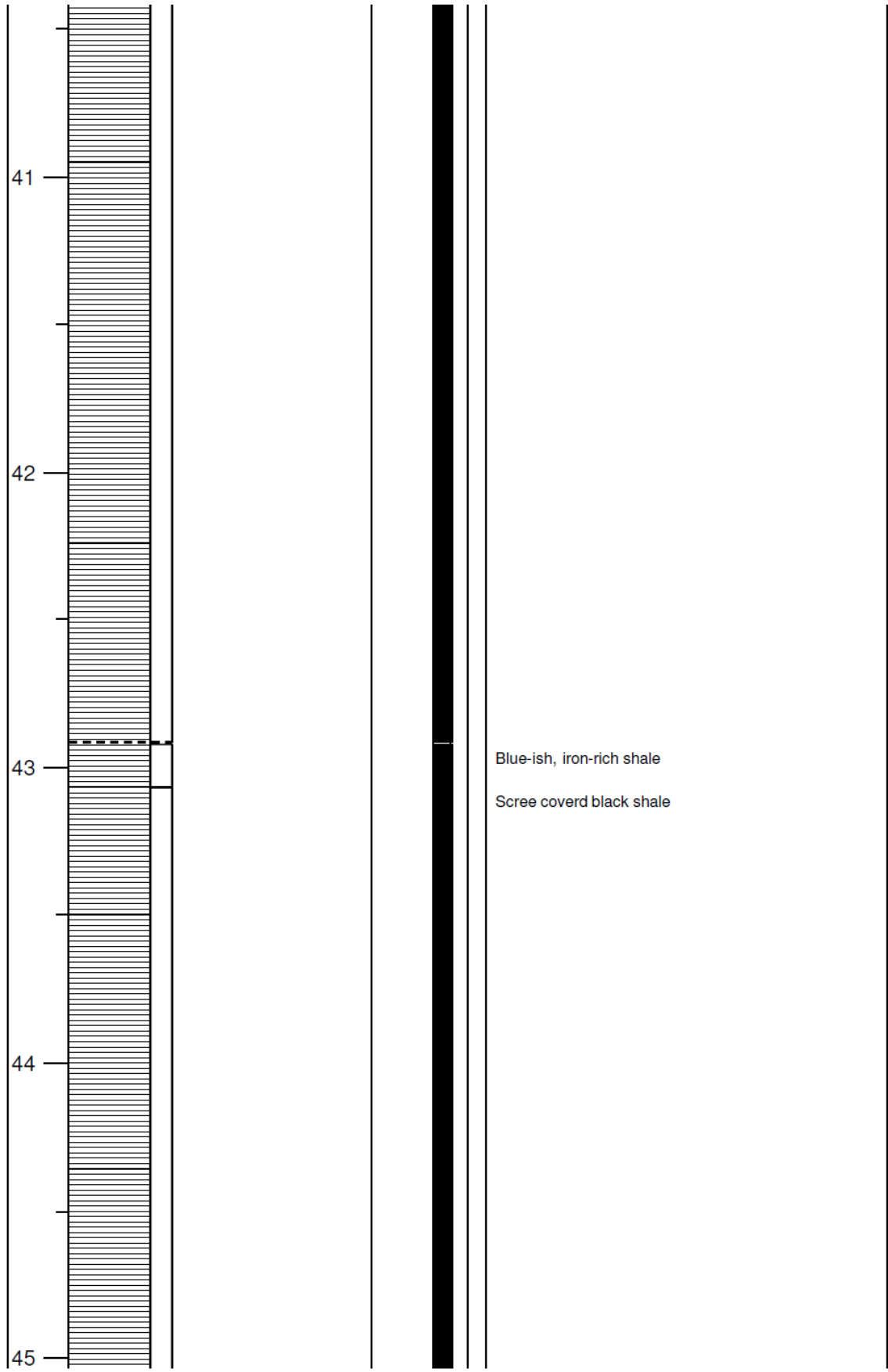


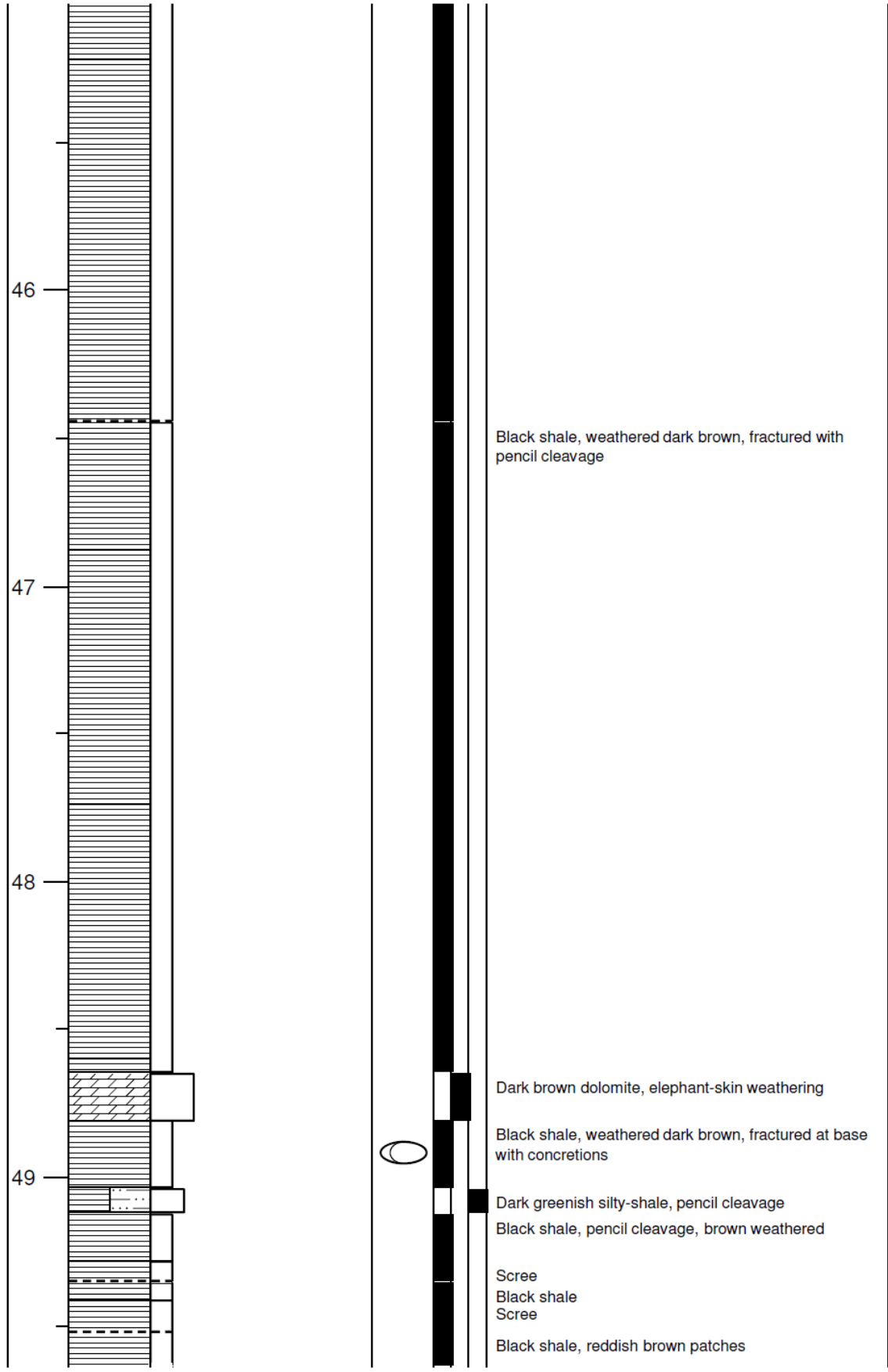


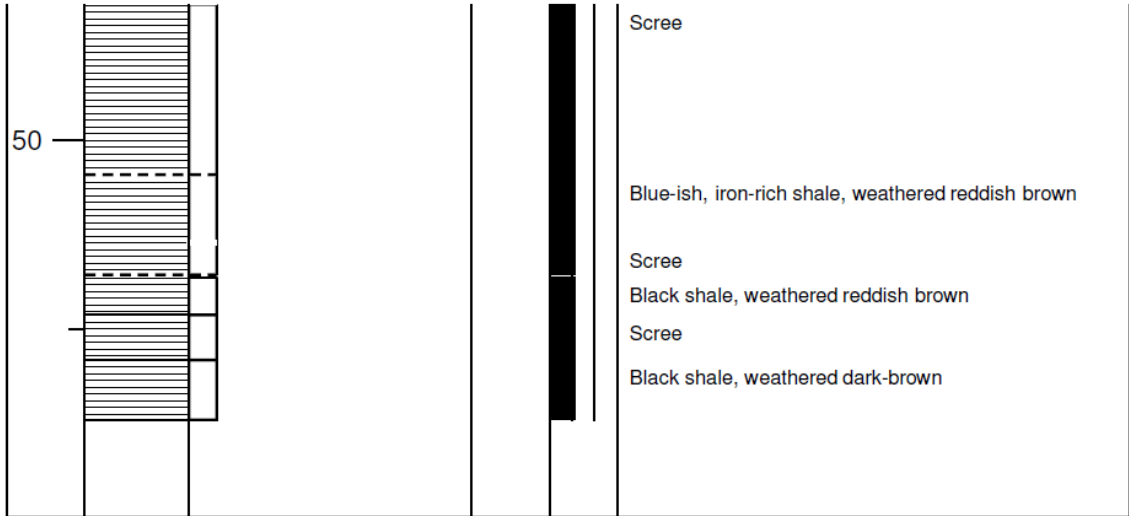








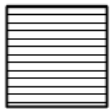




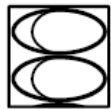
Lithologies

Symbols

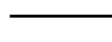
Base Boundaries



Shale



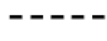
Nodules and concretions



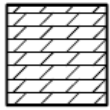
Sharp



Siltstone



Gradational



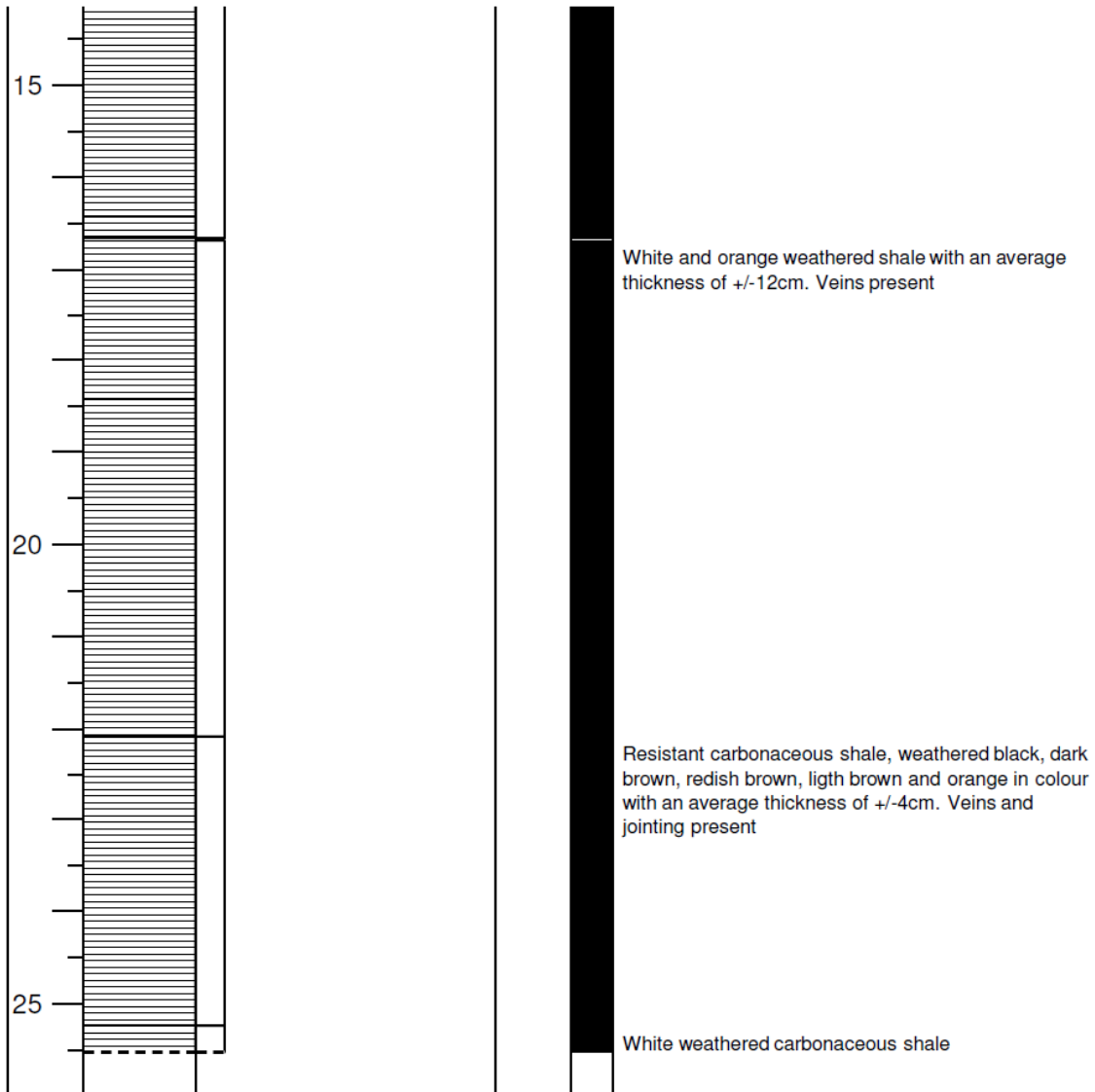
Dolomite



Appendix B

UNIVERSITY *of the*
WESTERN CAPE

Whitehill Formation						
SCALE (m)	LITHOLOGY	LIMESTONES		STRUCTURES / FOSSILS	FACIES	NOTES
		mud wacke pack grain	rud & bound			
		clay silt vf f c	m vc gran pebb cobb boul		1	
5						White, grey and cream weathered carbonaceous shale beds (+/-4cm thick) with fracturing. White weathered carbonaceous shale
						Resistant dark brown shale beds averaging +/-6cm in thickness
						Extremely weathered carbonaceous shale
						White weathered carbonaceous shale
						White, brown and orange weathered beds, averaging +/-8.5cm in thickness. Veins present
10						White weathered carbonaceous shale

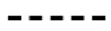


Lithologies

Base Boundaries



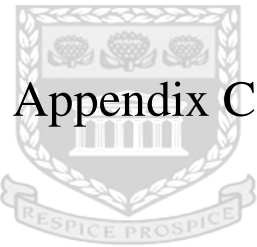
Shale



Gradational

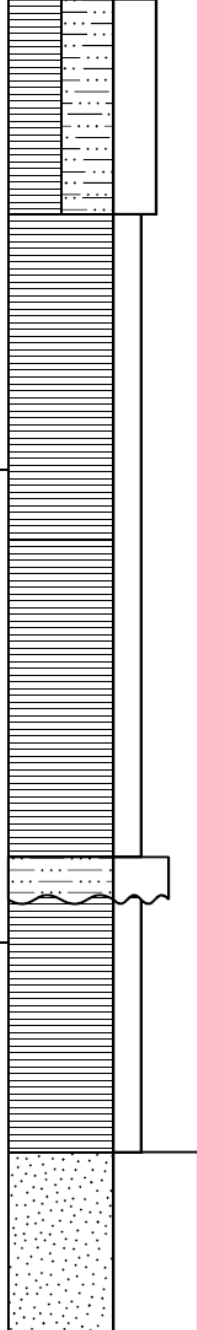


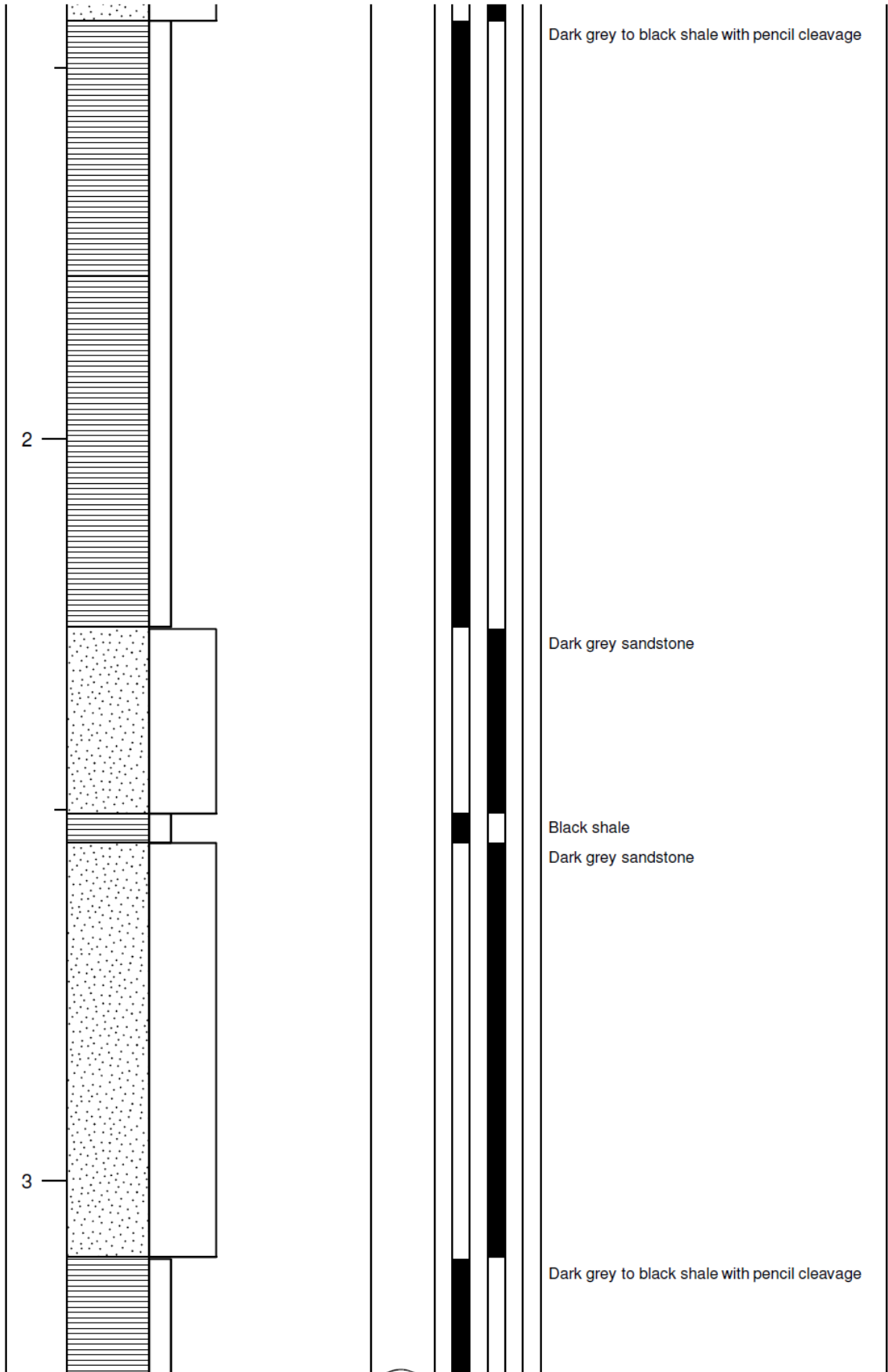
Sharp

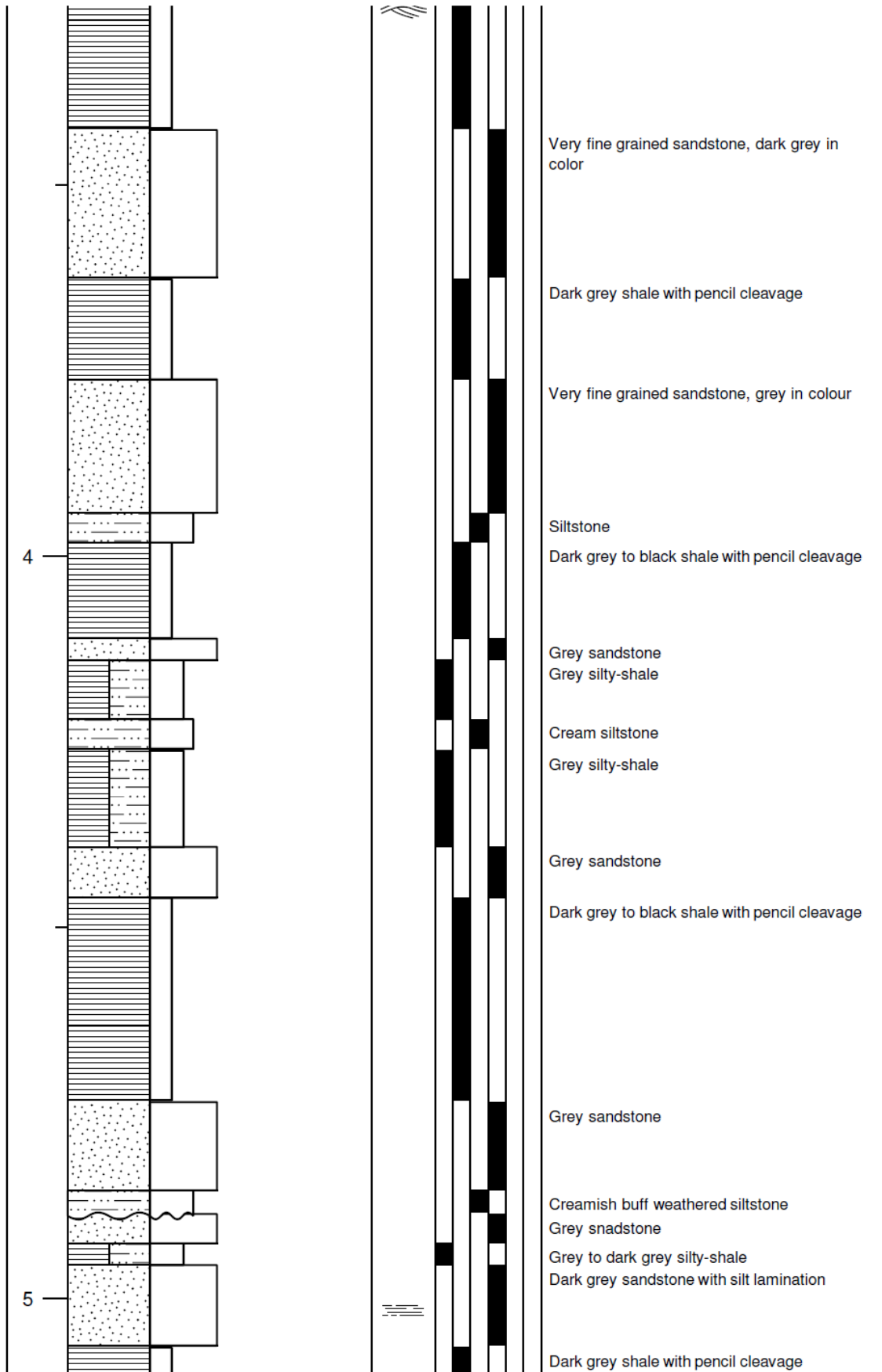


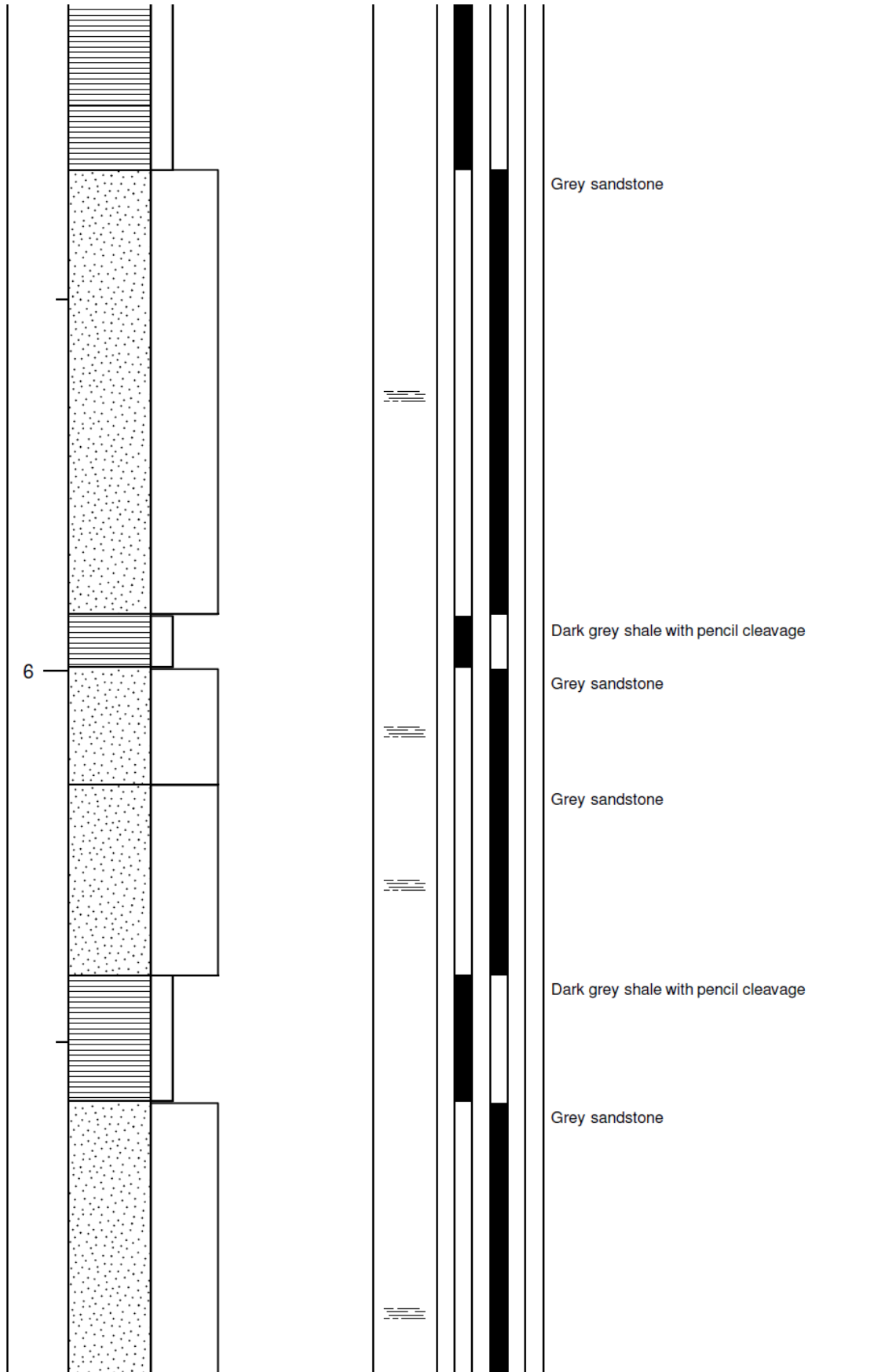
Appendix C

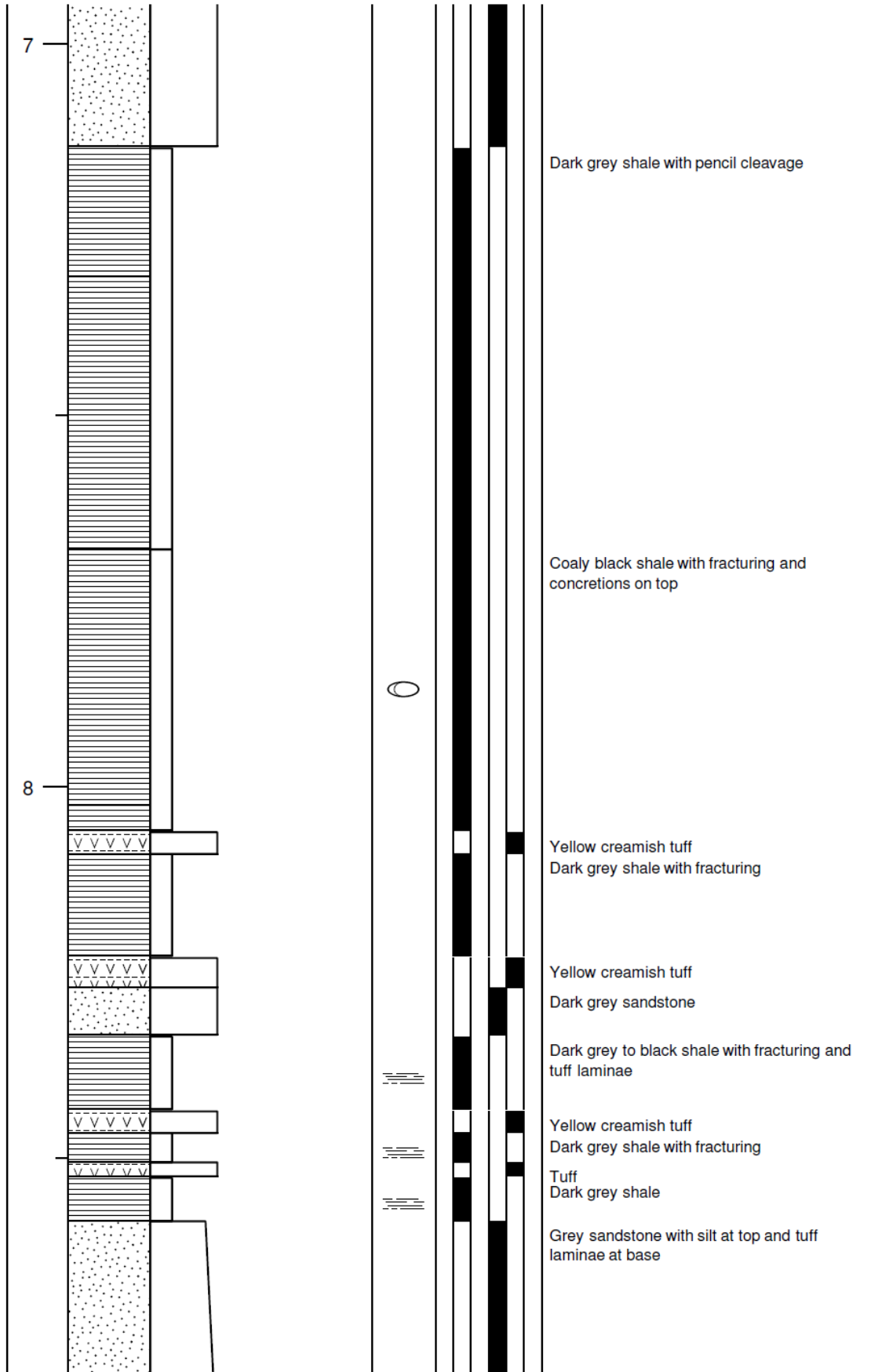
UNIVERSITY *of the*
WESTERN CAPE

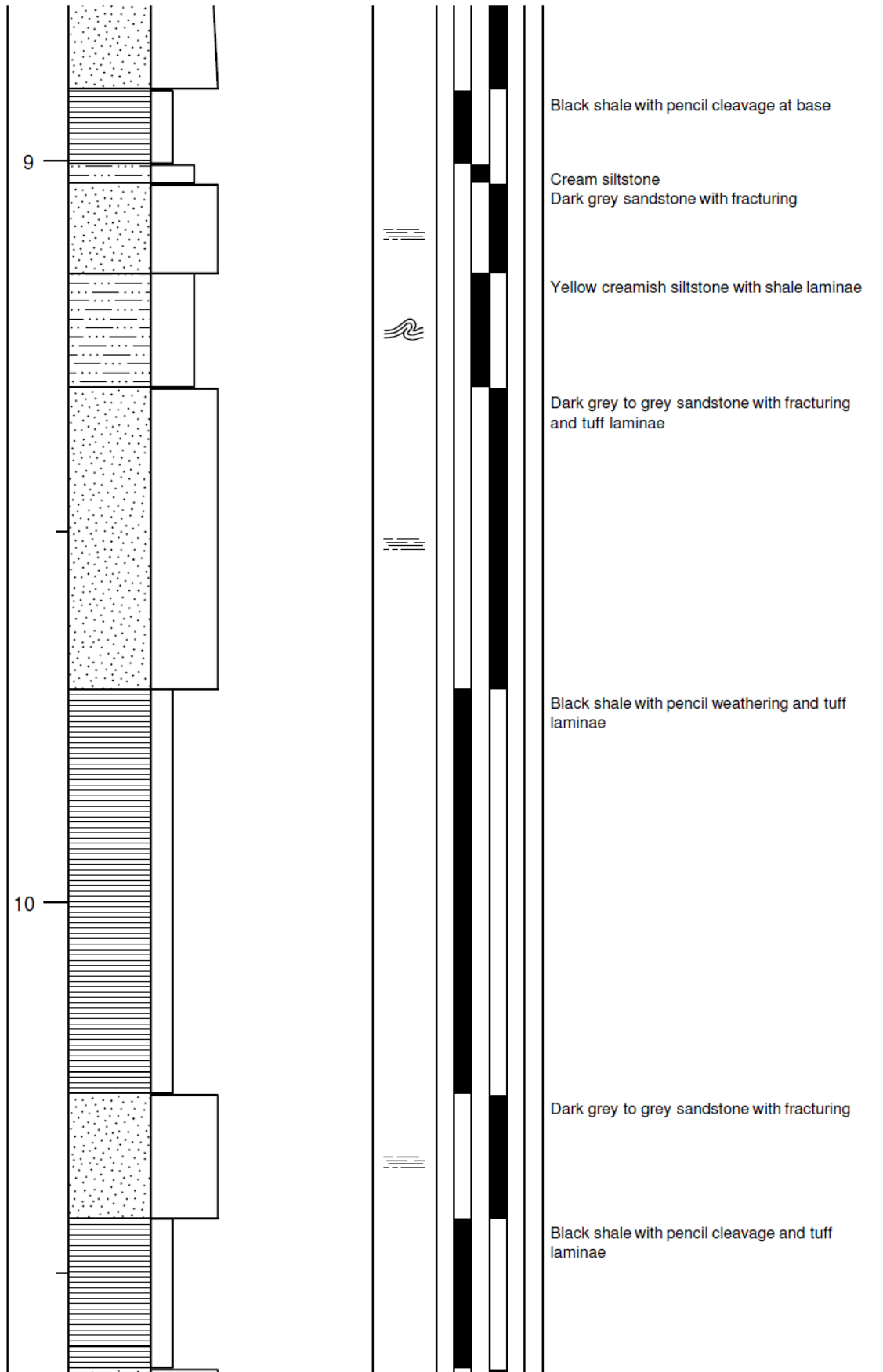
Collingham Formation													
SCALE (m)	LITHOLOGY	LIMESTONES					STRUCTURES / FOSSILS	FACIES	NOTES				
		mud	wacke	pack	grain	rud & bound							
		MUD SANDGRAVEL											
		clay	silt	vf	m	vc	gran	pebb	cobb	boul		1 2 3 4 5 6	
													Grey silty-shale
													Dark grey to black shale with pencil cleavage
													Buff weathered siltstone
													Dark grey to black shale with pencil cleavage
													Very fine grained sandstone, dark grey with dark brown weathering

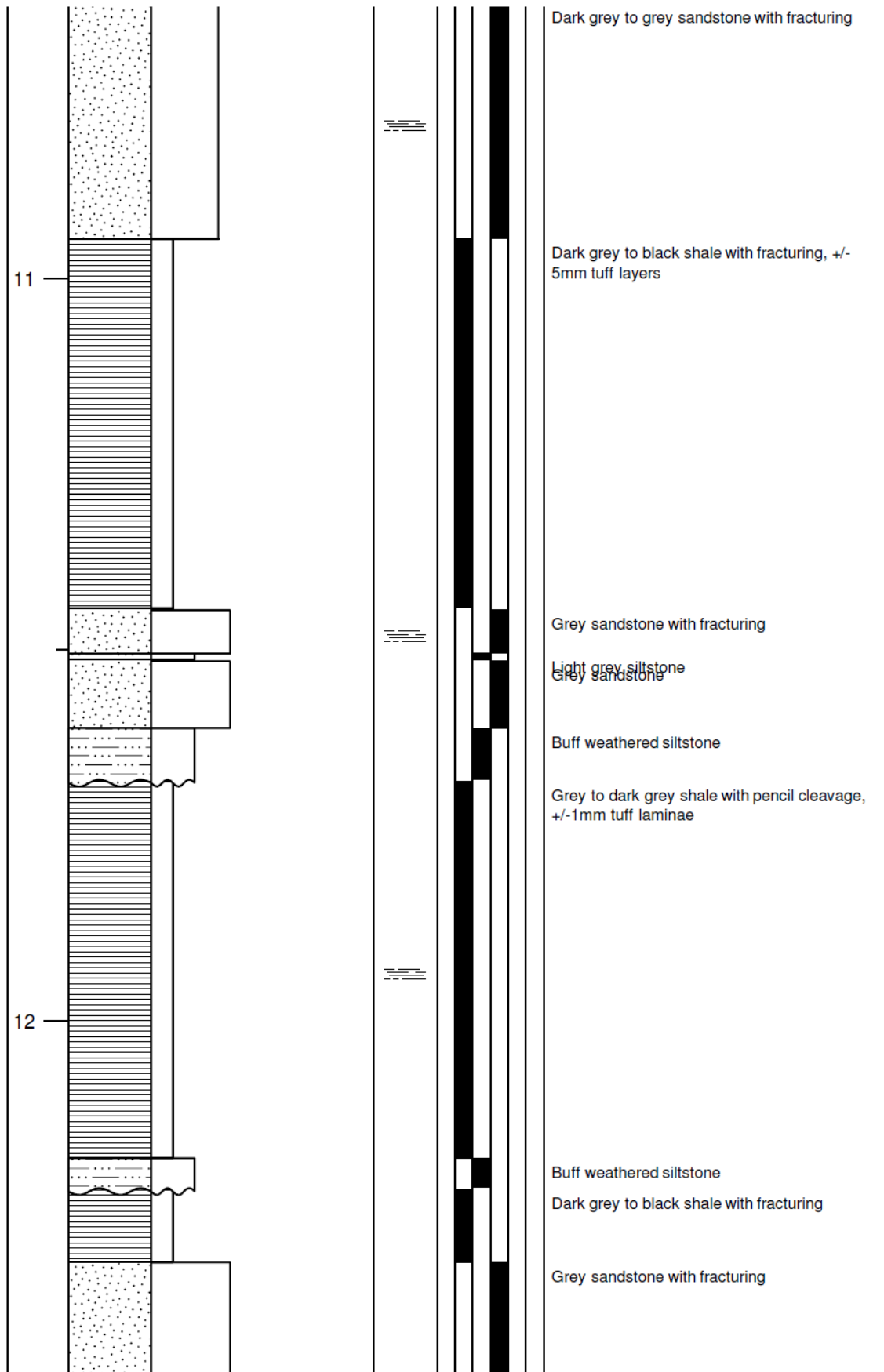


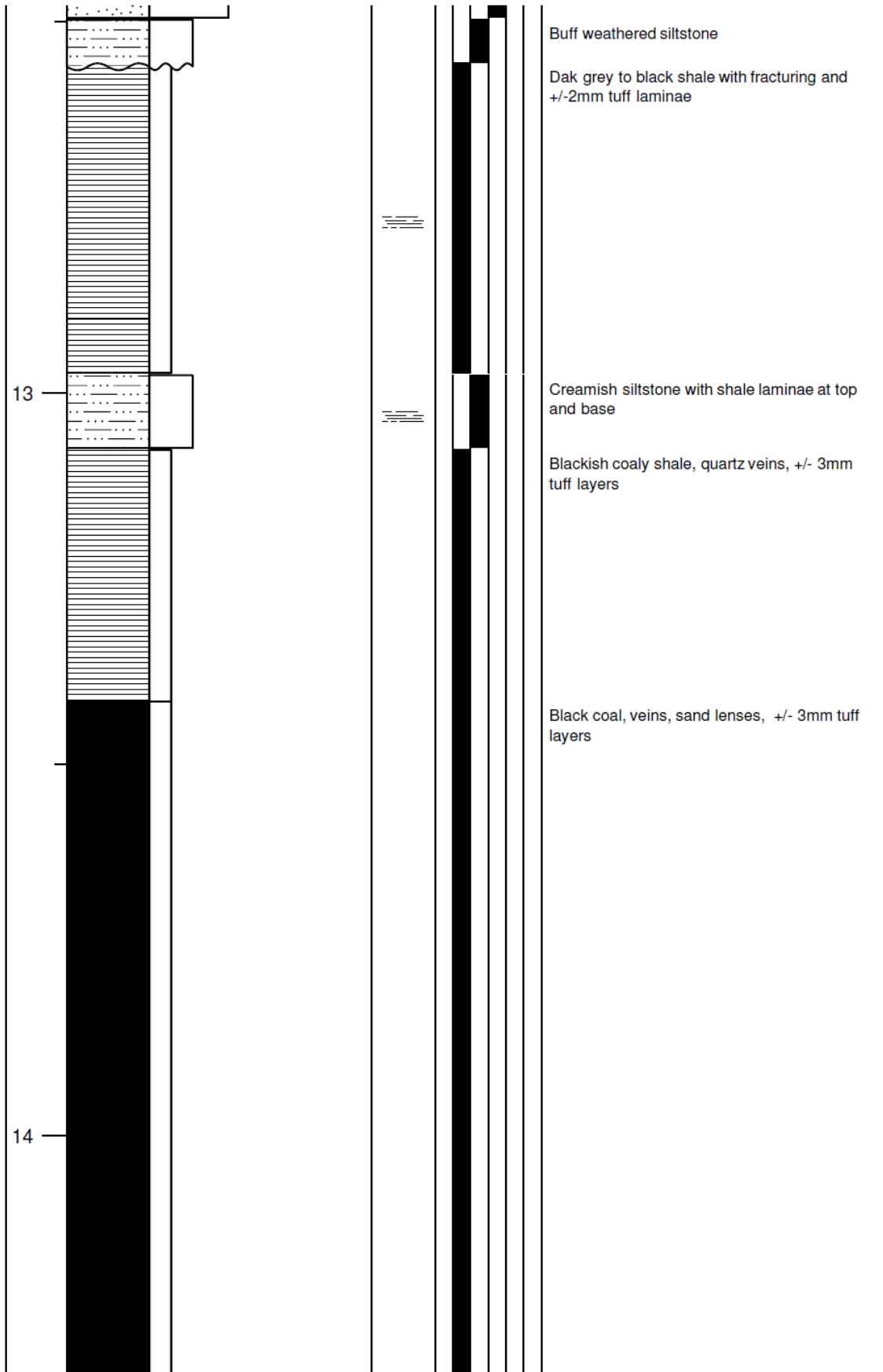


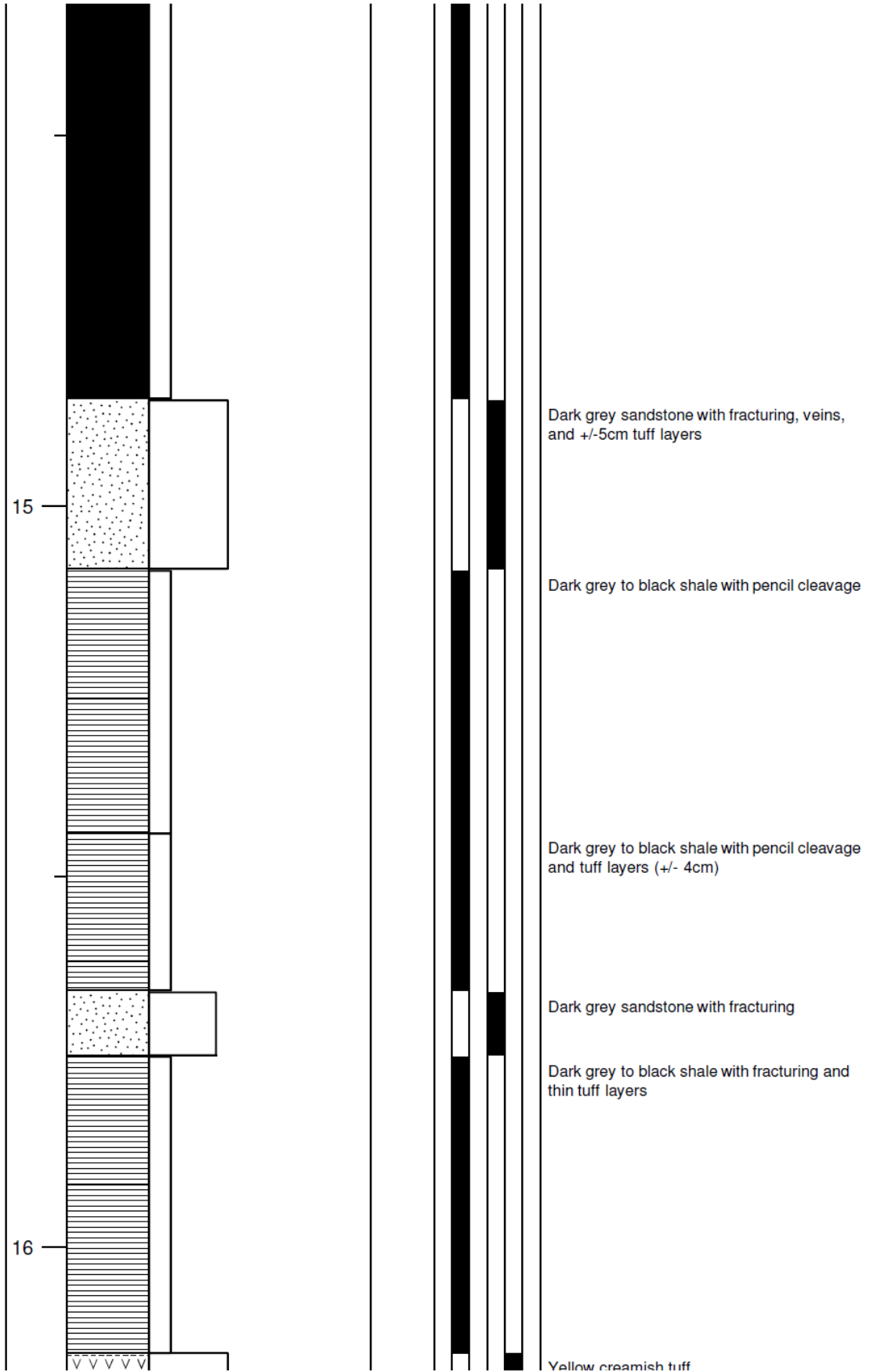


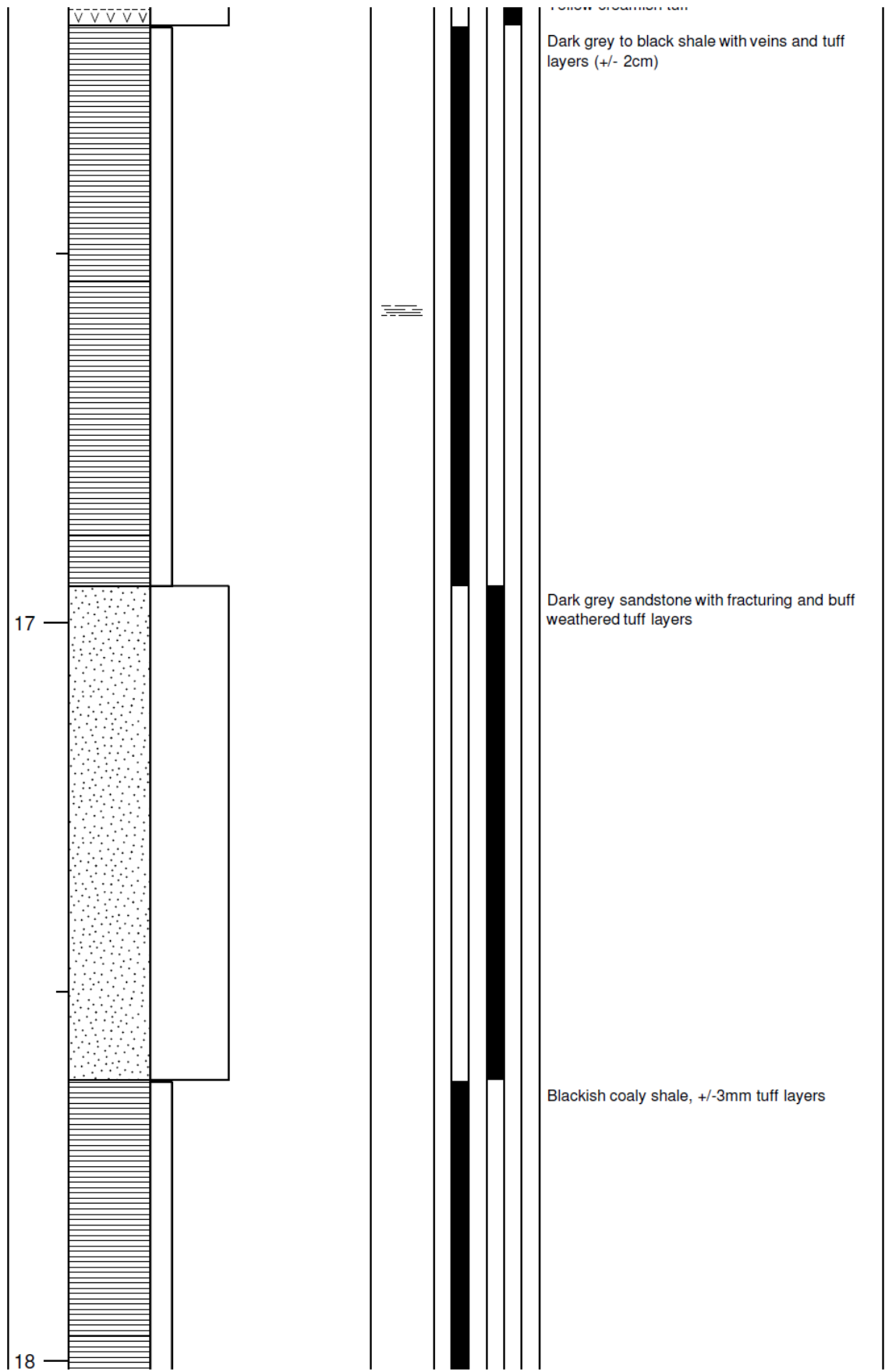


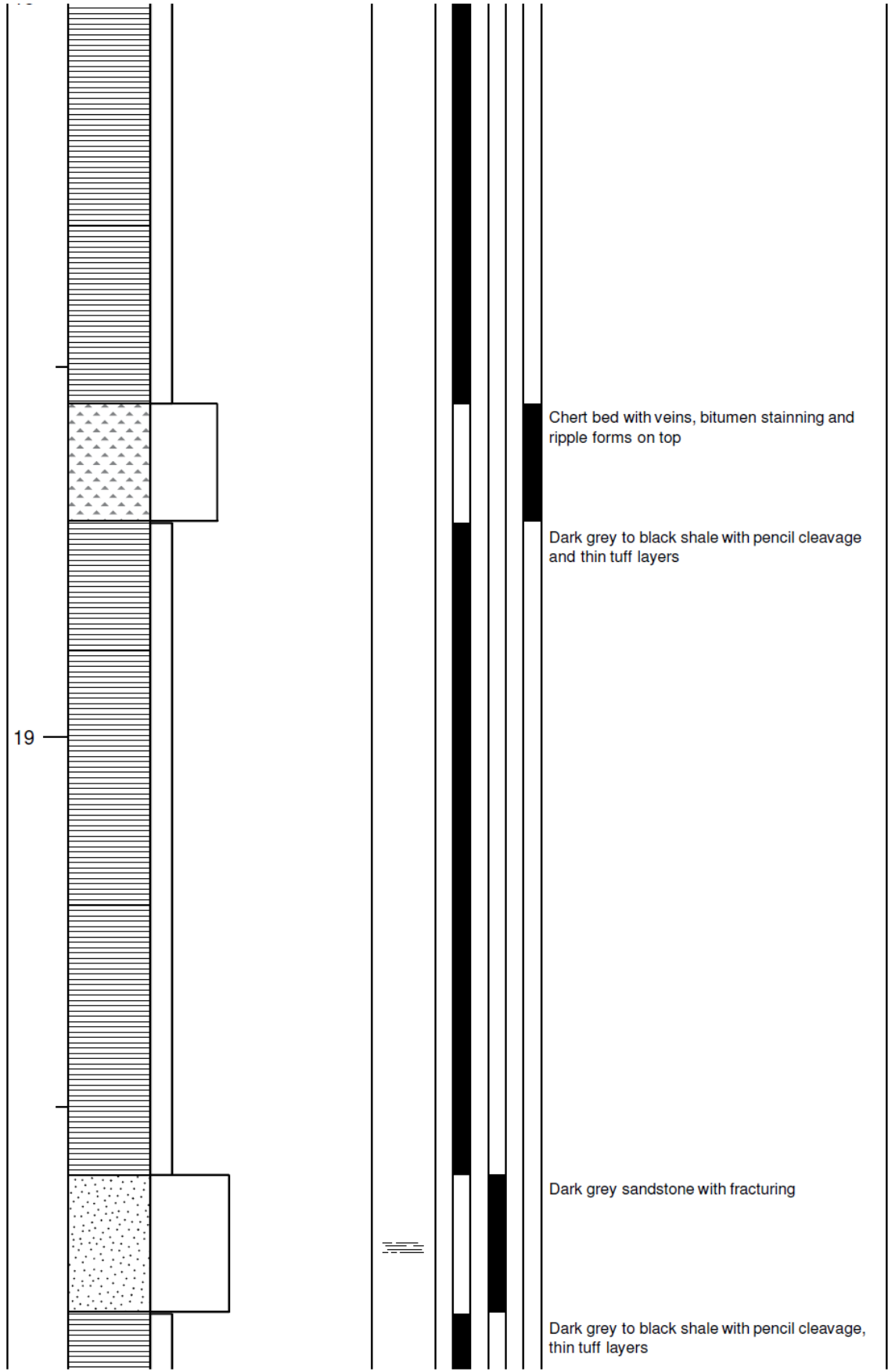


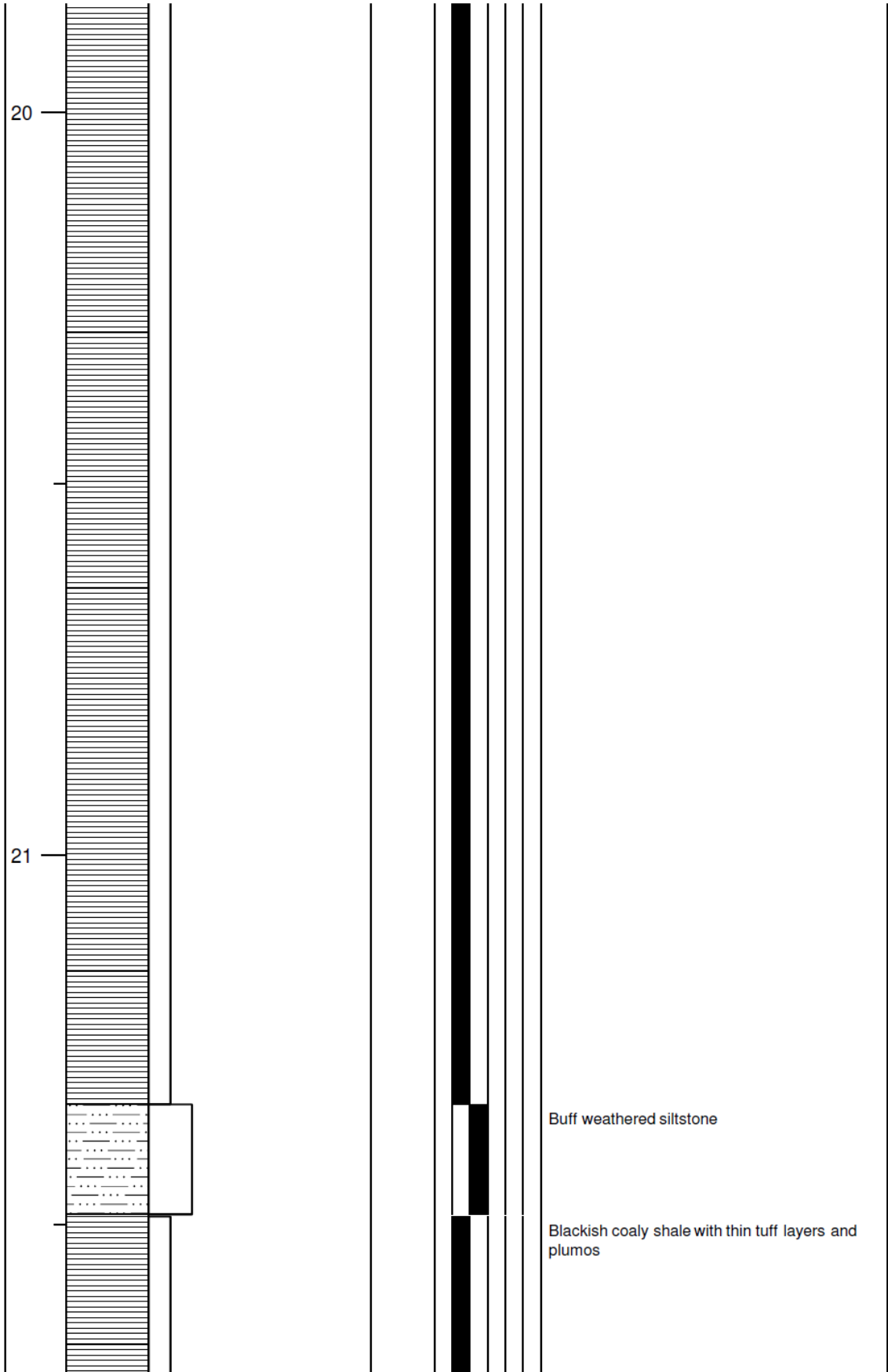


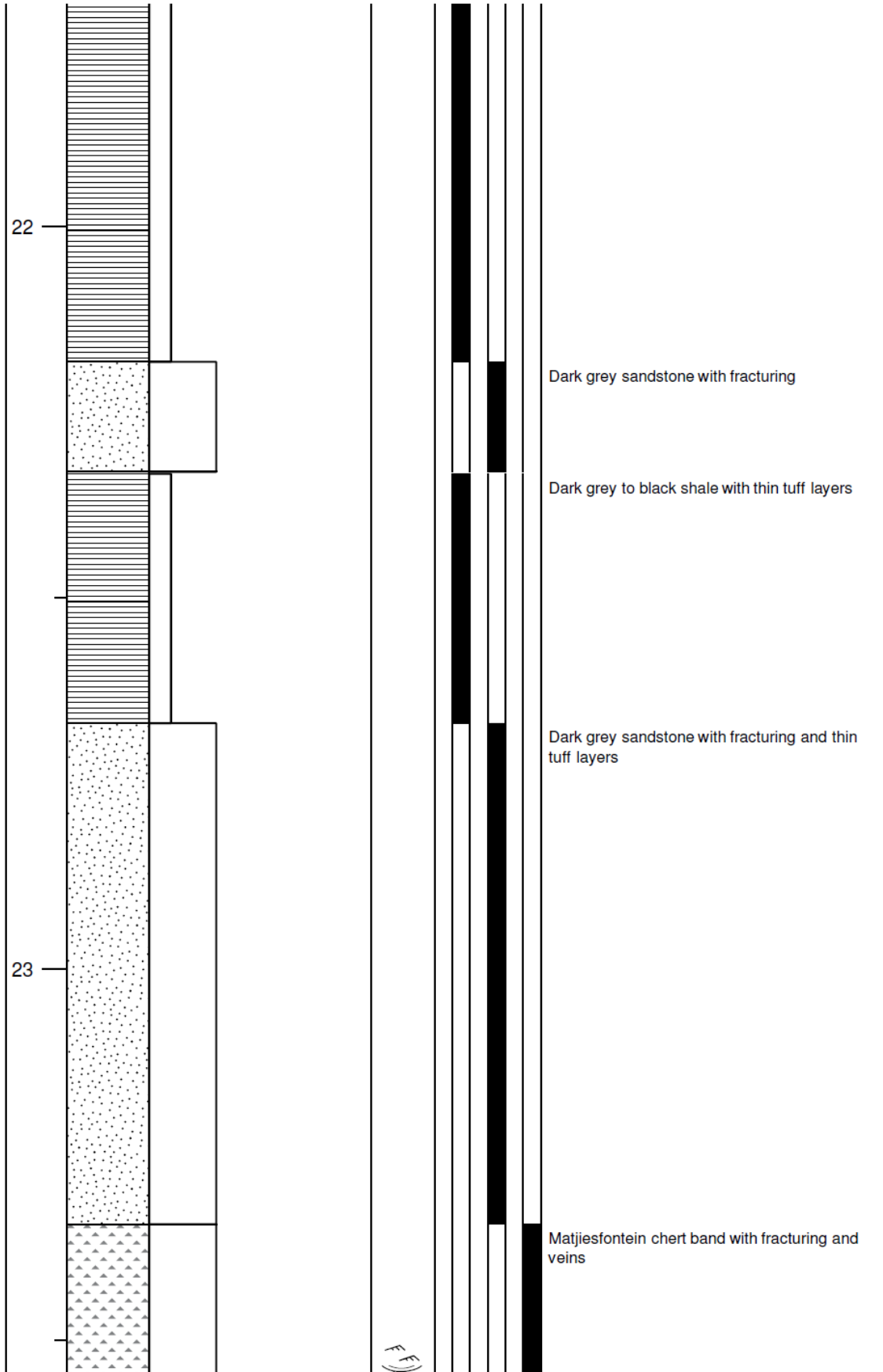


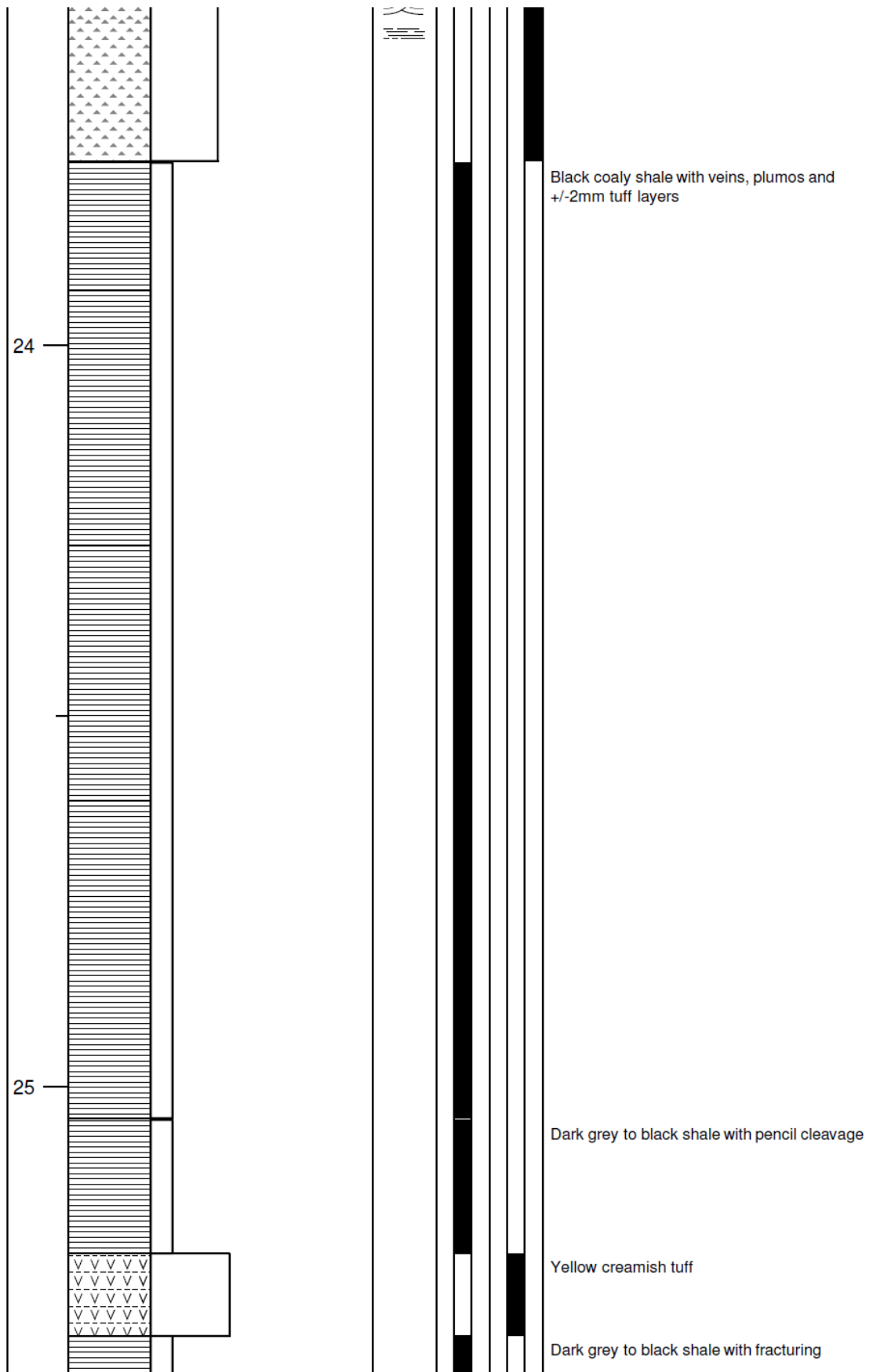


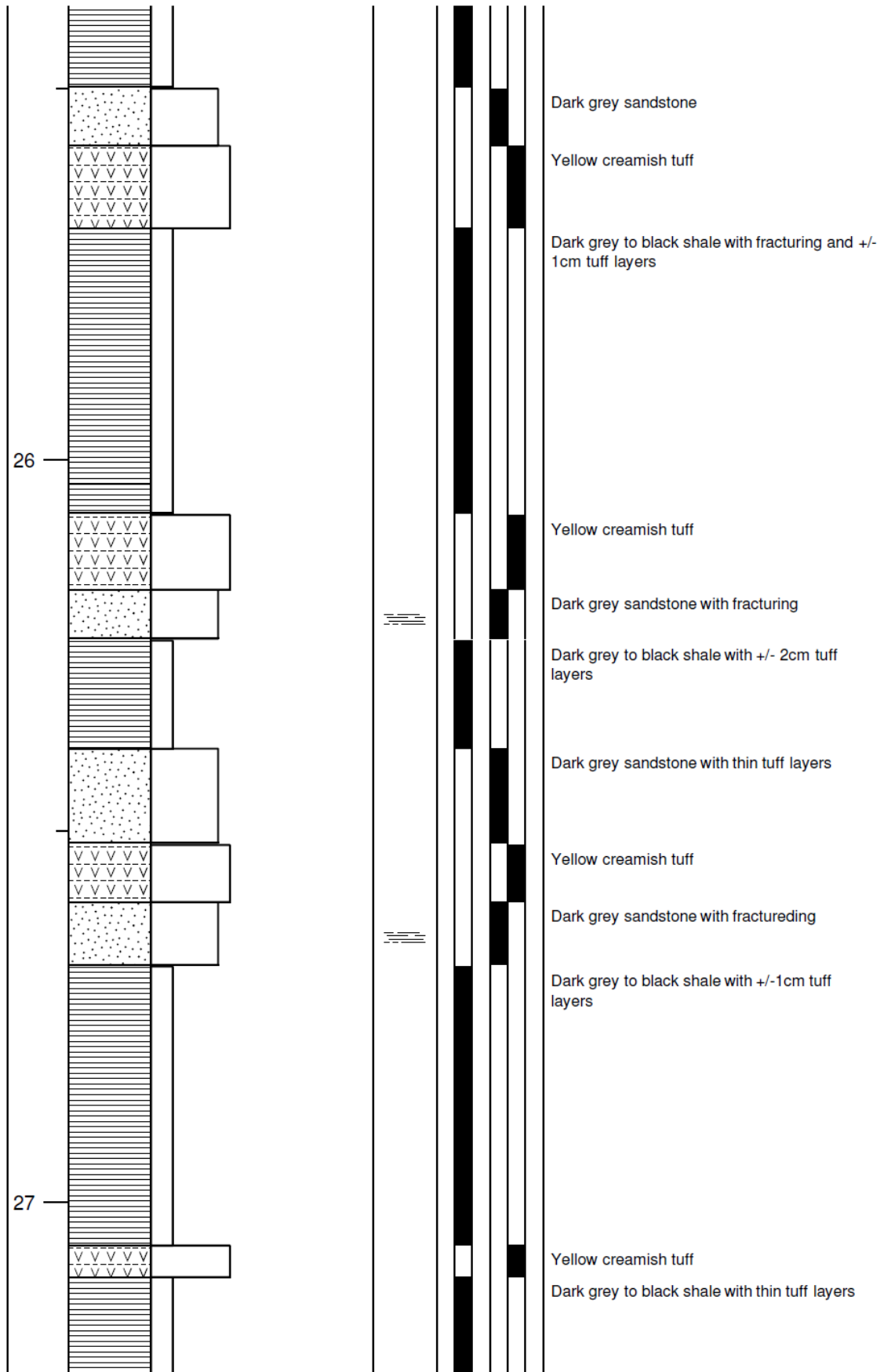


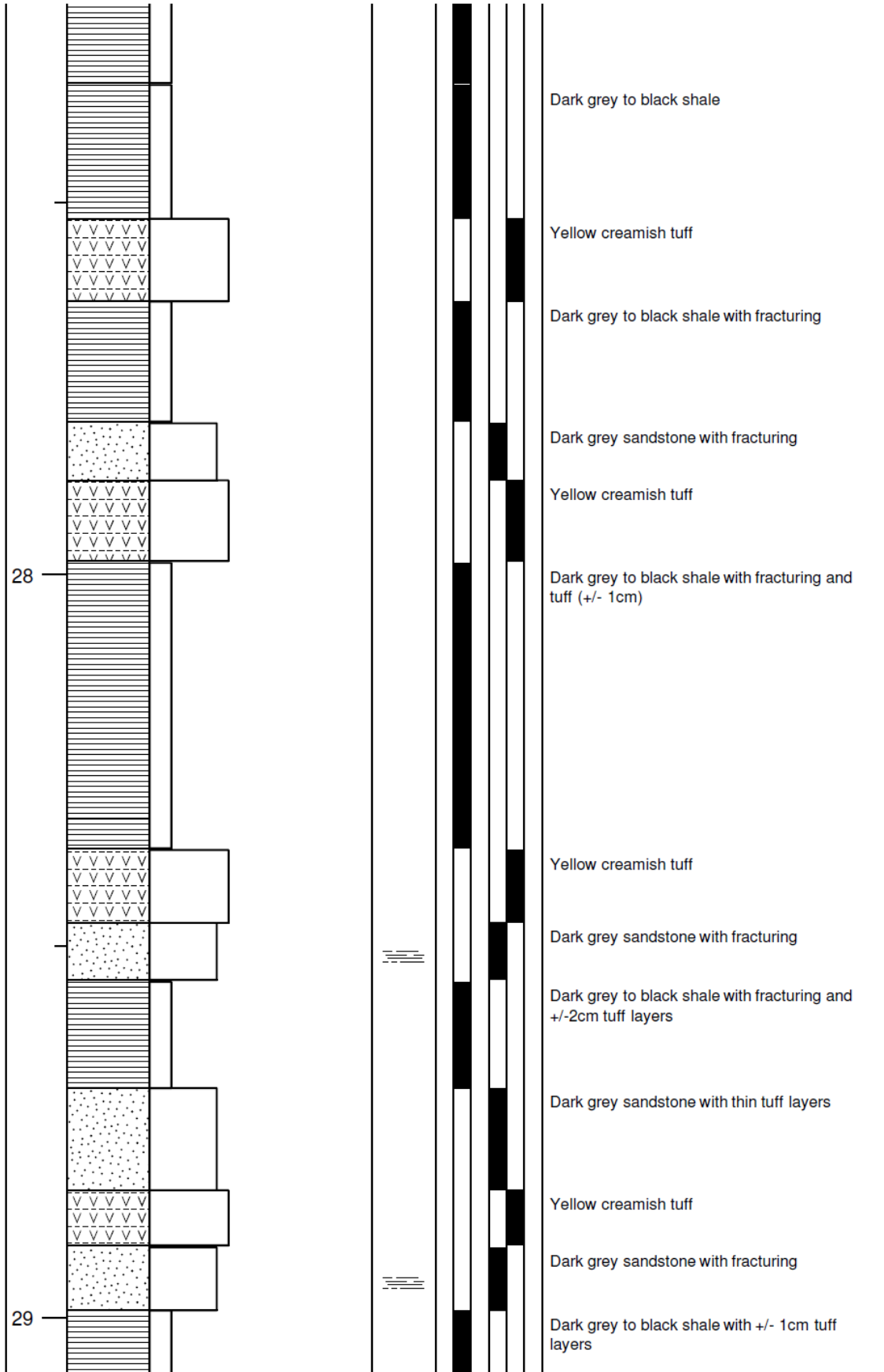


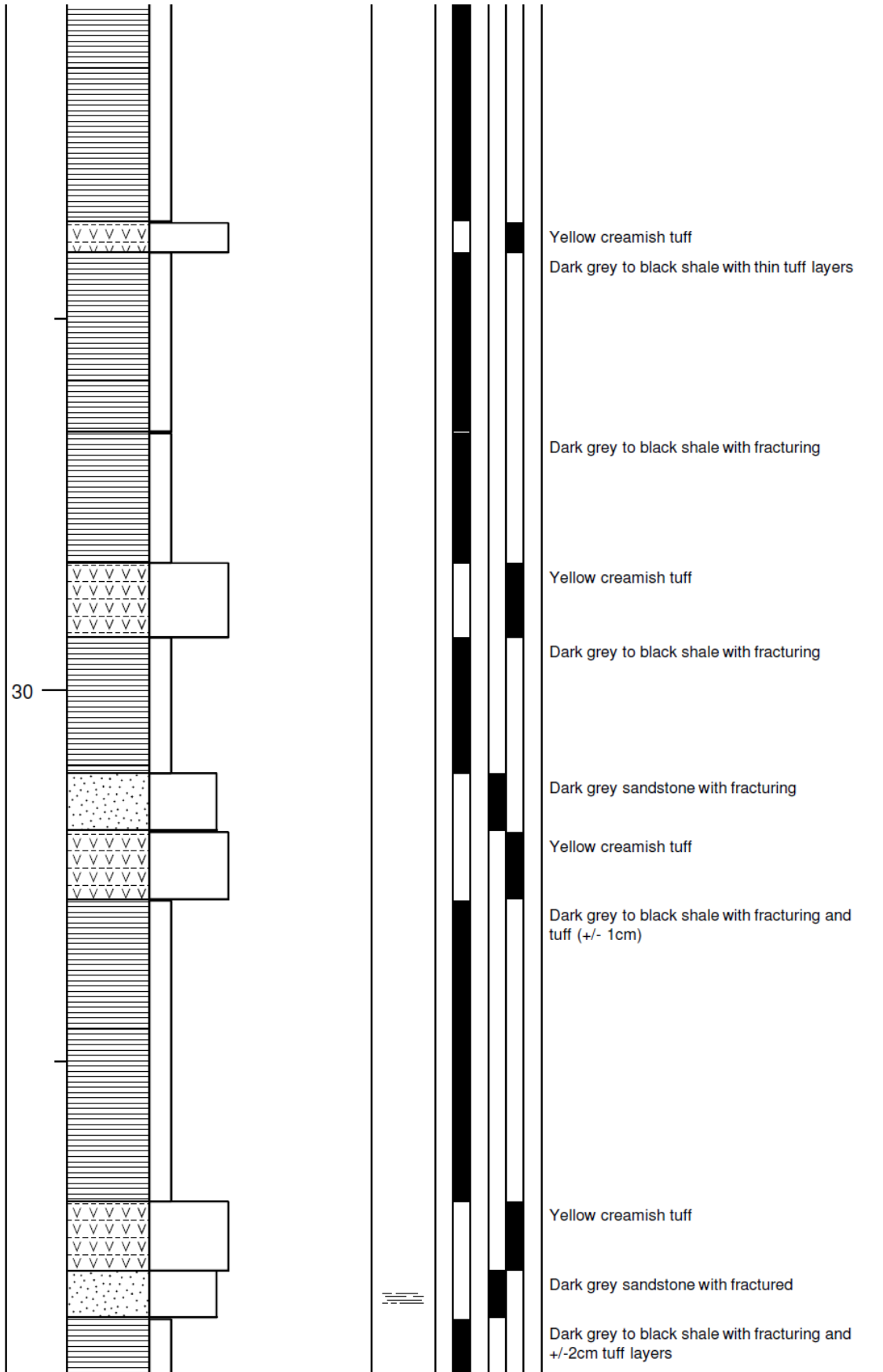


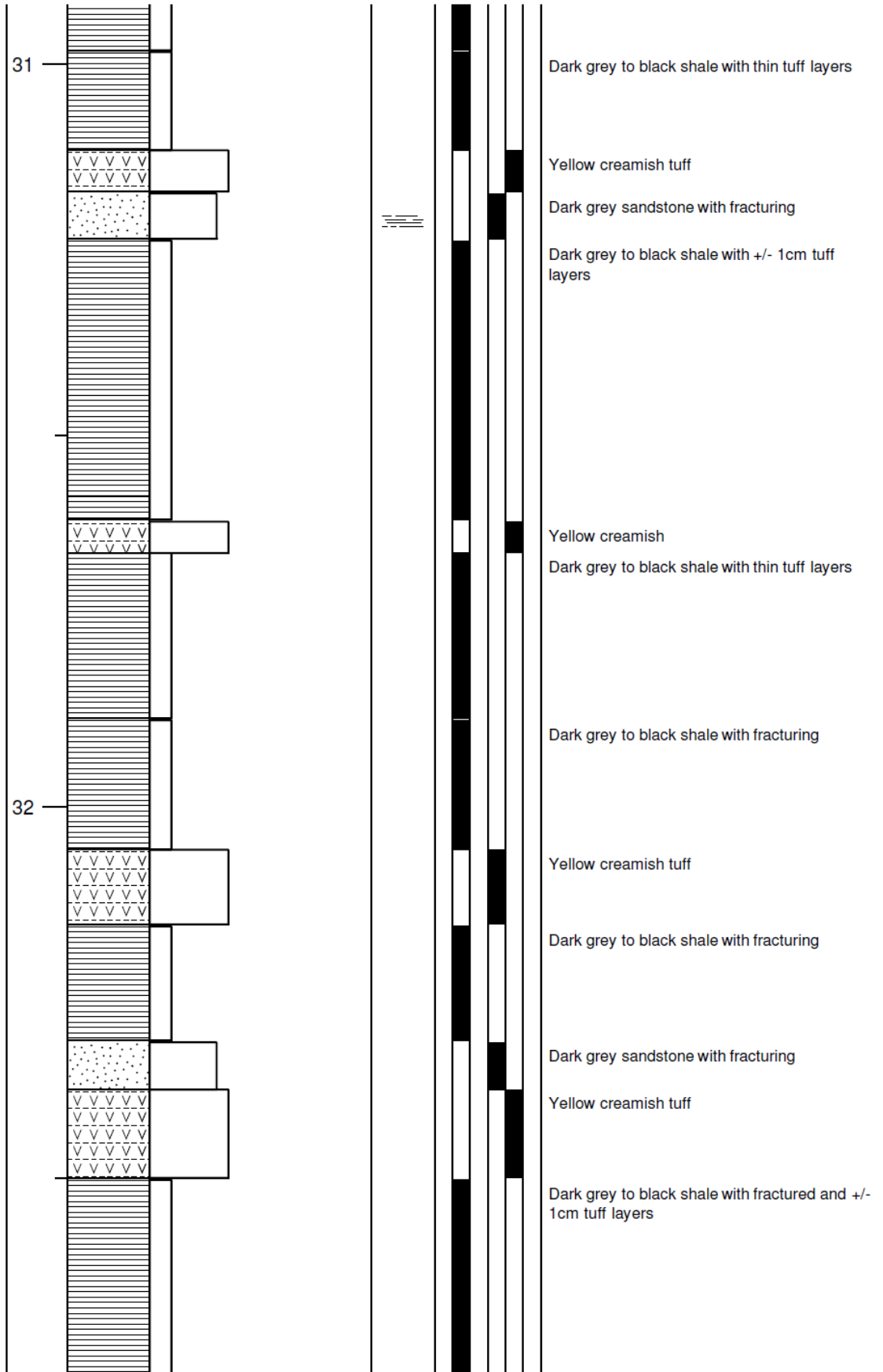


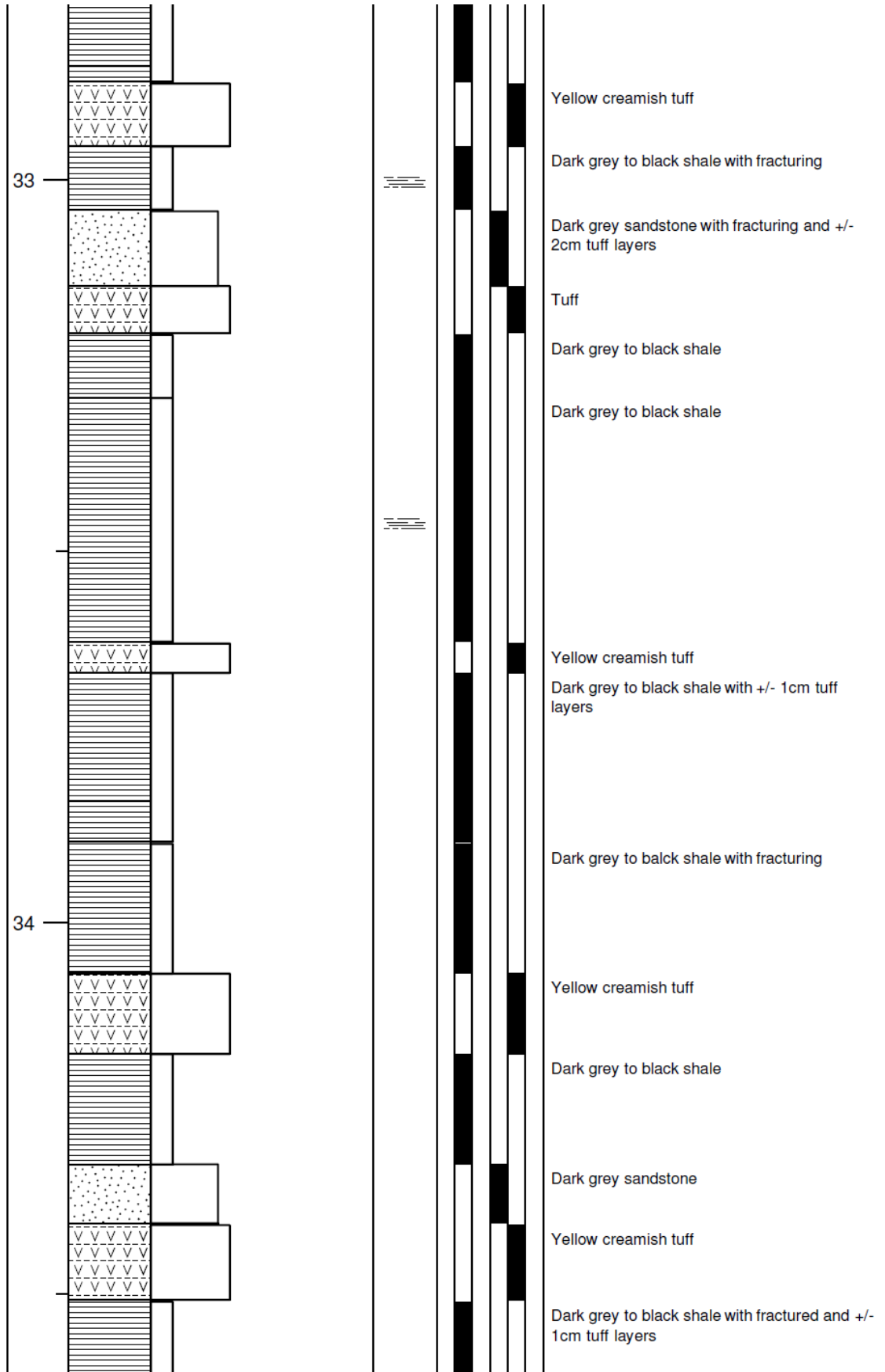


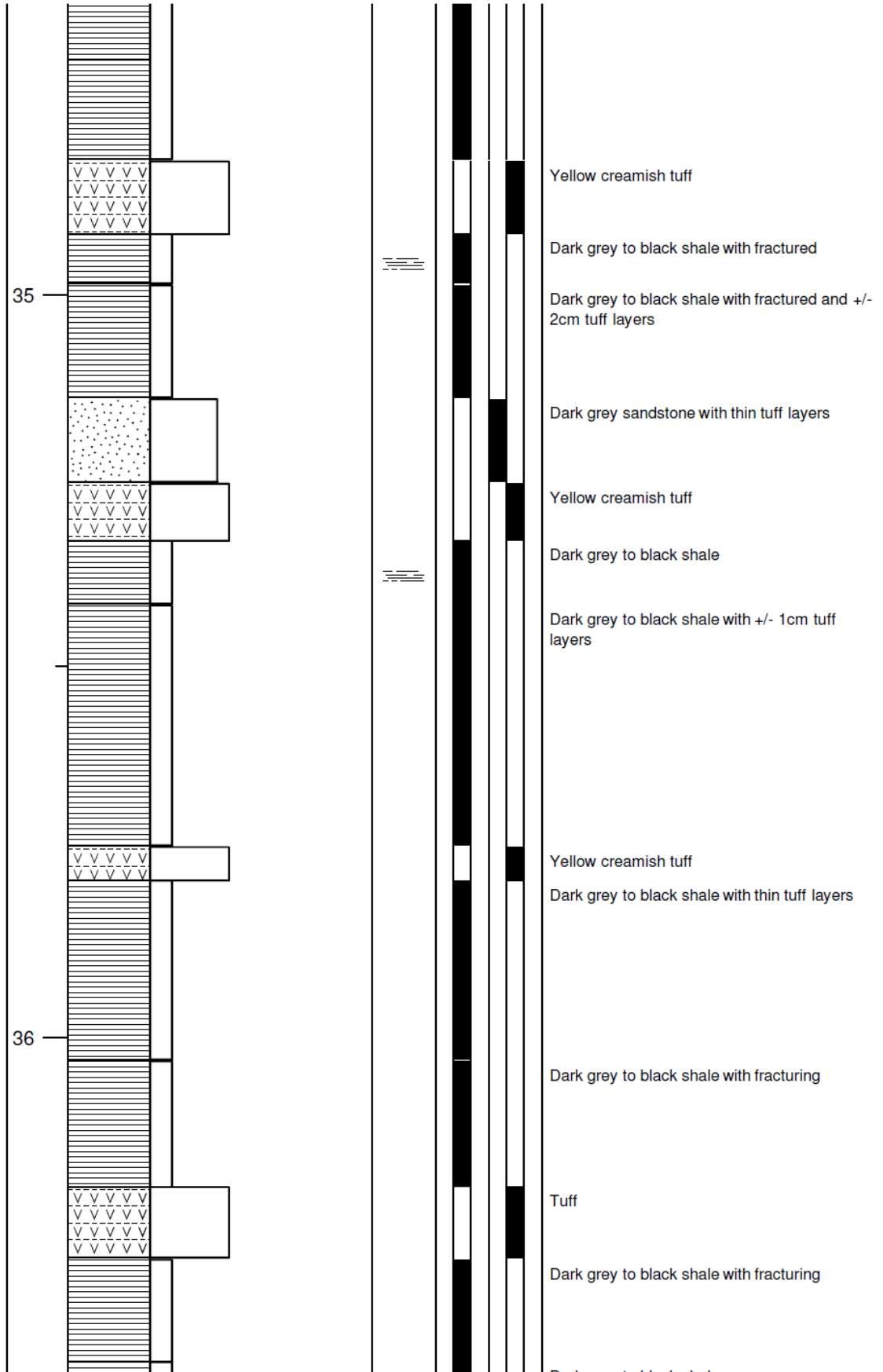


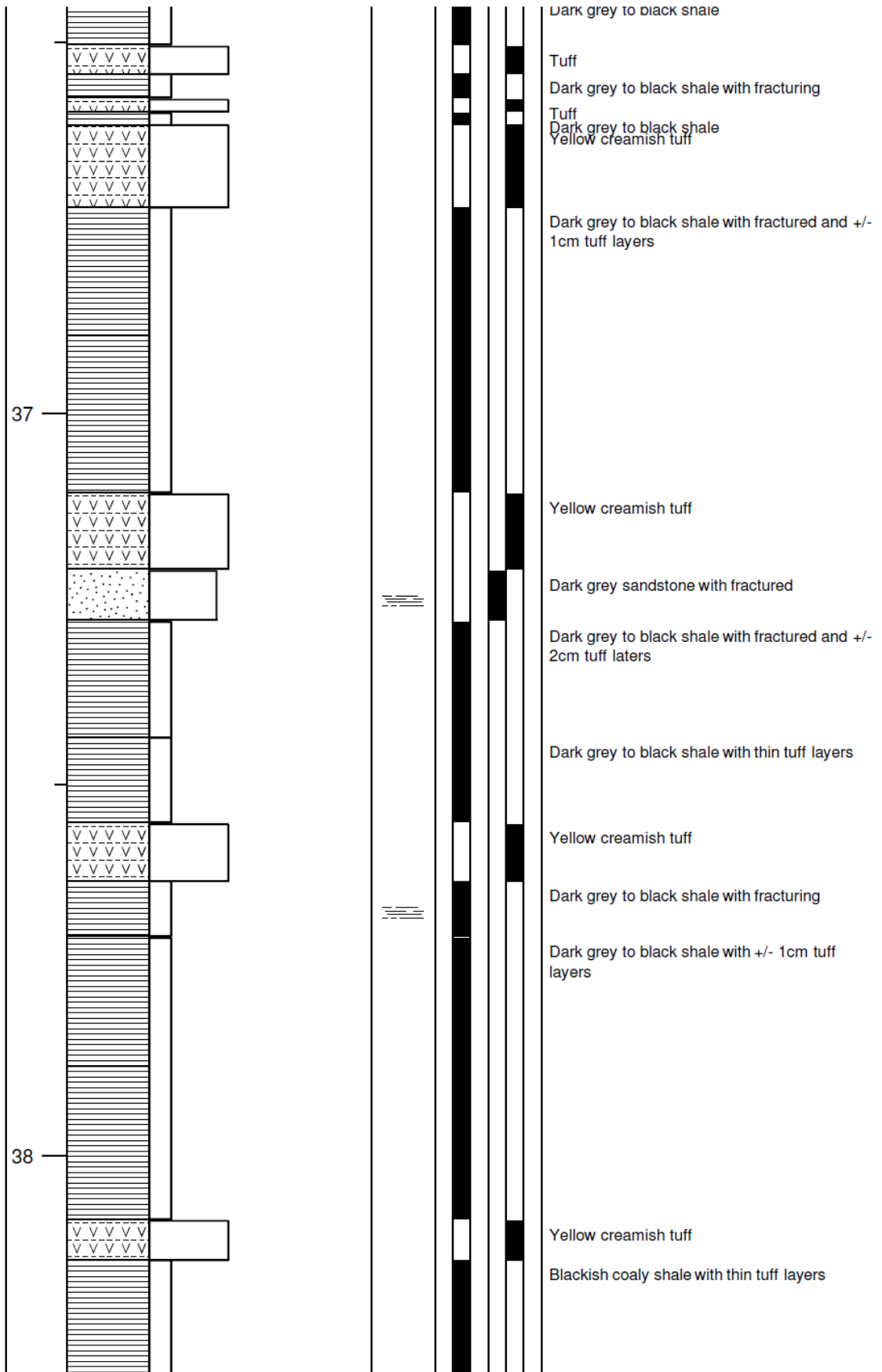


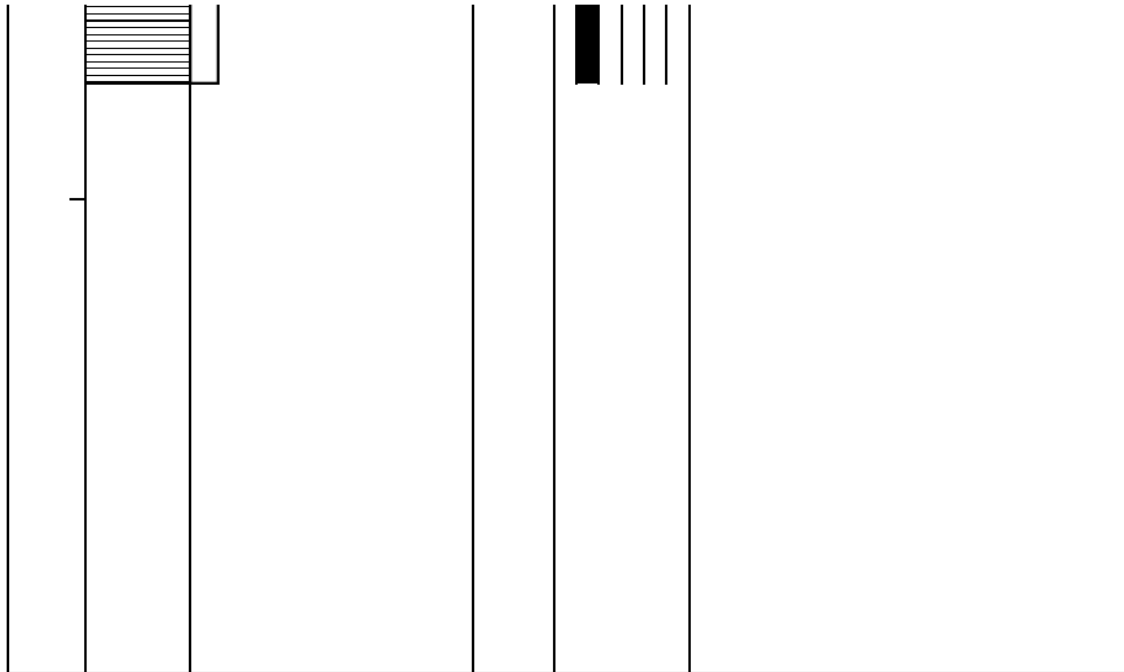












Lithologies

Symbols

Base Boundaries



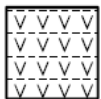
Shale



Horizontal planar lamination



Sharp



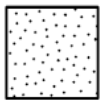
Fine ash



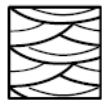
Current ripple cross-lamination



Erosion



Sandstone



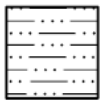
Trough cross bedding



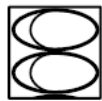
Chert



Convolute lamination



Siltstone



Nodules and concretions



Coal



Hummocky cross stratification



Appendix D

UNIVERSITY *of the*
WESTERN CAPE

Sample	Area	Long.	Lat.	Elevation	Description
PA1	Witteberg	S 33° 14,403'	E 20° 51, 995'	681	Shale
PA2	Witteberg	S 33° 14,399'	E 20° 51, 987'	681	Shale
PA3	Floriskraal	S 33° 16,651'	E 20° 56, 251'	667	Shale
PA4	Floriskraal	S 33° 16,694'	E 20° 57,034'	660	Shale
PA5	Floriskraal	S 33° 16,659'	E 20° 57, 028'	663	Shale
PA6	Floriskraal	S 33° 16,651'	E 20° 56, 251'	667	Shale
PA7	Floriskraal	S 33° 16' 35,6"	E 20° 57' 02,0"	651	Shale
PA8	Witteberg	S 33° 14' 26,2"	E 20° 51' 57,5"	680	Shale
PA9	Witteberg	S 33° 14' 26"	E 20° 51' 56,9"	683	Shale
PA10	Witteberg	S 33° 14' 24,1"	E 20° 51' 55,8"	681	Coaly shale
PA11	Geelbek	S 33° 14' 25,7"	E 20° 53' 29,1"	662	Shale
WH1	Witteberg	S 33° 14,343'	E 20° 51, 984'	681	Shale
WH2	Witteberg	S 33° 14,343'	E 20° 51, 003'	681	Shale
WH3	Floriskraal	S 33° 16,804'	E 20° 57, 066'	682	Shale
WH4	Floriskraal	S 33° 16' 48,7"	E 20° 57' 05,4"	691	Shale
WH5	Geelbek	S 33° 14' 23,5"	E 20° 53' 36,6"	680	Shale
WH6	Geelbek	S 33° 14' 21,7"	E 20° 53' 32,2"	674	Shale
WH7	Geelbek	S 33° 14' 23,9"	E 20° 53' 39,3"		Shale
WH8	Witteberg	S 33° 14' 20,6"	E 20° 52' 0"	670	Coaly shale
WH9	Witteberg	S 33° 14' 20,6"	E 20° 52' 0"	670	Coaly shale
CH1	Witteberg	S 33° 14,306'	E 20° 51, 948'	674	Shale
CH2	Witteberg	S 33° 14,312'	E 20° 51, 953'	681	Shale
CH3	Witteberg	S 33° 14,313'	E 20° 51, 957'	659	Coaly shale
CH4	Witteberg	S 33° 14,318'	E 20° 51, 962'	668	Shale
CH5	Floriskraal	S 33° 16,871'	E 20° 57,116'	696	Shale
CH6	Floriskraal	S 33° 16' 51,3"	E 20° 57' 06,7"	700	Shale
CH7	Geelbek	S 33° 14' 21,8"	E 20° 53' 33,8"	679	Shale
CH8	Witteberg	S 33° 14' 19,9"	E 20° 51' 58"	676	Shale

Appendix E



UNIVERSITY *of the*
WESTERN CAPE

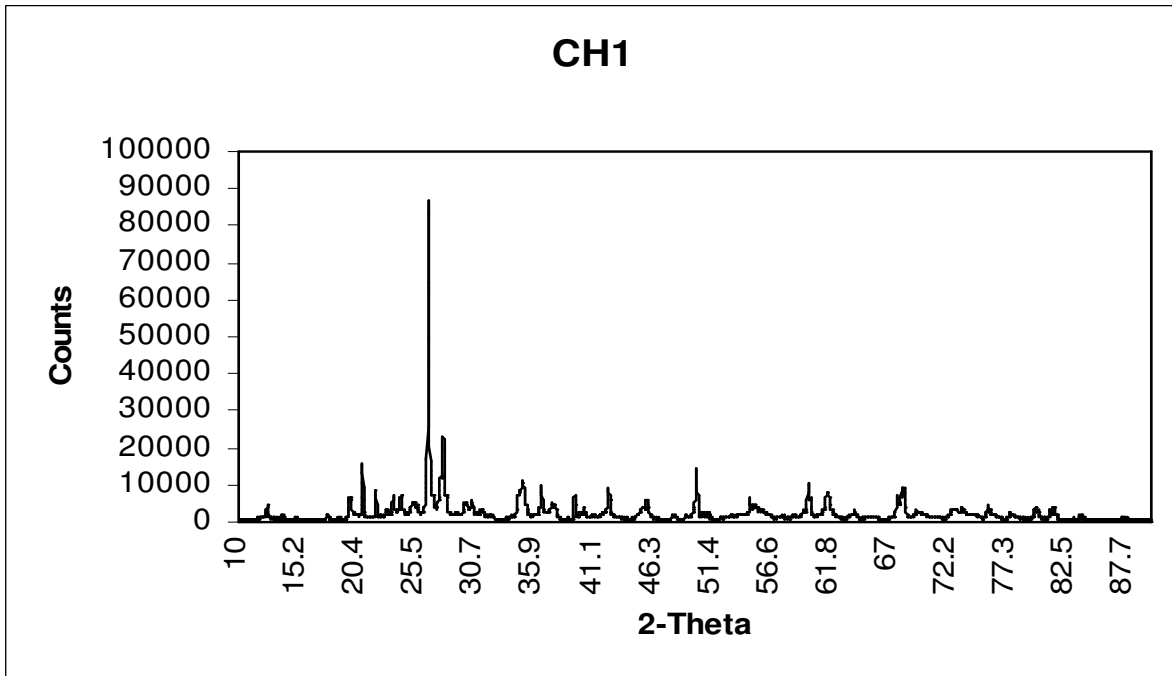


Figure 1. Representative profile of X-ray diffraction patterns for studied shale of the Collingham Formation, Witteburg.

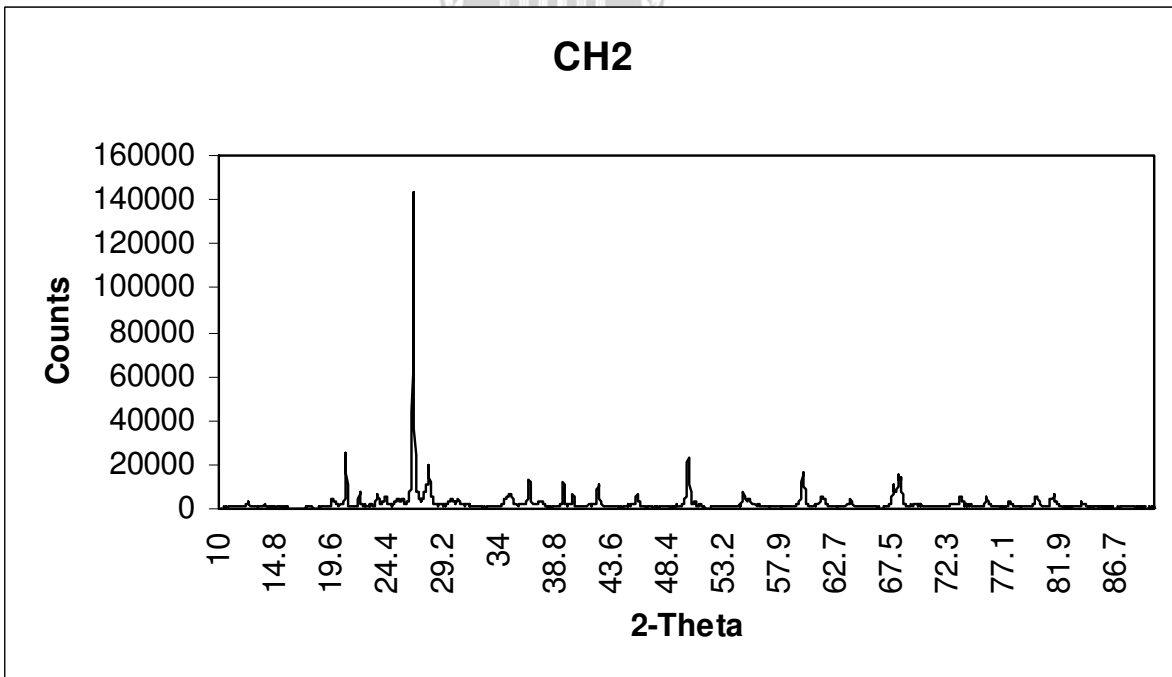


Figure 2. Representative profile of X-ray diffraction patterns for studied shale of the Collingham Formation, Witteburg.

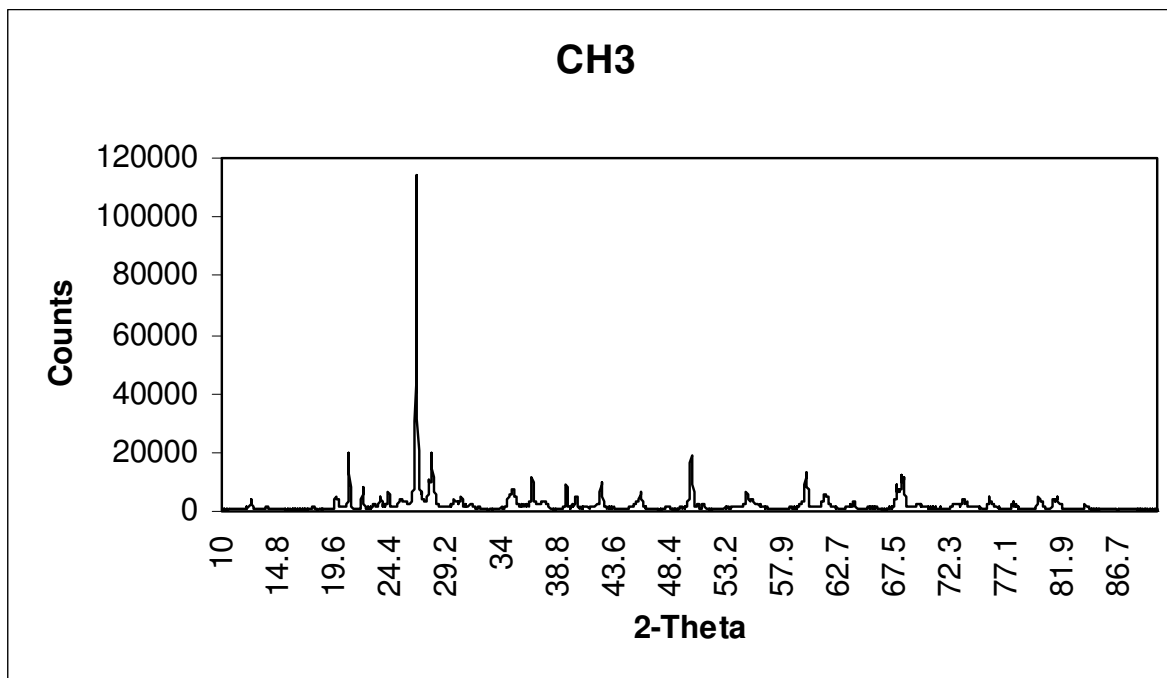


Figure 3. Representative profile of X-ray diffraction patterns for studied shale of the Collingham Formation, Witteburg.

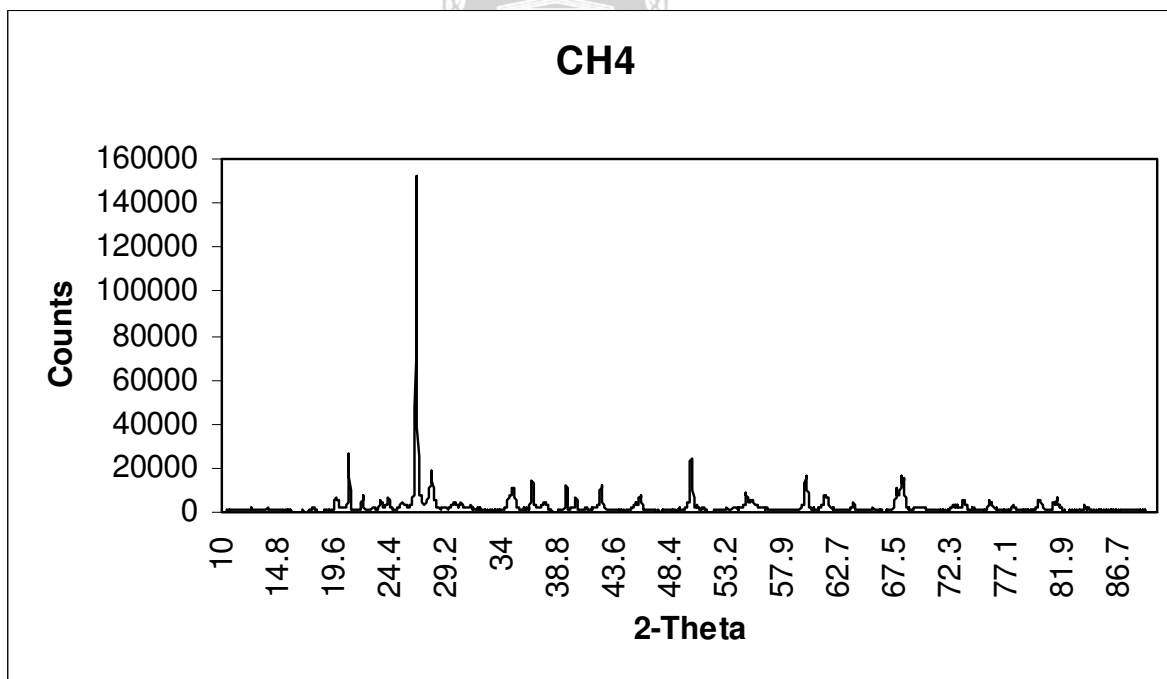


Figure 4. Representative profile of X-ray diffraction patterns for studied shale of the Collingham Formation, Witteburg.

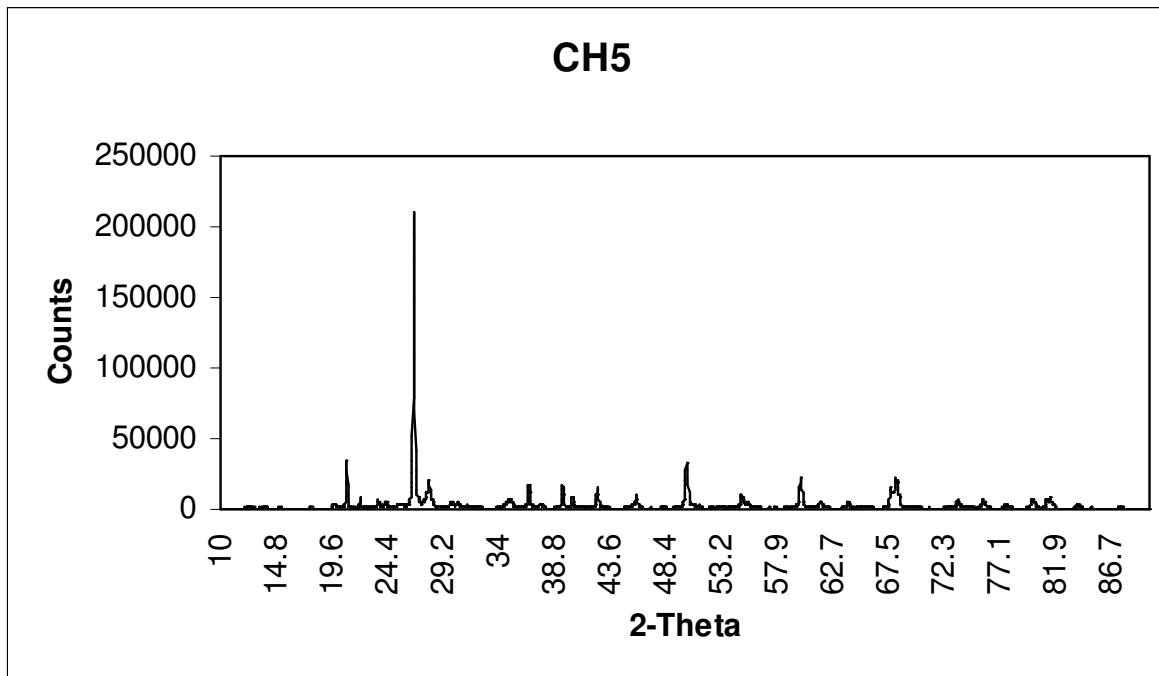


Figure 5. Representative profile of X-ray diffraction patterns for studied shale of the Collingham Formation, Floriskraal.

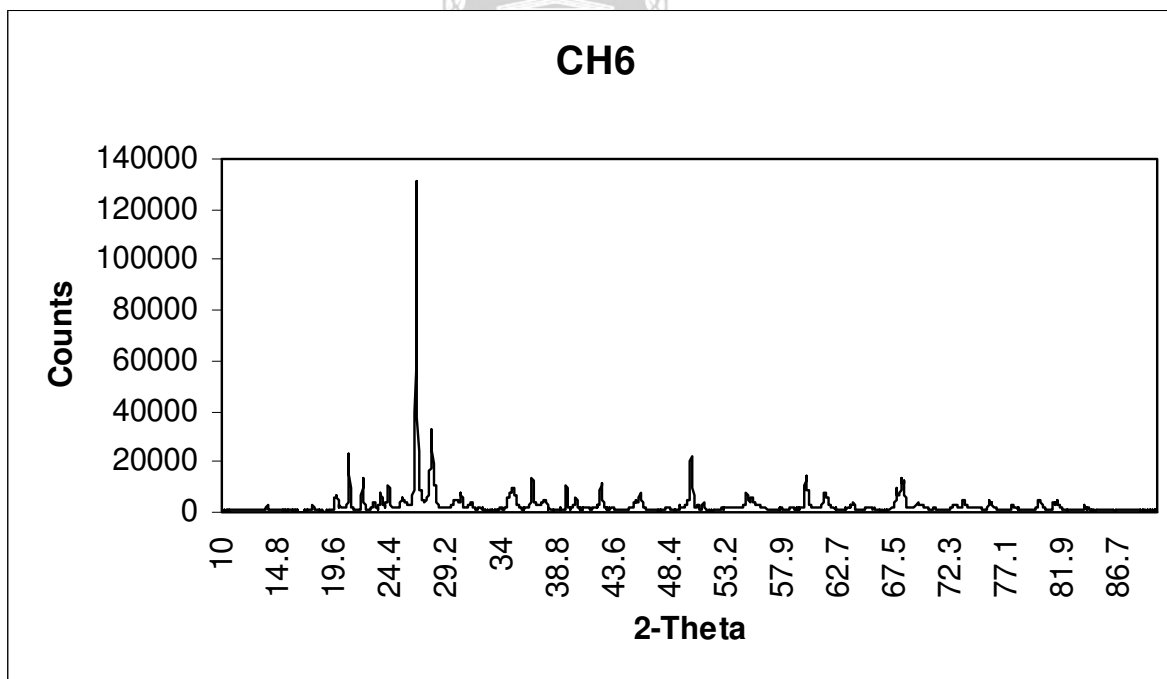


Figure 6. Representative profile of X-ray diffraction patterns for studied shale of the Collingham Formation, Floriskraal.

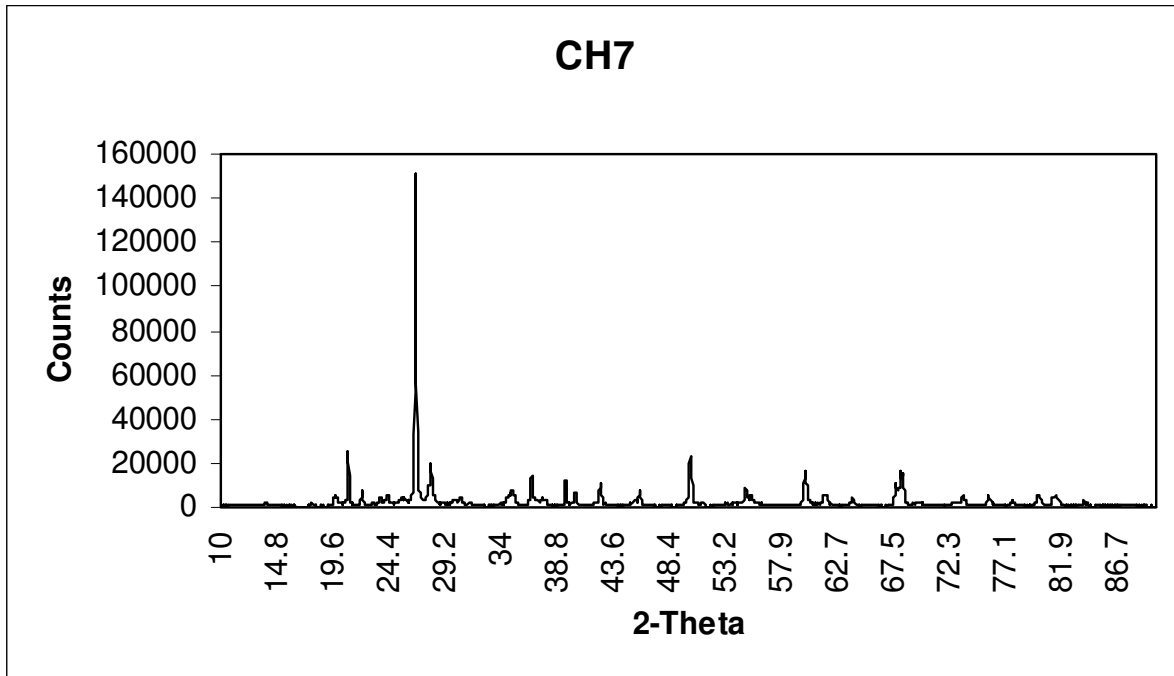


Figure 7. Representative profile of X-ray diffraction patterns for studied shale of the Collingham Formation, Geelbek.

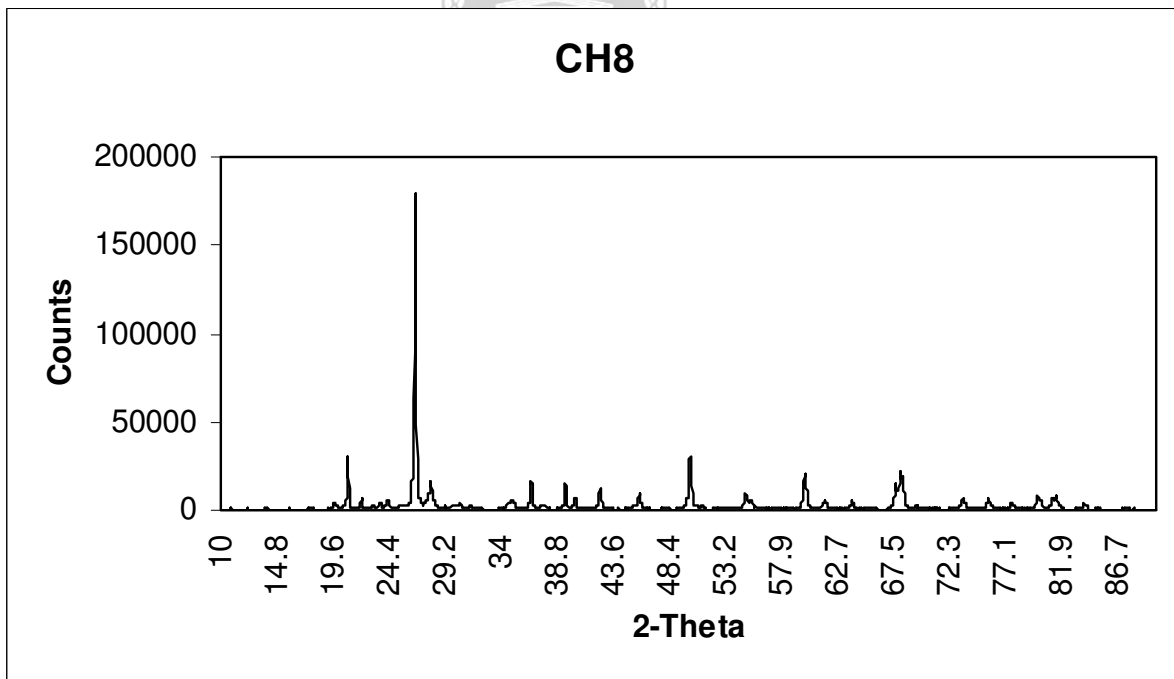


Figure 8. Representative profile of X-ray diffraction patterns for studied shale of the Collingham Formation, Witteburg.

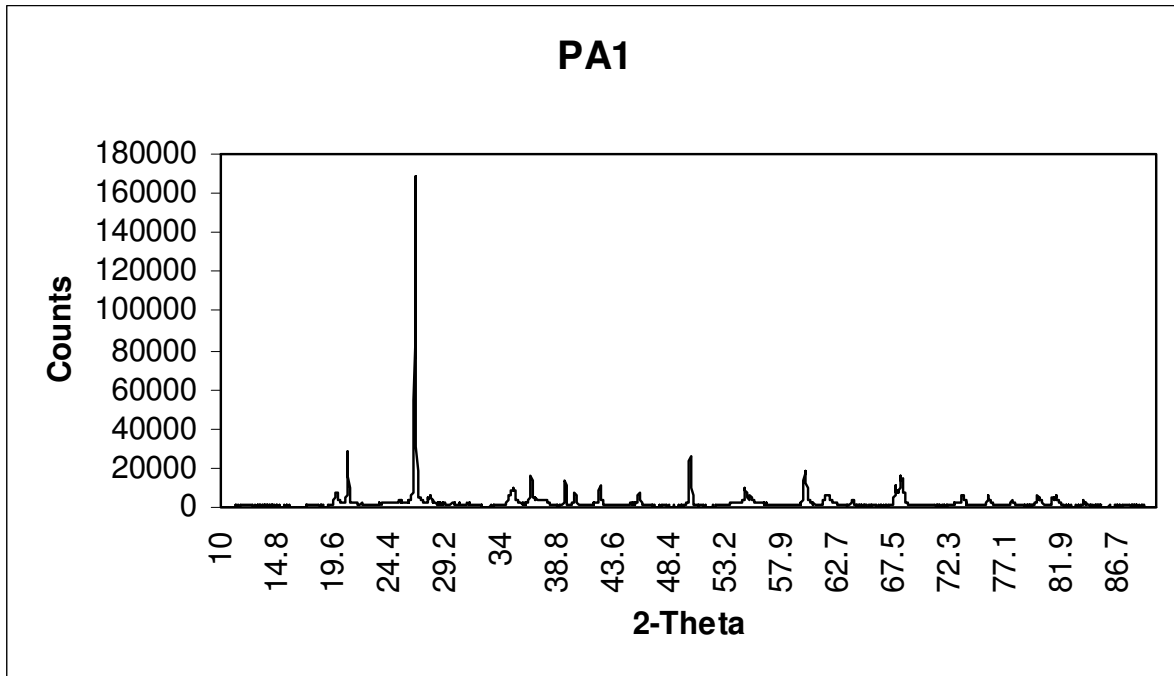


Figure 9. Representative profile of X-ray diffraction patterns for studied shale of the Prince Albert Formation, Witteburg.

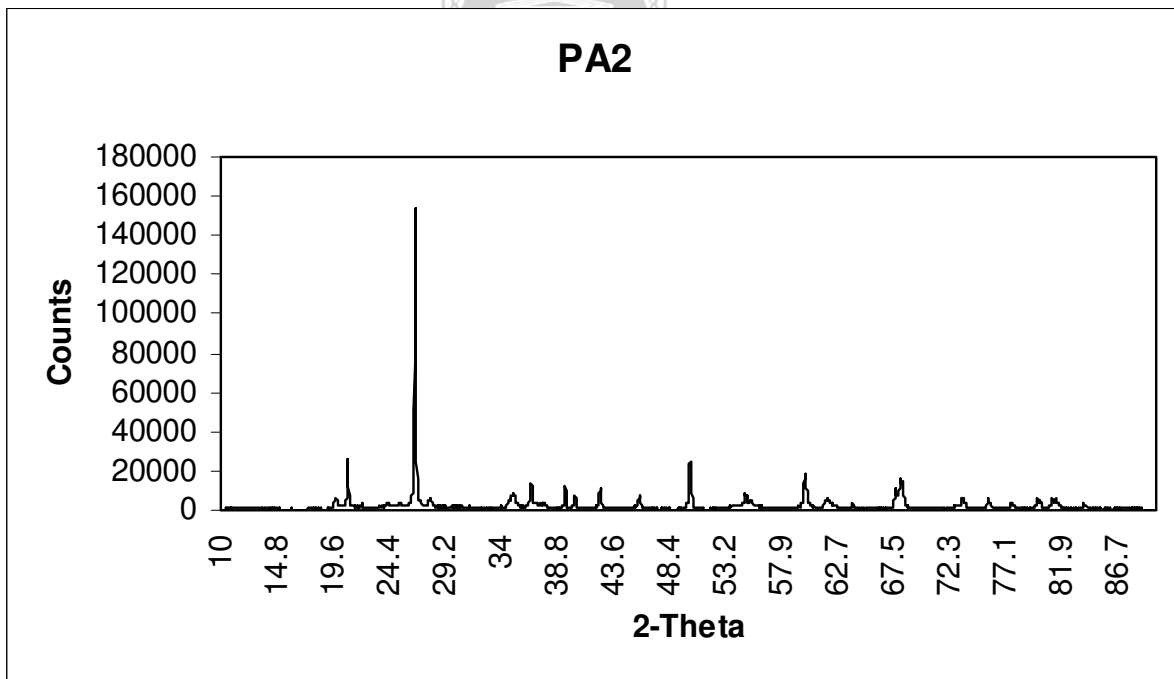


Figure 10. Representative profile of X-ray diffraction patterns for studied shale of the Prince Albert Formation, Witteburg.

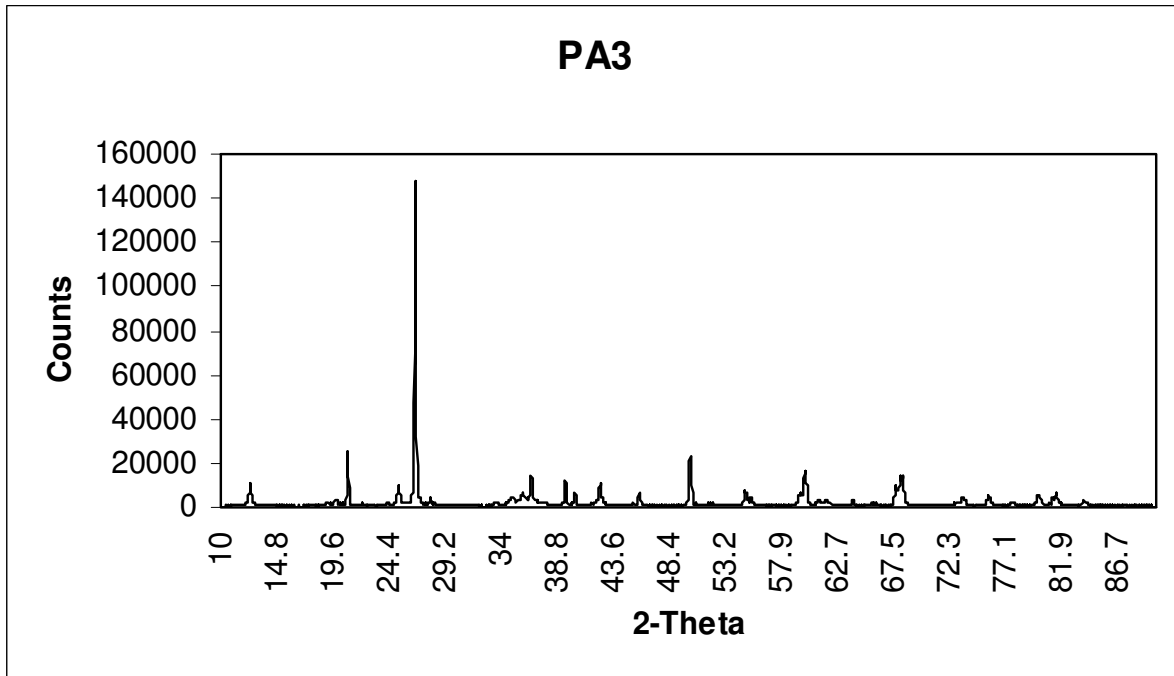


Figure 11. Representative profile of X-ray diffraction patterns for studied shale of the Prince Albert Formation, Floriskraal.

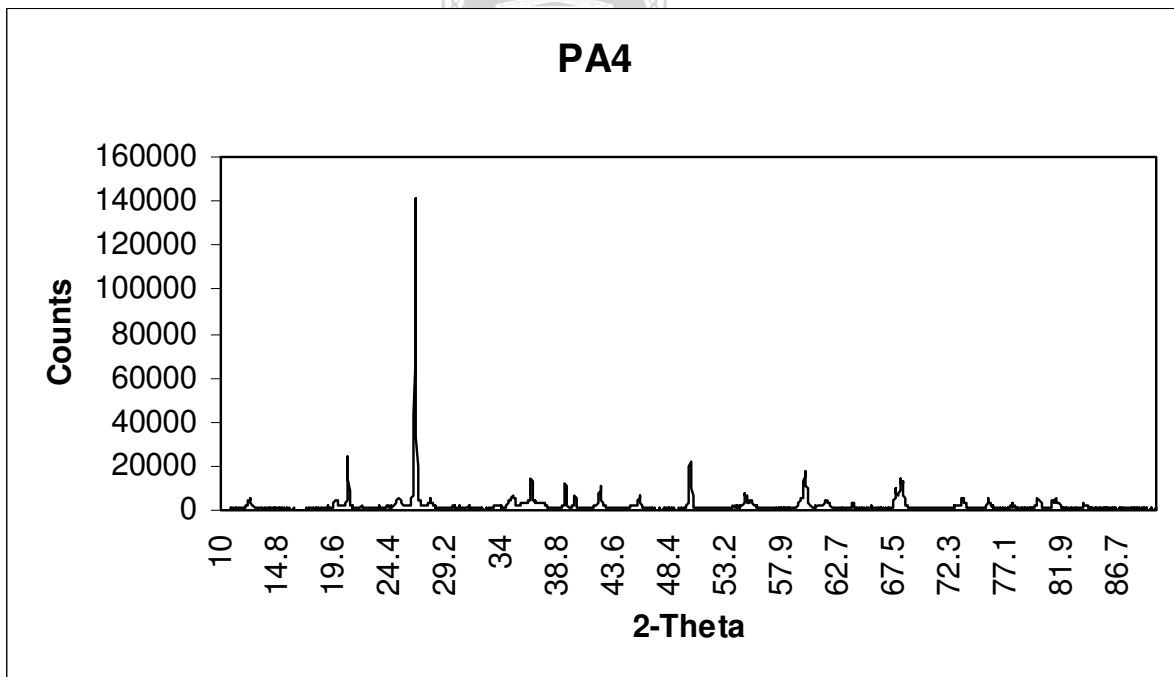


Figure 12. Representative profile of X-ray diffraction patterns for studied shale of the Prince Albert Formation, Floriskraal.

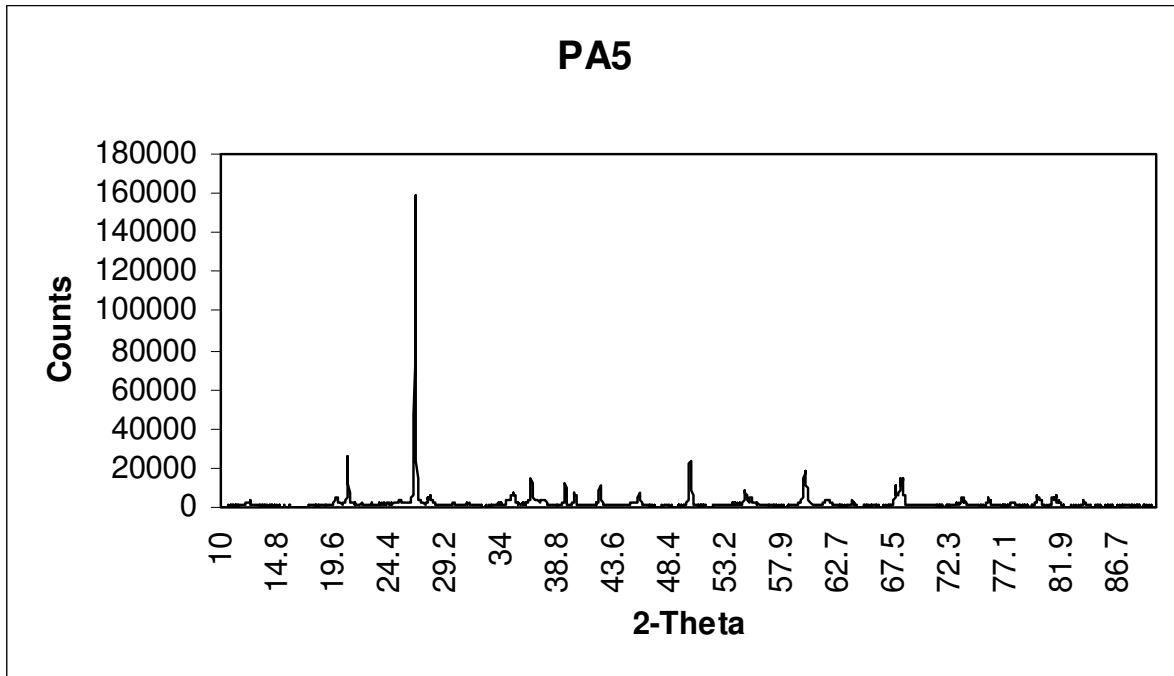


Figure 13. Representative profile of X-ray diffraction patterns for studied shale of the Prince Albert Formation, Floriskraal.

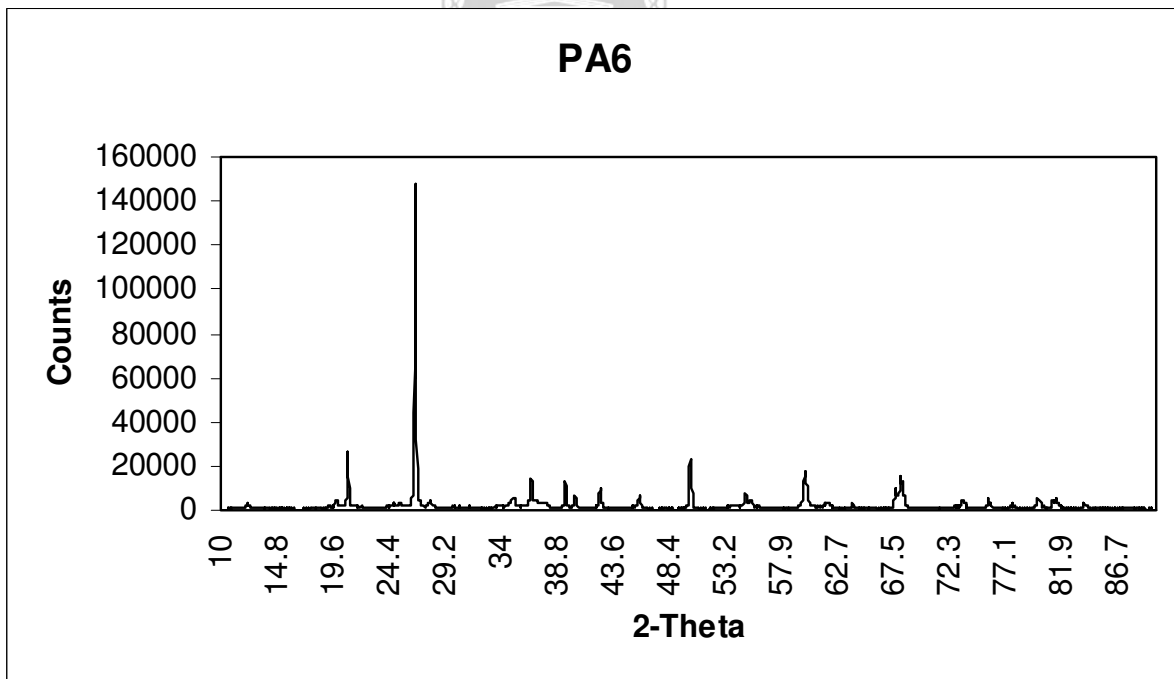


Figure 14. Representative profile of X-ray diffraction patterns for studied shale of the Prince Albert Formation, Floriskraal.

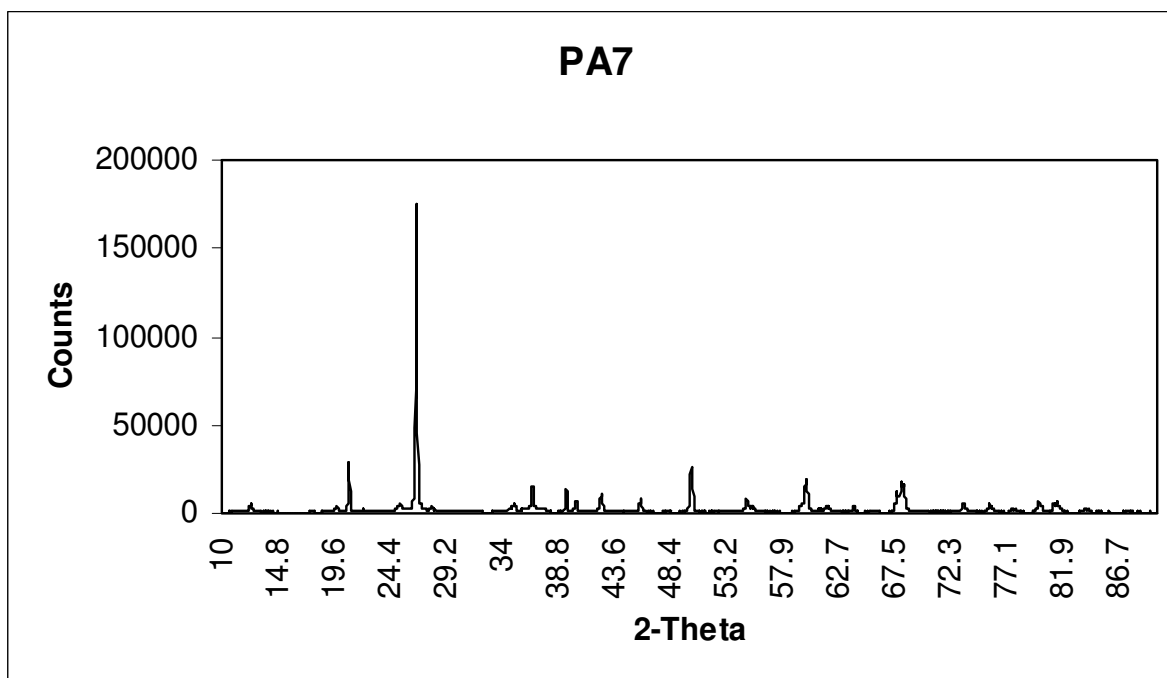


Figure 15. Representative profile of X-ray diffraction patterns for studied shale of the Prince Albert Formation, Floriskraal.

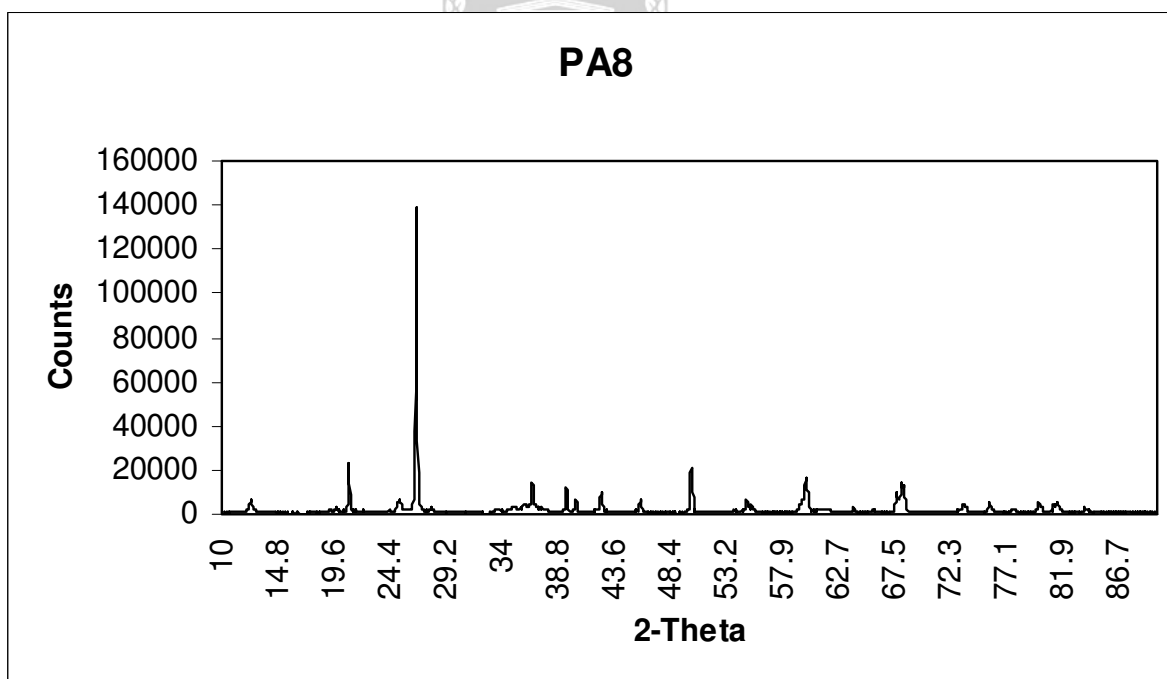


Figure 16. Representative profile of X-ray diffraction patterns for studied shale of the Prince Albert Formation, Witteburg.

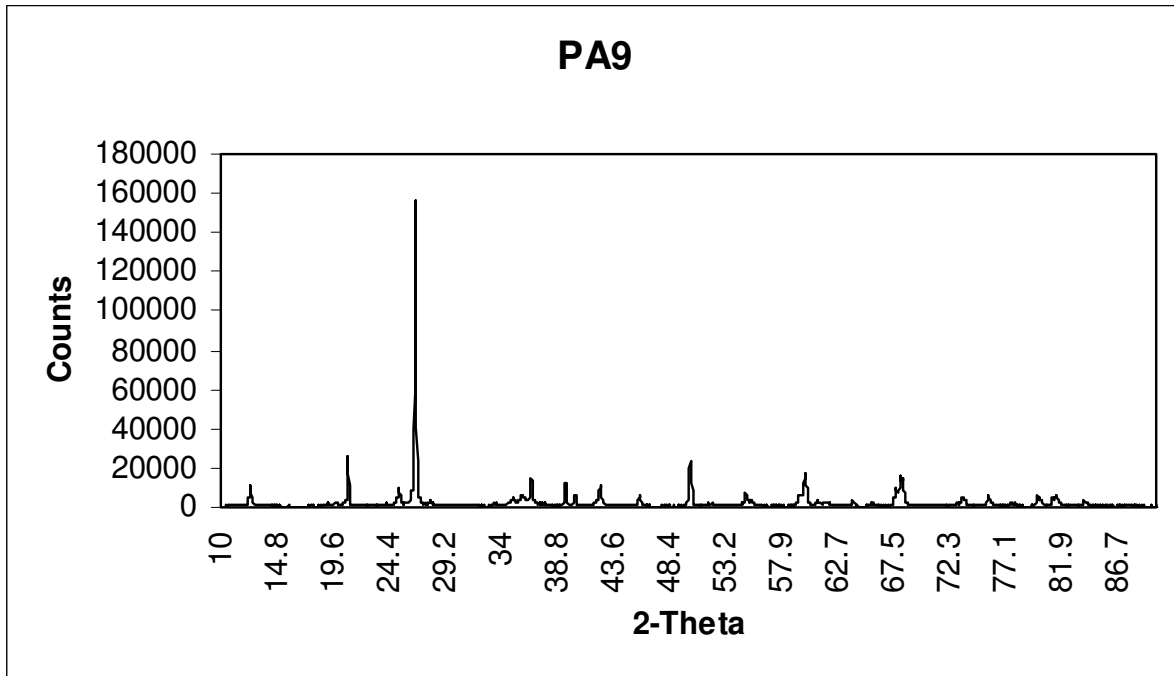


Figure 17. Representative profile of X-ray diffraction patterns for studied shale of the Prince Albert Formation, Witteburg.

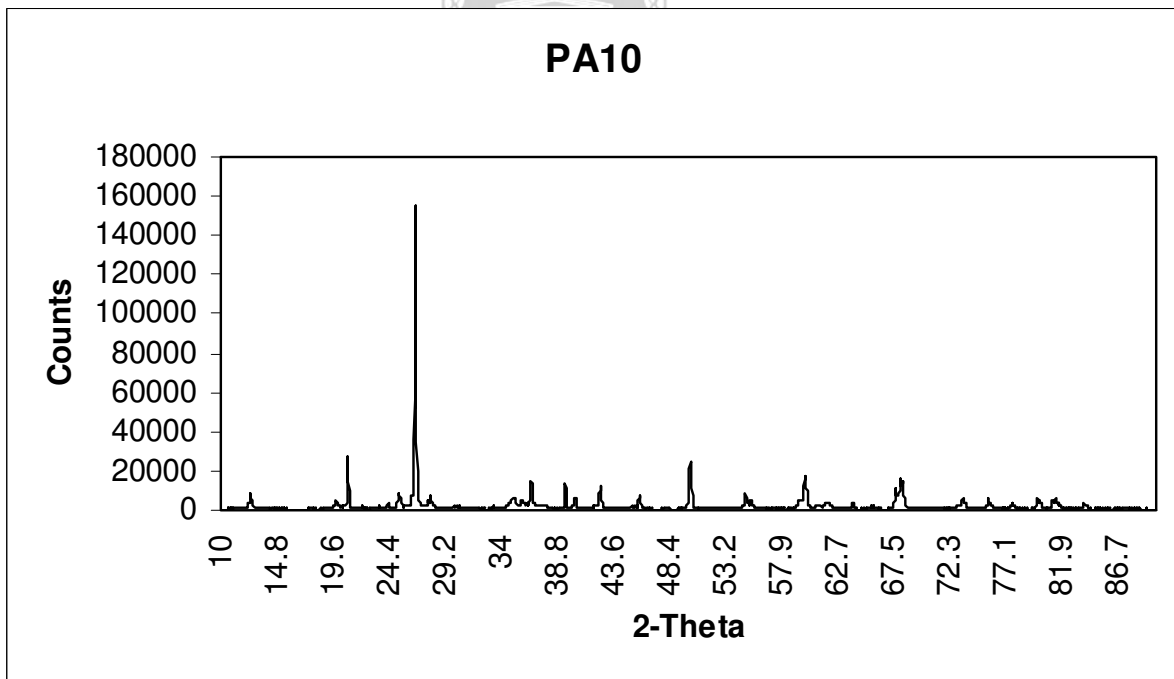


Figure 18. Representative profile of X-ray diffraction patterns for studied shale of the Prince Albert Formation, Witteburg.

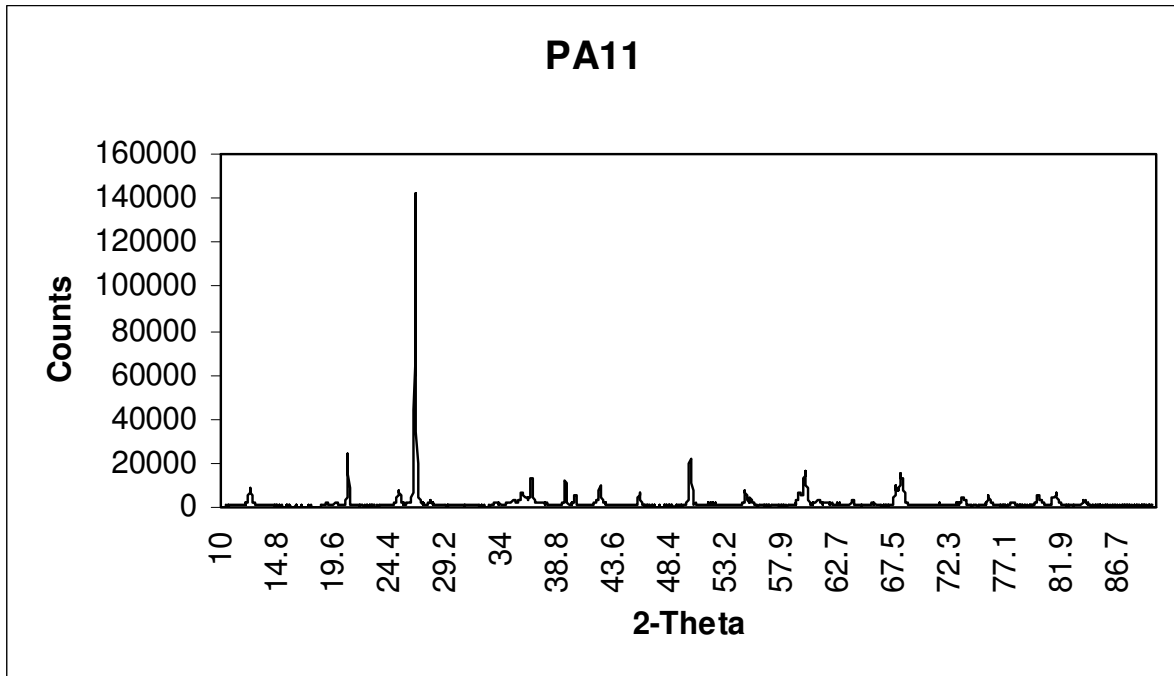


Figure 19. Representative profile of X-ray diffraction patterns for studied shale of the Prince Albert Formation, Geelbek.

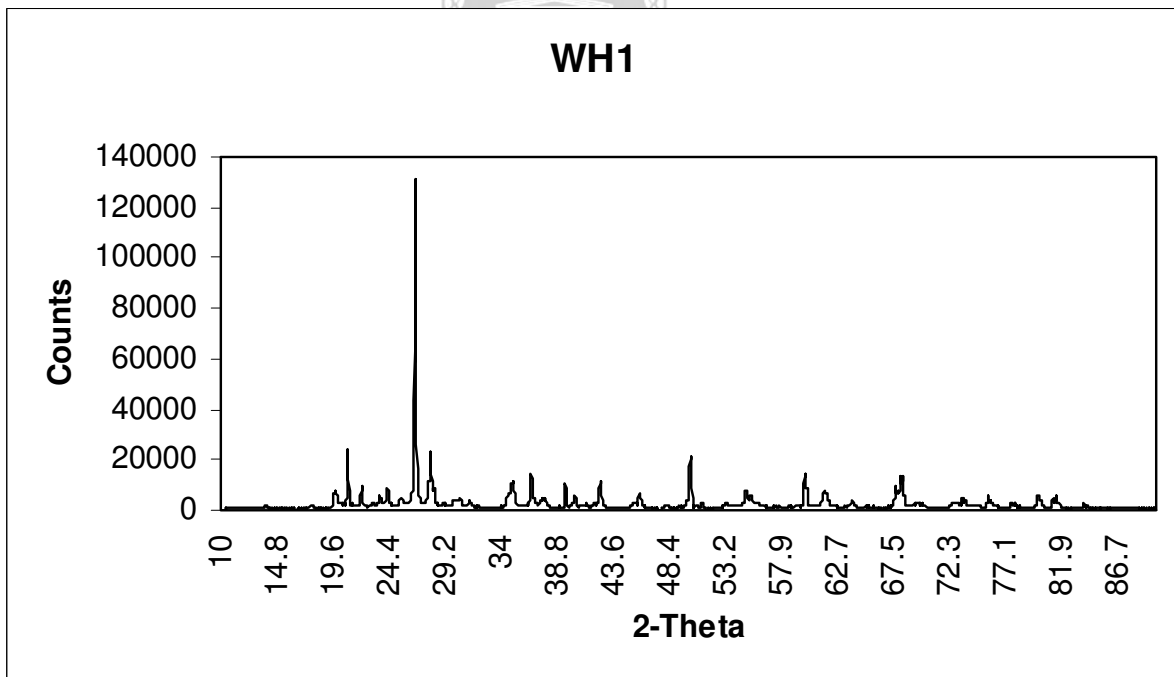


Figure 20. Representative profile of X-ray diffraction patterns for studied shale of the Whitehill Formation, Witteburg.

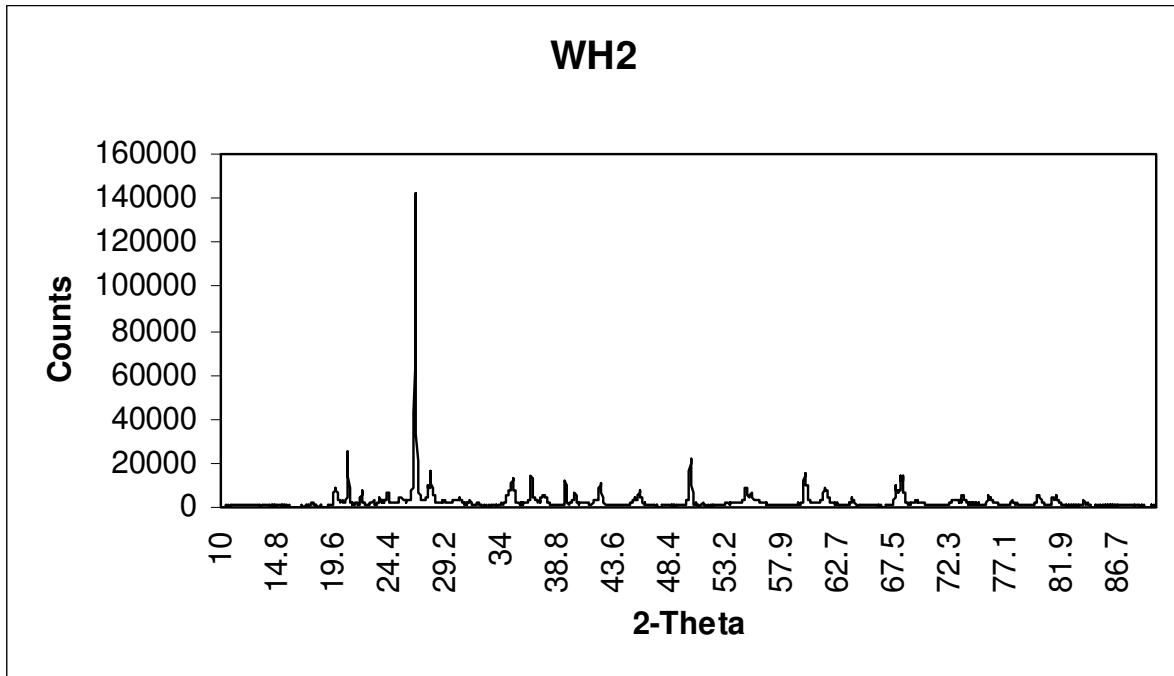


Figure 21. Representative profile of X-ray diffraction patterns for studied shale of the Whitehill Formation, Witteburg.

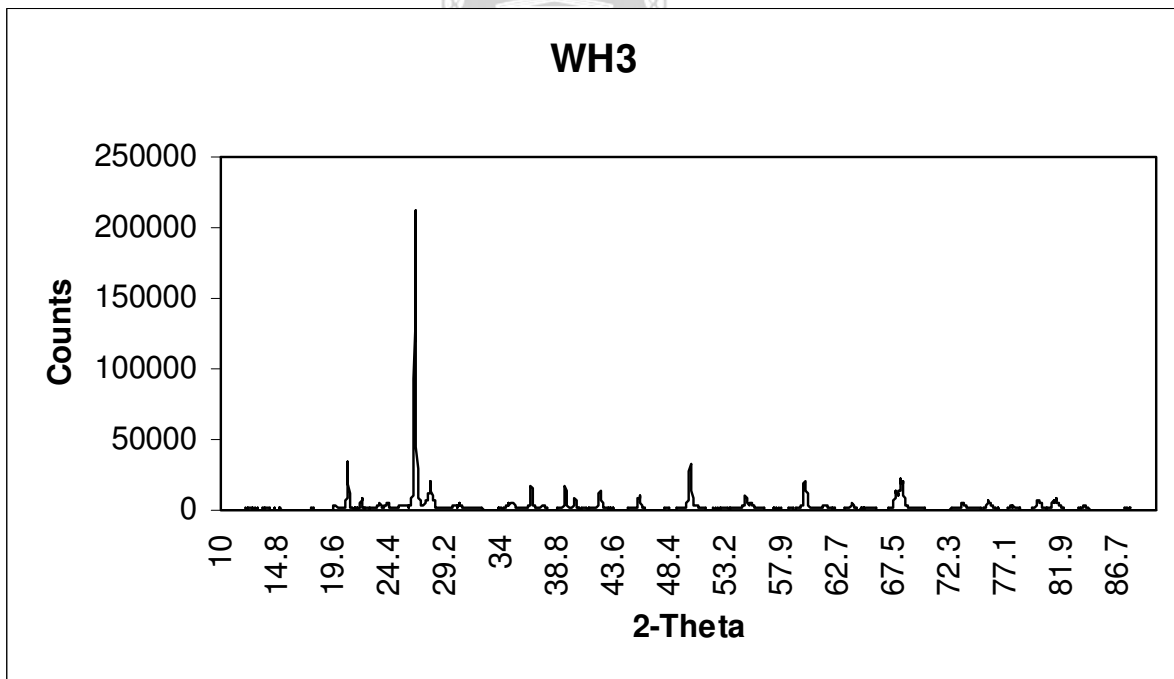


Figure 22. Representative profile of X-ray diffraction patterns for studied shale of the Whitehill Formation, Floriskraal.

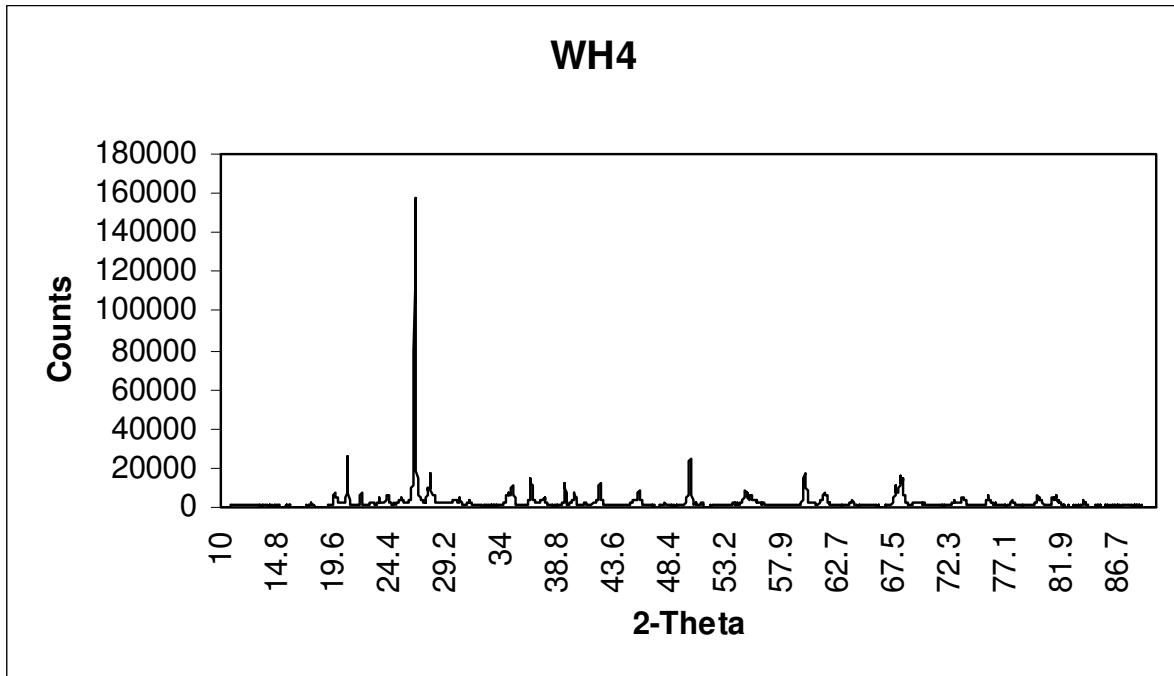


Figure 23. Representative profile of X-ray diffraction patterns for studied shale of the Whitehill Formation, Floriskraal.

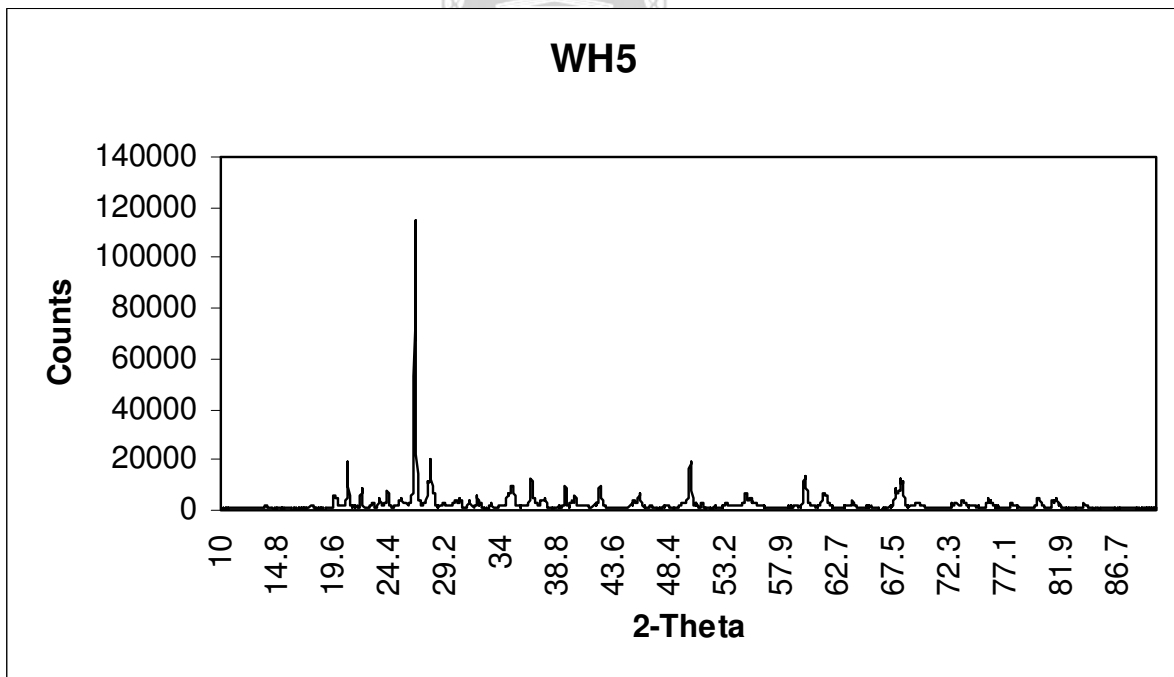


Figure 24. Representative profile of X-ray diffraction patterns for studied shale of the Whitehill Formation, Geelbek.

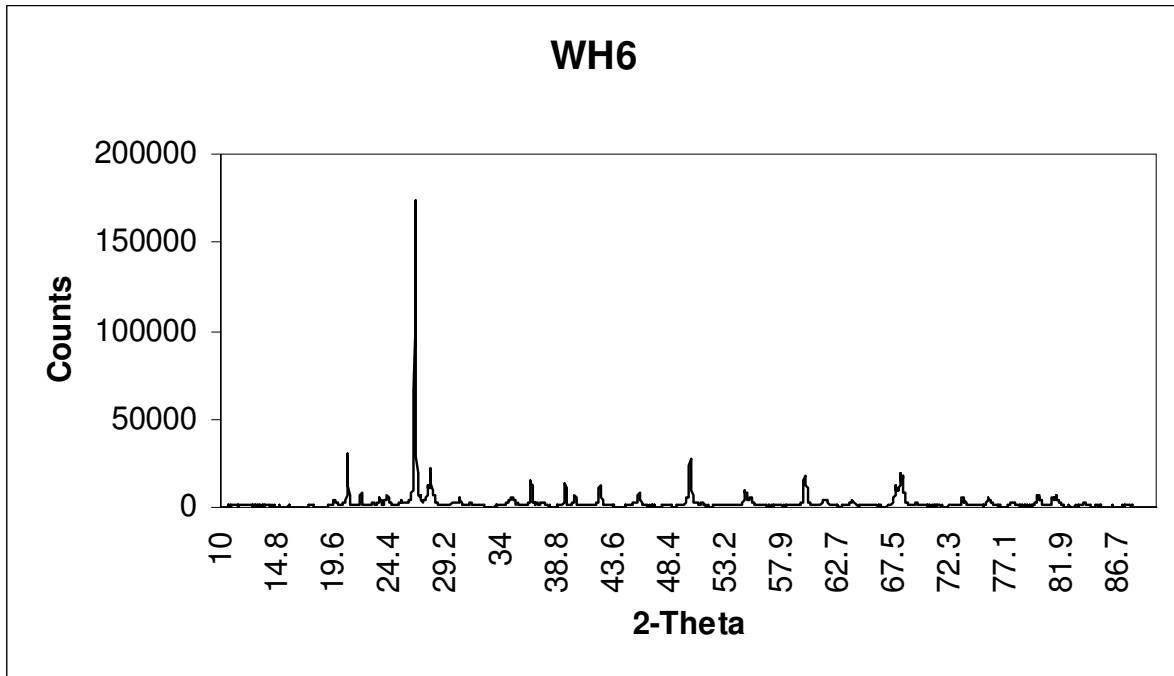


Figure 25. Representative profile of X-ray diffraction patterns for studied shale of Whitehill Formation, Geelbek.

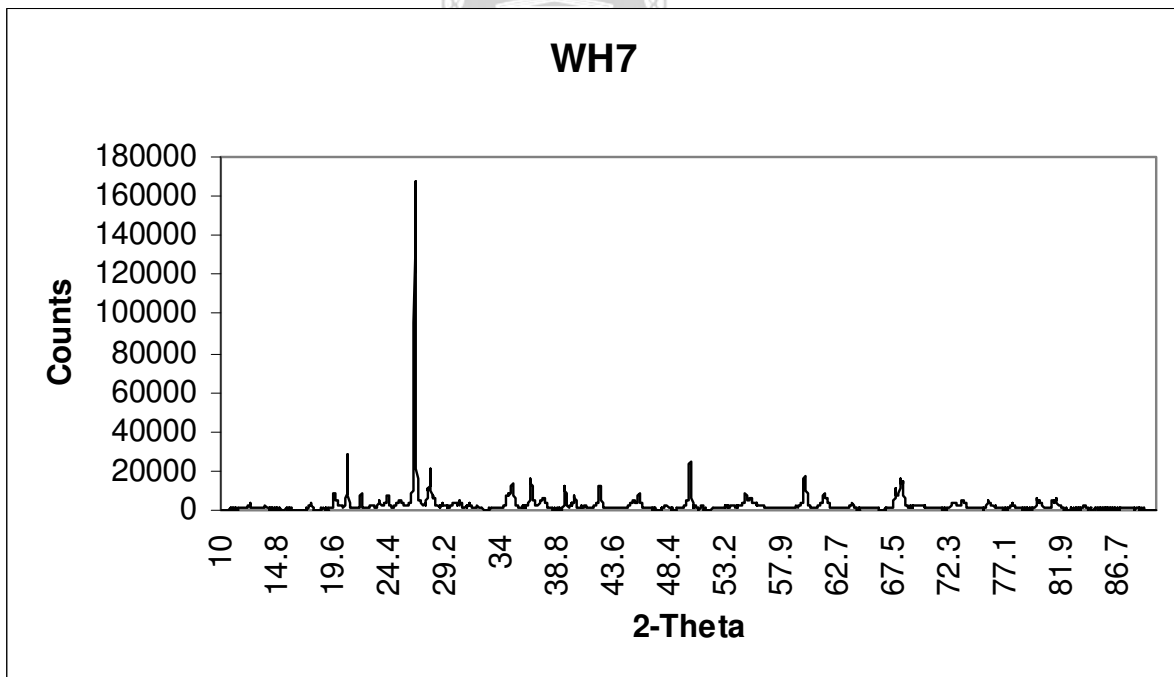


Figure 26. Representative profile of X-ray diffraction patterns for studied shale of the Whitehill Formation, Geelbek.

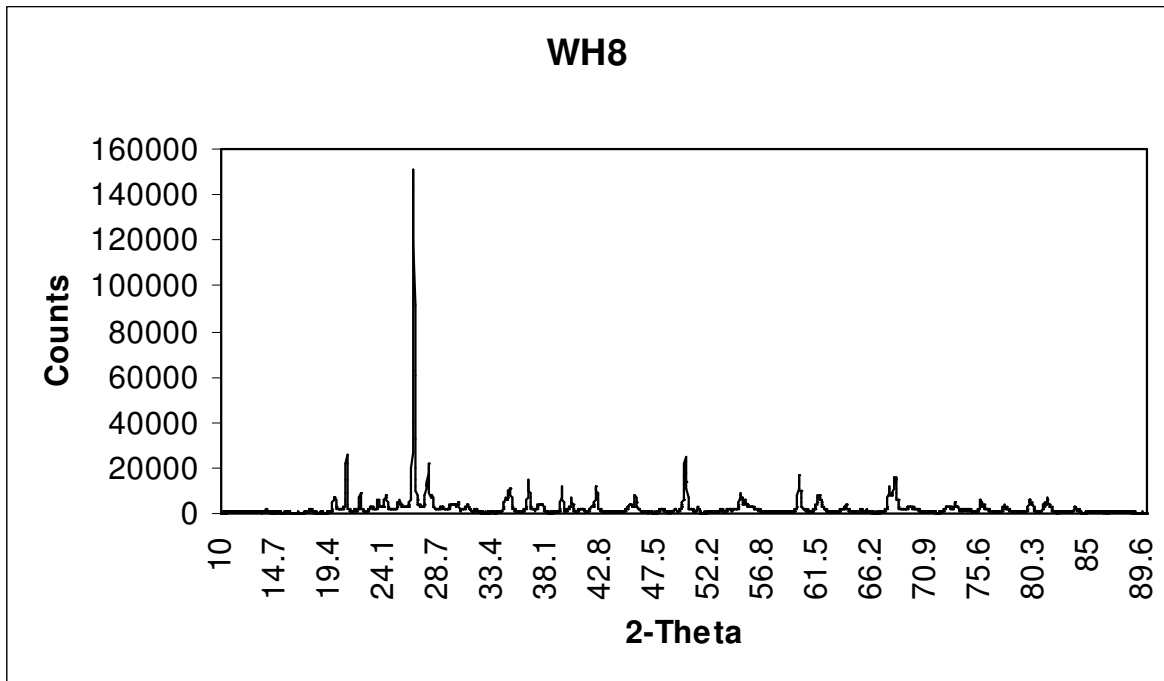


Figure 27. Representative profile of X-ray diffraction patterns for studied shale of the Whitehill Formation, Witteburg.

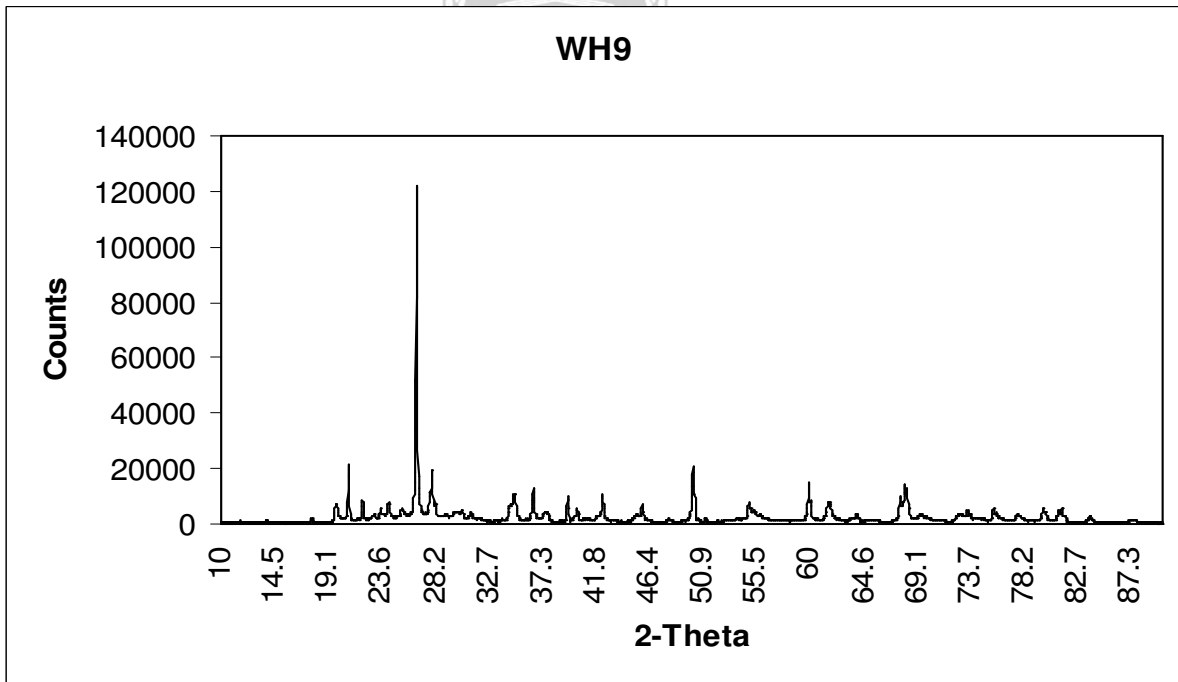


Figure 28. Representative profile of X-ray diffraction patterns for studied shale of the Whitehill Formation, Witteburg.



Appendix F

UNIVERSITY *of the*
WESTERN CAPE

Appendix F

Plate 1

Figure A. SEM micrograph of shale of the Collingham Formation shows partially altered grain along the edges.

Figure B. SEM micrograph of shale of the Collingham Formation shows white illite flake.

Plate 2

Figure A. SEM micrograph of shale of the Prince Albert Formation shows clay minerals showing signs of alteration along edges.

Figure B. SEM micrograph of shale of the Prince Albert Formation shows partially coated albite grains with white illite flake growths.

Plate 3

Figure A. SEM micrograph of shale of the Whitehill Formation shows paper structure of montmorillonite (right and left) of a white flake.

Figure B. SEM micrograph of shale of the Whitehill Formation shows flower structure of montmorillonite.

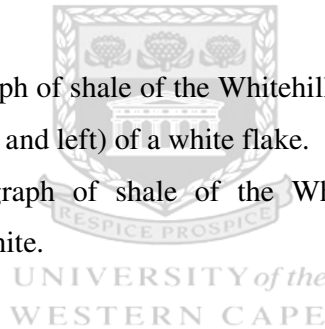


Plate 4

Figure A and B. SEM micrograph and EDS of shale of the Whitehill Formation reveals composition of montmorillonite

Plate 5

Figure A and B. SEM micrograph and EDS of shale of the Whitehill Formation reveals coated grain with a chemical composition typical of muscovite.

Plate 1

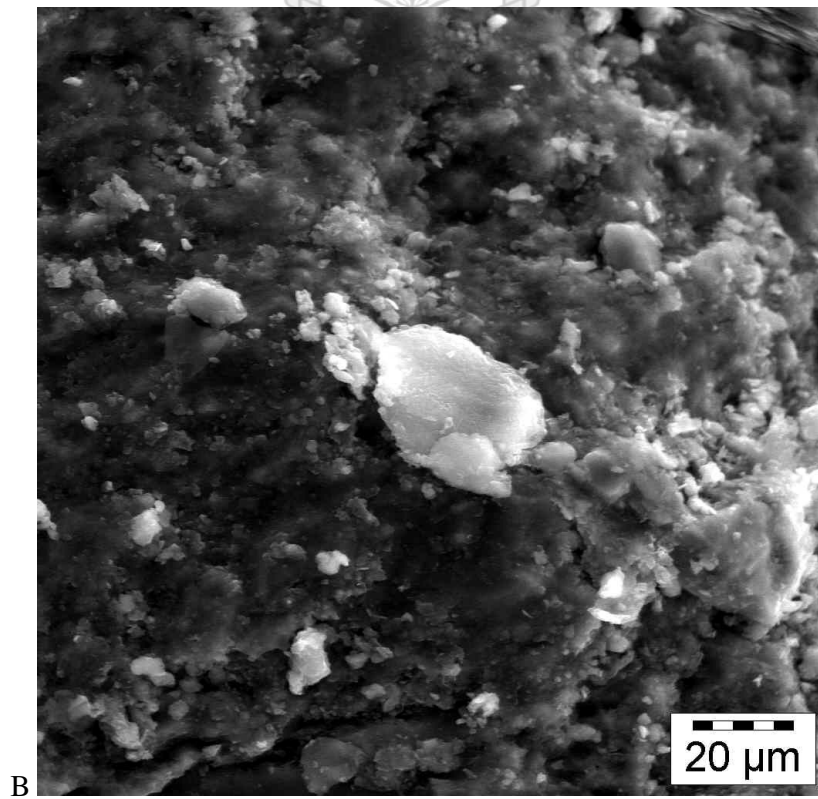
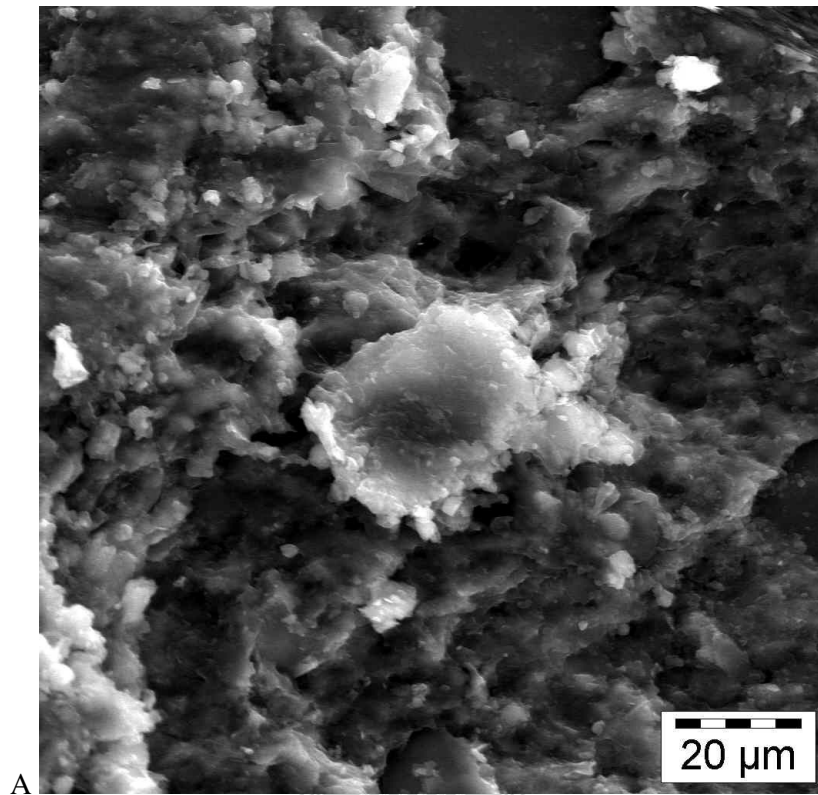


Plate 2

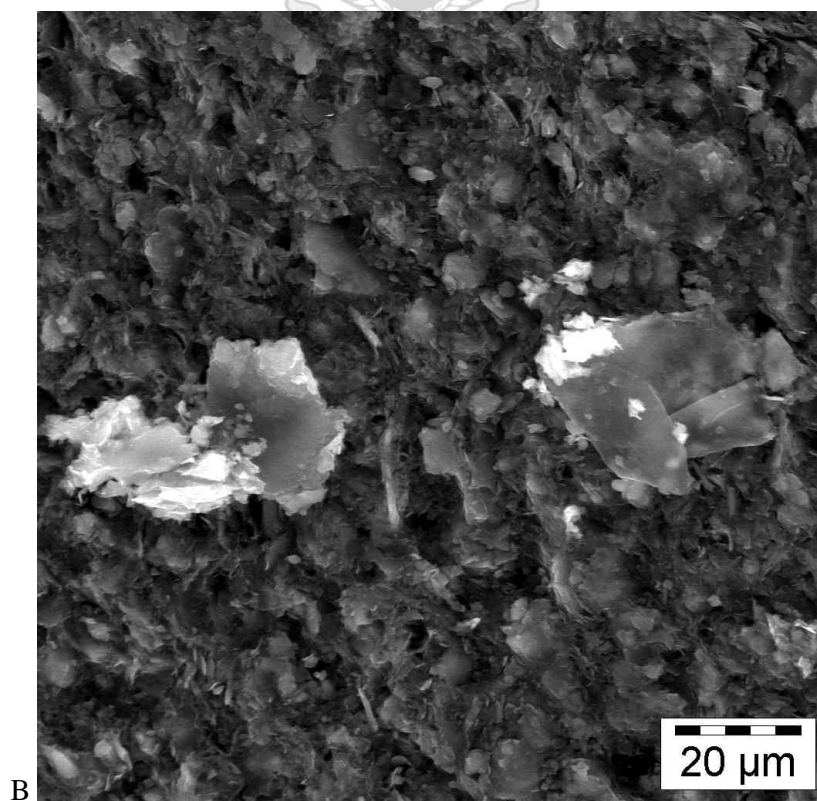
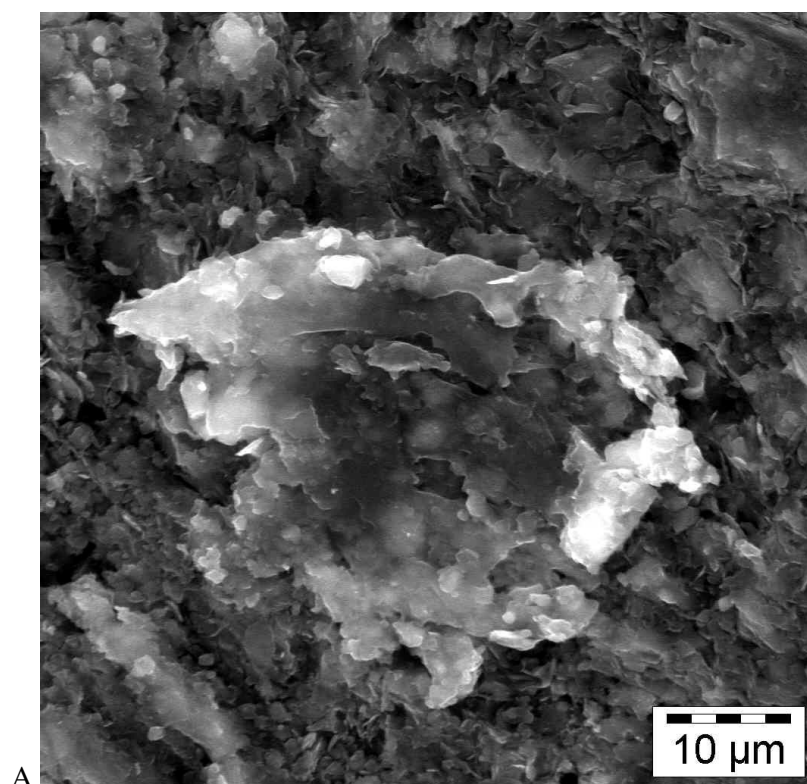


Plate 3

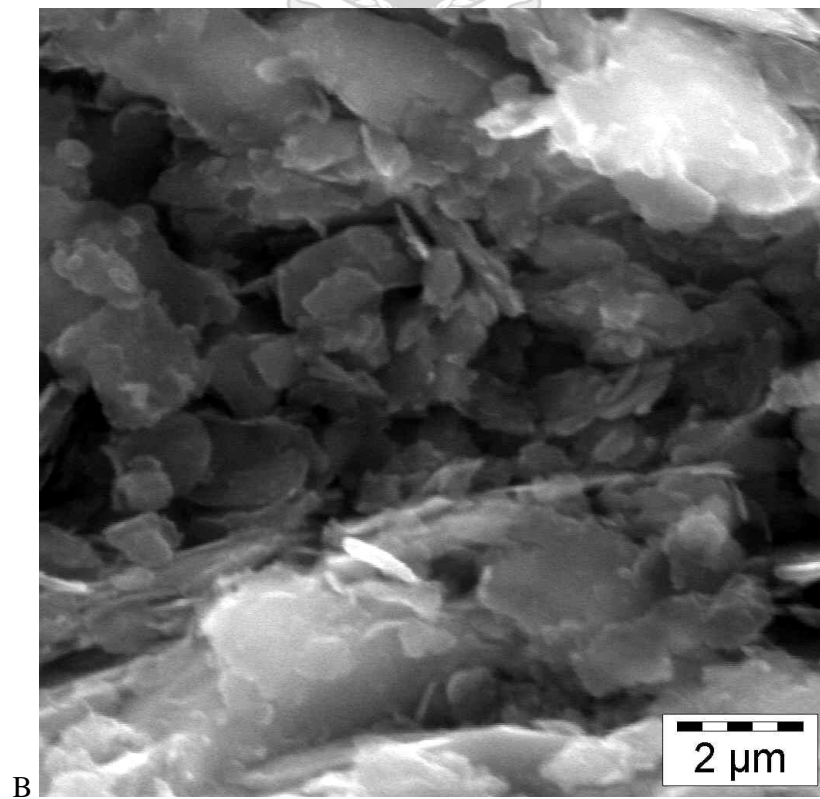
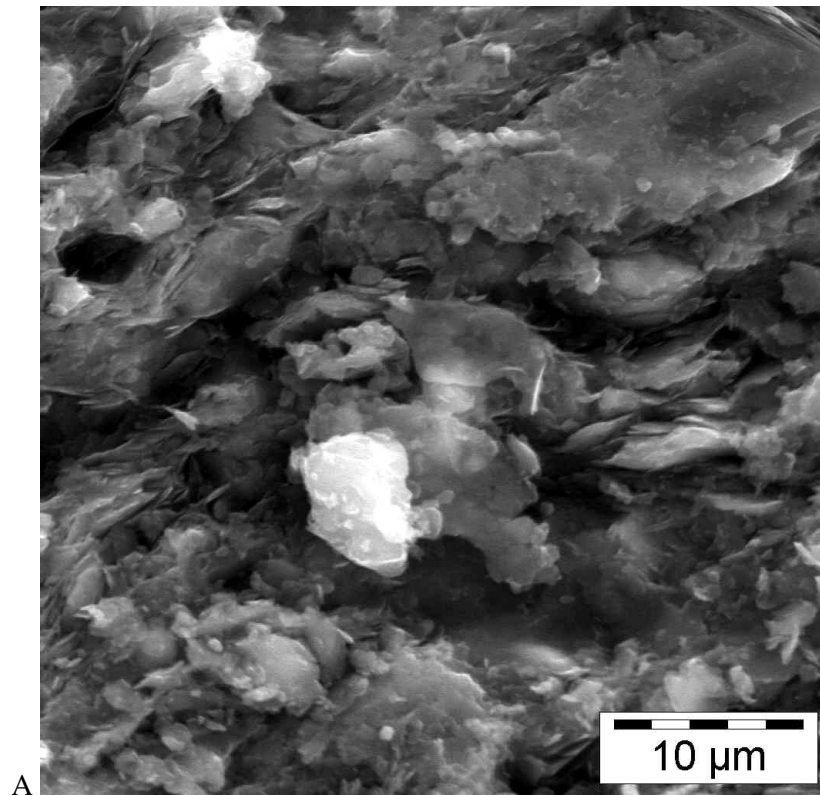
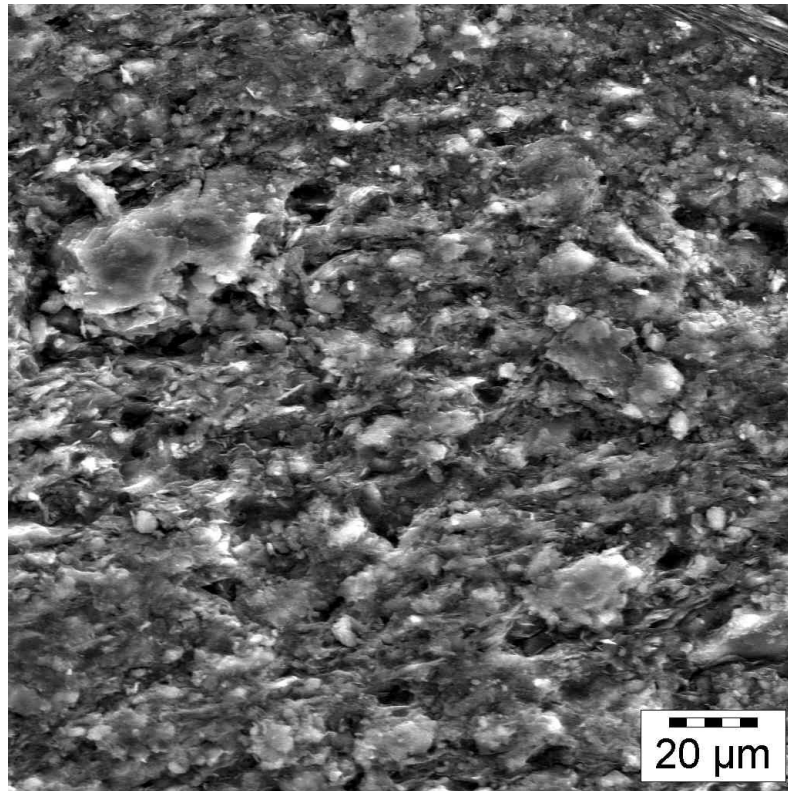
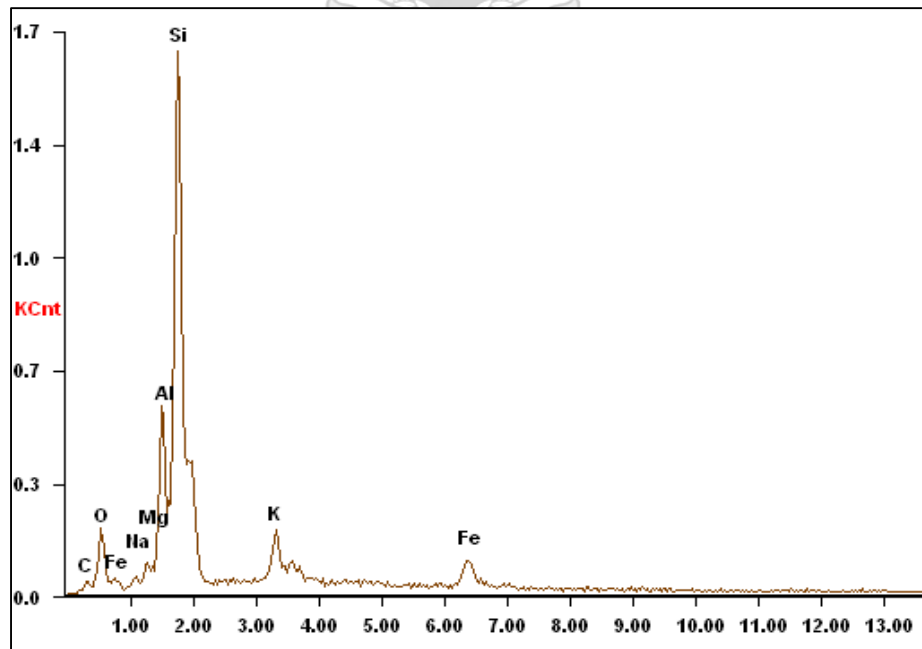


Plate 4

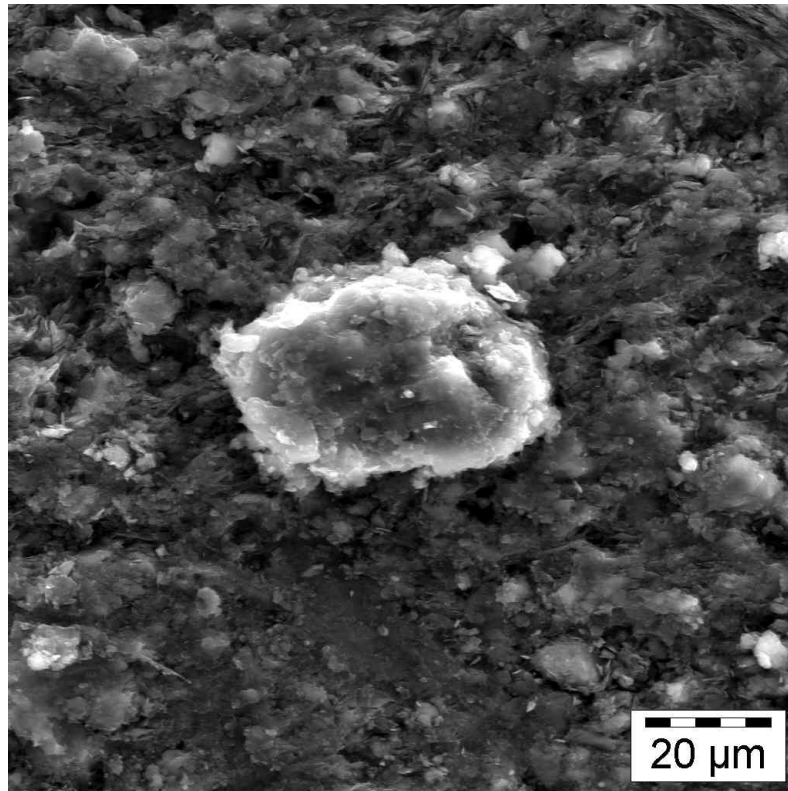


A

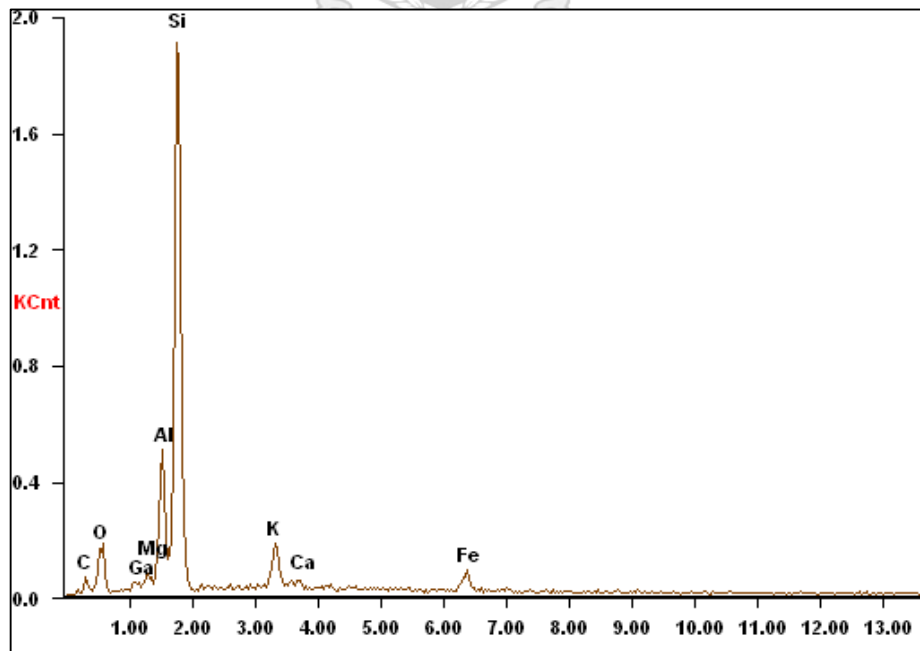


B

Plate 5



A



B